

Pit Arnold

Master Thesis 2018 supervised by:
Univ.-Prof. Dipl.-Phys. Dr.habil. Holger Ott

Experimental investigation of interfacial tension for alkaline flooding

To my beloved parents and sister

Declaration

I hereby declare that except where specific reference is made to the work of others, the contents of this dissertation are original and have not been published elsewhere. This dissertation is the outcome of my own work using only cited literature.

Erklärung

Hiermit erkläre ich, dass der Inhalt dieser Dissertation, sofern nicht ausdrücklich auf die Arbeit Dritter Bezug genommen wird, ursprünglich ist und nicht an anderer Stelle veröffentlicht wurde. Diese Dissertation ist das Ergebnis meiner eigenen Arbeit mit nur zitierter Literatur.

Name, 04 June 2018

Acknowledgements

I would like to thank Prof. Holger Ott for his supervision throughout my entire masters. All the discussions and his vast knowledge motivated and helped me a lot to complete my studies and this thesis.

I also want to thank Dr. Torsten Clemens and the OMV for providing materials as well as support.

In addition, I want to thank my colleagues Roman Manasipov, Mostafa Borji and Kata Kurgyis for their moral support and helpful advices.

Last but not least I want to thank my family and friends who supported me throughout my entire studies in all possible ways. Especially, Alexandra Groiss and Mario Dragovits who were there for me, whenever I needed them.

Abstract

Even after waterflooding is applied, the average recovery factor from conventional oil fields is between 25-45%, which means that a major part of the oil still remains in the reservoir. In case of field in Austria, waterflooding is already applied for several decades. A large portion of the produced fluids is reservoir water (i.e. 96% water cut) implying that the remaining oil is largely trapped. Therefore, new methods and techniques need to be applied. Enhanced oil recovery (EOR), as the name indicates, summarizes techniques that deal with the increase of hydrocarbon recovery from fields depleted by conventional means. One family of techniques is chemical flooding, for which the targeted field is suitable. Alkaline flooding is one promising method, creating in-situ surfactants thus lower the interfacial tension between oil and water. Furthermore, alkaline flooding preconditions the reservoir for a subsequent surfactant polymer (SP) flood.

The present thesis investigates the behavior of the interfacial tension (IFT) between various oils and injection water of different chemical compositions. The oil samples crude 8 and crude 16 are characterized by a relatively high total acid number (TAN), which makes them a target for alkaline flooding. As alkalic EOR agent, sodium carbonate (Na_2CO_3) has been added in different concentrations to distilled water and synthetic brine mimicking the reservoir water.

For first orientation classical phase behavior experiments were conducted to investigate the degree of emulsion formation. To measure IFT pendant drop and spinning drop methods were applied. During the study it turned out that spinning drop can be applied throughout the whole range of investigated IFT, while pendant drop failed below a value of 1 mN/m. The bulk of experiments were performed at ambient conditions, and temperature dependencies were determined for selected interesting cases.

Experiments conducted with distilled water solutions showed a distinct reduction of IFT and pronounced emulsion formation. However, different oil samples showed different trends without a clear link to the TAN. The synthetic brine solutions on the other hand showed neither a distinct reduction nor visible emulsion formation, not in spinning drop nor in the phase behavior experiments. At last, temperature dependencies were investigated which showed that IFT readings are sensitive to it. The individual fluid combinations show distinct behavior, but without an obvious trend with respect to alkali concentration and TAN. Further statements require additional experiments.

Zusammenfassung

Auch nach sekundärer Produktion von Öllagerstätten (Wasserflutung), bleiben im Schnitt 55-75% des Öls in der Lagerstätte zurück. In Feldern Österreichs wurden Wasserflutungen bereits über mehrere Jahrzehnte angewendet. Der Hauptanteil der produzierten Flüssigkeiten ist Wasser (d.h. 96% Wassergehalt), was bedeutet, dass ein Großteil des Öls gefangen ist. Daher müssen neue Methoden und Techniken angewandt werden. Wie der Name impliziert, umfasst Enhanced Oil Recovery (EOR), Techniken, welche sich mit der Erhöhung der Ölgewinnung aus Feldern beschäftigen, die bereits durch gewöhnliche Methoden erschöpft wurden. Das angestrebte Feld eignet sich für die Zugabe von Chemikalien zum Injektionswasser, was eine der Techniken ist. Eine vielversprechende Methode ist dabei die Verwendung von Alkalien, welche in-situ Tenside bilden und dadurch die Grenzflächenspannung zwischen Öl und Wasser senken. Des Weiteren konditioniert eine Alkaliflutung die Lagerstätte für eine Sequenz aus Tensid- und Polymerflutungen.

In dieser Diplomarbeit wird das Verhalten der Grenzflächenspannung zwischen verschiedenen Ölen und Wässern unterschiedlicher chemischer Zusammensetzungen untersucht. Ein höherer Entölungsgrad kann dabei durch eine Senkung der Grenzflächenspannung, durch Erzeugung von Tensiden aus der Ölphase, erreicht werden. Als alkalisches EOR Mittel wurde Natrium Carbonat (Na_2CO_3) in verschiedenen Konzentrationen zu destilliertem Wasser und synthetischer Sole, welche dem Lagerstättenwasser nahekommt, hinzugefügt. Daher wird in dieser Arbeit die Änderung der Grenzflächenspannung der zwei unterschiedlichen Rohöle crude 8 und crude 16 untersucht. Beide haben ähnlich hohe Gesamtsäurezahlen.

Für einen ersten Überblick wurden klassische Phasenverhaltensexperimente durchgeführt, um die Bildung von Emulsionen abzuschätzen. Um die Grenzflächenspannung zu messen wurden die Pendant Drop und Spinning Drop Methoden benutzt. Während der Untersuchungen wurde festgestellt, das Spinning Drop für den gesamten Bereich der untersuchten Grenzflächenspannungen geeignet ist, wohingegen Pendant Drop sich für Werte unter 1 mN/m als ungeeignet herausstellte. Ein Großteil der Experimente wurde unter Umgebungsbedingungen durchgeführt, während Temperaturabhängigkeiten nur für vereinzelte interessante Fälle untersucht wurden.

Experimente mit destilliertem Wasser Lösungen zeigten eine deutliche Verringerung der Grenzflächenspannung, sowie ausgeprägte Emulsionsbildungen. Die verschiedenen Ölproben

zeigten zwar unterschiedliche Ergebnisverläufe, jedoch ohne eine klare Verbindung zur Gesamtsäurezahl. Dahingegen zeigte sich im Falle der synthetischen Solen Lösungen weder eine deutliche Verringerung der Grenzflächenspannung noch eine sichtbare Bildung von Emulsionen, nicht im Spinning Drop und auch nicht in den Phasenverhaltensexperimenten. Zuletzt wurde die Temperaturabhängigkeit untersucht, welche zeigte, dass die Grenzflächenspannung gegenüber dieser empfindlich ist. Aus den einzelnen Kombinationen gingen deutliche Verhalten hervor, aus welchen sich jedoch keine klaren Verläufe hinsichtlich des Alkaligehaltes und der Gesamtsäurezahl abzeichneten. Für weitere Feststellungen bedarf es zusätzlicher Experimente.

Table of Contents

Declaration	iii
Erklärung	iii
Acknowledgements	iv
Abstract	v
Zusammenfassung	vi
List of Figures	xi
List of Tables	xiii
Nomenclature	xv
Abbreviations	xvii
Chapter 1	1
1.1 Background and Context	1
1.2 Scope and Objectives	2
Chapter 2	3
2.1 EOR	3
2.1.1 Alkaline Flooding	3
2.1.2 Soap generation	4
2.1.3 Total Acid Number (TAN)	5
2.2 Phase behavior	5
2.3 Interfacial Tension	7
2.3.1 IFT measurement via pendant drop method	7
2.3.2 IFT measurement via spinning drop tensiometer	8
2.3.3 Temperature dependency of IFT	11
2.3.4 Capillary Number	11
Chapter 3	13
3.1 Materials	13
3.2 Measurement Set up	17
3.2.1 Preparation of solutions	17
3.2.2 Phase behavior	17
3.2.3 Syringes	17
3.2.4 Pendant drop	18
3.2.5 Spinning Drop	19
3.3 Cleaning Procedure	21
Chapter 4	25
4.1 Phase Behavior	25
4.1.1 Phase behavior distilled water solutions	25
4.1.2 Phase behavior synthetic water solutions	28

4.2	IFT measurements.....	30
4.2.1	Pendant Drop	30
4.2.2	Spinning Drop	33
4.2.3	Distilled water	39
4.2.4	Synthetic water.....	41
4.2.5	Alkali solutions	44
4.2.6	Temperature	61
Chapter 5.....		65
5.1	Alkali concentration dependency.....	65
5.2	Temperature dependency	70
5.3	Summary	73
5.4	Future Work.....	74
Chapter 6.....		75

List of Figures

Figure 2-1 Schematic of alkali recovery process (deZabala, et al., 1982)	5
Figure 2-2 Three types of microemulsions and the effect of salinity on phase behavior (Sheng, 2010).....	6
Figure 2-3 Pendant drop showing the geometrical variable (Zeppieri, et al., 2001).....	8
Figure 2-4 Drop shapes depending on the rotational speed when gravitational forces are neglected (Viades-Trejo & Gracia-Fadrique, 2007)	9
Figure 2-5 Shape parameter for usage of CSW- and LY-Method calculations (Dataphysics, 2013).....	10
Figure 2-6 Schematic capillary desaturation curve (Lake, et al., 2014).....	12
Figure 3-1 Spinning Drop Tensiometer SVT 20N set up	15
Figure 3-2 FEC 622/400-HT capillary.....	16
Figure 3-3 Set up for pendant drop measurement.....	18
Figure 3-4 Calibration via needle for a magnification of 1.0x.....	19
Figure 3-5 Example of a droplet within the measuring box.....	21
Figure 3-6 Cleaning steps of the capillary	23
Figure 4-1 Phase behavior of crude 8 (top) and crude 16 (bottom) oil with alkali solutions prepared with distilled water (left to right: 3,000, 4,500, 6,000, 7,500, 9,000, 10,500, 12,000 ppm)	27
Figure 4-2 Phase behavior of crude 8 (top) and crude 16 (bottom) oil with alkali solutions prepared with synthetic water (left to right: pure synthetic water, 3,000 ppm, 7,500 ppm and 12,000 ppm).....	29
Figure 4-3 IFT vs. time of crude 8 and crude 16 oil in distilled water via pendant drop.....	31
Figure 4-4 IFT vs. time of crude 8 and crude 16 oil in synthetic water via pendant drop	32
Figure 4-5 No droplet formation of crude 8 oil in distilled water with 3,000 ppm Na ₂ CO ₃ (left: picture of needle inside cuvette; right: picture within the software).....	33
Figure 4-6 Overview of drop types and calculation methods	33
Figure 4-7 Drop Type comparison with standard deviation	34
Figure 4-8 IFT of all three calculation methods vs. time with horizontal to vertical ratio	35
Figure 4-9 Measured IFT difference to the ratio of the drop	36
Figure 4-10 Measured IFT values with LY and CSW method for a droplet with a ratio of 1.01	36
Figure 4-11 Histogram of IFT values for almost spherical drop	37
Figure 4-12 Almost spherical drop view via software	37
Figure 4-13 IFT dependency on rotational speed	38
Figure 4-14 IFT median with standard deviation depending on rotational speed.....	38
Figure 4-15 IFT vs. time of crude 8 oil in distilled water via spinning drop	40
Figure 4-16 Crude 8 oil in distilled water	40
Figure 4-17 IFT vs. time of crude 16 oil in distilled water via spinning drop	41
Figure 4-18 Crude 16 oil in distilled water.....	41
Figure 4-19 IFT vs. time of crude 8 oil in synthetic water	42
Figure 4-20 Crude 8 oil in synthetic water over time.....	42
Figure 4-21 IFT vs. time of crude 16 oil in synthetic water	43
Figure 4-22 Crude 16 oil in synthetic water	43
Figure 4-23 Example of oil touching both sides of the capillary	44
Figure 4-24 IFT vs. time of crude 8 oil in 3,000 ppm distilled water solution	45
Figure 4-25 Crude 8 oil in 3,000 ppm distilled water solution over time (left to right: 274 s, 6450 s, 20600 s).....	45
Figure 4-26 IFT vs. time of crude 8 oil in 7,500 ppm distilled water solution	46
Figure 4-27 Crude 8 oil in 7,500 ppm distilled water solution over time (left to right: 10 s, 380 s, 1730 s, 6300 s)	47

Figure 4-28 IFT vs. time of crude 8 oil in 7,500 ppm distilled water solution with rpm decrease	48
Figure 4-29 Crude 8 oil in 7,500 ppm distilled water solution after emulsion reattached.....	48
Figure 4-30 IFT vs. time of crude 8 oil in 12,000 ppm alkali distilled water solution	49
Figure 4-31 Crude 8 oil in 12000 ppm distilled water solution	49
Figure 4-32 IFT vs. time of crude 16 oil in 3,000 ppm alkali distilled water solution	50
Figure 4-33 Crude 16 oil in 3,000 ppm distilled water solution (first experiment)	51
Figure 4-34 Crude 16 oil in 3,000 ppm distilled water solution (second experiment)	51
Figure 4-35 Evolution of crude 16 oil drop formation in 7,500 ppm distilled water solution software (left to right: 33s, 140s, 470s, 714s, 1031s, 1110s, 1400s and 2640s)	52
Figure 4-36 Evolution of crude 16 oil drop formation in 7,500 ppm distilled water solution photos (left to right: 145s, 720s, 2700s).....	52
Figure 4-37 IFT vs. time crude 16 oil in 7,500 ppm distilled water solution of two different experiments with different drop volumes (left: 0.9 μ L; right: 0.03 μ L)	53
Figure 4-38 Crude 16 oil in 7,500ppm distilled water solution of two different experiments with different drop volumes (left: 0.9 μ L; right: 0.03 μ L).....	53
Figure 4-39 IFT vs. time of crude 16 oil in 12,000 ppm distilled water solution	54
Figure 4-40 Crude 16 oil in 12,000 ppm distilled water solution	54
Figure 4-41 IFT vs. time of crude 8 oil in 3,000 ppm synthetic water solution.....	55
Figure 4-42 Crude 8 oil in 3,000 ppm synthetic water solution.....	56
Figure 4-43 IFT vs. time and rotational speed of crude 8 oil in 7,500 ppm synthetic water solution.....	57
Figure 4-44 Crude 8 oil in 7,500 ppm synthetic water solution	57
Figure 4-45 IFT vs time of crude 8 oil in 12,000 ppm synthetic water solution.....	58
Figure 4-46 Crude 8 oil in 12,000 ppm synthetic water solution.....	58
Figure 4-47 IFT vs. time of crude 16 oil in 3,000 ppm synthetic water solution.....	59
Figure 4-48 Histogram of stable crude 16 oil drop in synthetic water solution.....	59
Figure 4-49 Crude 16 oil in 3,000 ppm synthetic water.....	59
Figure 4-50 IFT vs. time of crude 16 oil in 7,500 ppm synthetic water solution.....	60
Figure 4-51 Crude 16 oil in 7,500 ppm synthetic water solution.....	60
Figure 4-52 IFT vs. time of crude 16 oil in 12,000 ppm synthetic water solution.....	61
Figure 4-53 Histogram of crude 16 oil in 12,000 ppm synthetic water solution	61
Figure 4-54 Crude 16 oil in 12,000 ppm synthetic water solution.....	61
Figure 4-55 IFT vs. time and temperature of crude 8 oil in 3,000 ppm distilled water solution	63
Figure 4-56 Distancing and conjoining of droplets exemplary in the case of crude 8 and 3000 ppm distilled water solution (top to bottom: 20, 30, 40 and 50°C).....	64
Figure 5-1 Schematic of an elliptical droplet with different phase contacts	66
Figure 5-2 IFT vs. Na ₂ CO ₃ solutions prepared with distilled (top) and synthetic (bottom) water	69
Figure 5-3 IFT vs. temperature of crude 8 (top) and crude 16 (bottom) oil.....	71

List of Tables

Table 3-1 Oil samples properties	14
Table 3-2 Calibration values for the spinning drop	20
Table 4-1 Statistics for rotational speed dependency.....	39
Table 6-1 Water density depending on temperature [g/ml] (Weast, 1972).....	A-1

Nomenclature

f_{rot} or n	frequency	[1/min]
t	time	[s]
r	radius	[m]
γ	Interfacial tension	[mN/m]

Abbreviations

DW	Distilled water
EOR	Enhanced oil recovery
IFT	Interfacial tension
LY	Laplace Young
PD	Pendant drop
RF	Recovery factor
RPM	Rounds per minute
SD	Spinning drop
SW	Synthetic water
TAN	Total acid number

Chapter 1

Introduction

Crude oil is still one of the major primary energy sources. Since the worldwide energy demand is steadily increasing the demand for oil is also on the rise. Yet most of them are still within their reservoirs since the average recovery factors are only between 25% to 45% (Deutsche Bank, 2013), leaving a vast majority within the fields. Most of the reservoirs have yet only undergone secondary recovery techniques leaving room for improvement. Over the years the understanding of rock-rock, fluid-rock and fluid-fluid interactions has greatly improved giving opportunities of increasing the RF up to 60% in some fields. Those can be achieved by using tertiary recovery, also called enhanced oil recovery (EOR), methods.

EOR techniques rely on the above-named rock-fluid interactions and therefore need to be chosen on an individual basis depending on the specific reservoir.

1.1 Background and Context

Austrian oil fields have been producing over many decades. The targeted Field, which is object of this thesis, was discovered in 1949 (Hamilton, et al., 1999) 1940's, along with its oil and gas bearing horizons. Therefore, it is already producing for more than 60 years now. Secondary recovery techniques were applied in form of water injection for over 40 years. Due to those circumstances the reservoir is already at residual conditions. Meaning that most of the oil left is trapped via capillary forces within the pores leading to a high-water production.

Interfacial tension is one of the main influences governing the magnitude of capillary forces. Increasing the pH of injection water tackles the capillary forces by reducing the interfacial tension. It works on the basis of chemical reactions between oil and water, similar to a saponification reaction. Since both, the crude 8 and crude 16 oil, which are found within the

targeted field are suitable for this technique their interfacial interaction between them and different alkali mixtures is studied.

1.2 Scope and Objectives

In this thesis the fluid-fluid interactions between different crude oils and aqueous solutions with different alkalinity is studied. More specifically the interfacial interactions have been studied as function of water alkalinity, salinity and temperature.

Many different IFT measurement methods are available, however with pendant drop and spinning drop two commonly applied techniques were chosen. A workflow for measuring the different systems was developed. Furthermore, the influence of adjustable parameters was investigated.

The goal is to find the influence of different alkali concentrations for each oil and to measure ultra-low interfacial tensions.

Chapter 2

Literature Review

The reduction of interfacial tension is one of the fundamentals in EOR, especially since it is the dominant force restricting flow on the microscopic scale. Therefore, I will give a brief introduction into its measurement as well as the mechanisms and purpose of its reduction.

2.1 EOR

The development of Enhanced Oil Recovery is one of the primary objectives in modern day reservoir engineering. It also refers to tertiary oil recovery, since it is often used on producing fields at the end of their life cycle where a water flood was already implied beforehand. Although EOR actually refers to the change of chemical rock and fluid properties. Some of the main parameters aimed for are IFT, viscosity and wettability, so even residual oil saturation can be targeted.

The classification of EOR methods varies in literature and is therefore not clearly defined. According to Lake the mechanisms can be divided into thermal, solvent, chemical and other (Lake, et al., 2014).

2.1.1 Alkaline Flooding

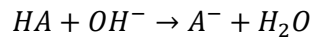
Injecting alkaline water solutions for oil recovery was already studied in the 1920's, but it took around another 50 years until it was subjected for field tests (Eremin & Nazarova, 2003). The idea behind the use of an alkaline water solution is the creation of in-situ surfactants. Due to the reaction between acidic components in the crude oil phase and the alkali, soaps are created. This may lead to a major reduction of IFT, formation of emulsions and even alteration of wettability. Former is especially important if the reservoir is at residual oil saturation, because the IFT stands in direct proportion to the capillary number, N_c , which will be discussed later. The correlation between wettability and oil recovery is studied since the 1970's. In general, it

has been shown that an increase of water-wetness results in an oil recovery increase (Owens & Archer, 1971) (Morrow, 1990). A change to water wetness alters relative permeabilities of oil and water leading to an increase of the displacement efficiency but it also increases residual oil saturation. However, it was later shown that sodium carbonate as alkali agent can lead to a wettability alteration in the opposite direction, meaning that water-wet systems change into oil-wet systems (Gong, et al., 2016). Yet it still has a positive effect by preventing water channeling which improves the sweep efficiency. This shows that making a statement about wettability alteration is not a simple task, especially since it depends on the rock composition and life cycle phase of the field. Since wettability alteration is not the main objective of alkaline flooding and of this thesis, I will focus in the following on fluid-fluid interactions and interfacial tension.

Alkaline floodings are seldomly standalone projects. They are often used in combination as ASP floodings, which stands for alkaline surfactant polymer flooding where the alkaline is used to precondition the reservoir. Additional to the three main mechanisms mentioned before, there is also oil entrainment, bubble entrapment and a reduction of surfactant adsorption (Johnson, 1976). Which are the main reasons why it is used before a surfactant/polymer flood.

2.1.2 Soap generation

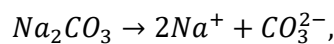
“...when an alkaline solution reacts with the acid component in a crude oil. The reaction equation is



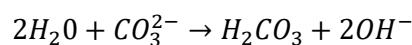
where HA is a pseudo-acid component and A⁻ is the soap component” (Sheng, 2014).

In Figure 2-1 a schematic of this reaction can be seen. The denotation o and w on the soap component refer to oleic and aqueous phase.

Whereas this is a general description of the reaction leading to the formation of a soap, below is the reaction in case of sodium carbonate which solely was used in this thesis. At first there is a dissociation of the Na₂CO₃ into:



which then removes free H⁺ ions by the formation of carbonic acid.



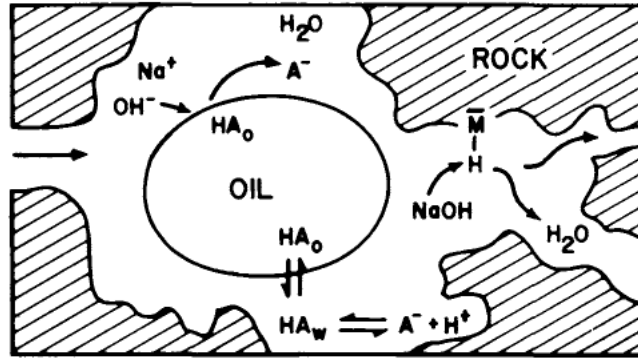


Figure 2-1 Schematic of alkali recovery process (deZabala, et al., 1982)

The so created OH^- can now react with the petroleum acids at the oil/water interface. Those are called naphthenic acid since it is an “unspecific mixture of several cyclopentyl and cyclohexyl carboxylic acids” (Sheng, 2010)

2.1.3 Total Acid Number (TAN)

As mentioned in the chapter above acids in the oil phase react with the hydroxide ions, in the aqueous phase, which is an acid-base reaction. Therefore, it is important to characterize the oil with respect to its acidic components. A measure to define the total acid concentration within a sample is the titration with potassium hydroxide (KOH). The procedure is clearly defined and standardized by ASTM International: A gram of oil is taken and the amount of KOH in milligram is measured which is needed to neutralize all acids within the oil. The unit is therefore given as [mg KOH / g oil]. Nowadays it is often done via potentiometric titration, which is working on the principal of electric resistance. For this the sample is needed as an aqueous phase and therefore is diluted in a mix of chloroform and isopropyl alcohol (D664, 2018).

One of the downsides is that only the total amount of acids present in the oil is measured. Therefore, it does not have to be a specific representation of the carboxylic acids within the oil. A better inside is given by the acid number (AN), since it also detects weak organic acids and strong inorganic acids. (Anon., 2018)

2.2 Phase behavior

In alkaline flooding, in-situ surfactants are generated, therefore the phase behavior between oil, brine and surfactant is a fundamental. Even though in the chapter before we called it soap it is actually a surfactant. In literature they use different names to distinguish between the in-situ produced surfactants and the ones injected via an ASP flooding.

Phase behavior is a complex topic since it is sensitive to many parameters. Each unique crude oil composition is adding to that complexity. The salinity of the brine is one of the major parameters influencing our system. In general, low salinity favors good water solubility for anionic surfactants. With increasing salinity of the brine, a change in tendency towards oil solubility develops. Phase behavior is already studied for over 70 years now and one of the first ones to discover it was Winsor (1948). Therefore, one of the naming conventions characterizing emulsion formation is Winsor Type I, II and III. Those represent solubilized oil in water, solubilized water in oil and a three-phase system with a stable microemulsion phase respectively. However, the convention of Type II(-), Type II(+) and Type III as a definition, can also be found. In this case the number stands for the amount of phases and the plus or minus stand for the slope of the tie lines in the ternary diagram. Generally, it results in two-phase systems unless an optimum is found and a thermodynamic stable microemulsion phase is formed which results in a three-phase system. In Figure 2-2 the simplified relation between salinity and phase behavior can be seen, furthermore exemplary ternary diagrams and phase behaviors are shown for the three named microemulsion cases. Additionally, it shows how to calculate the phase composition.

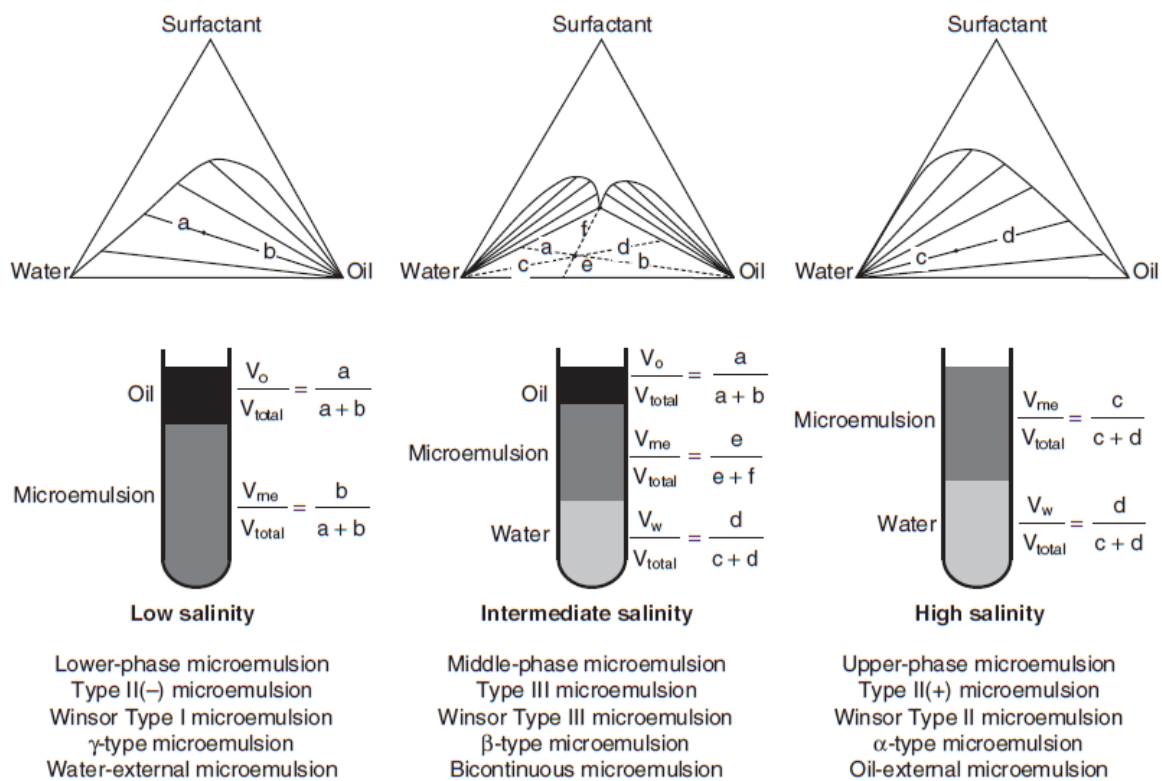


Figure 2-2 Three types of microemulsions and the effect of salinity on phase behavior (Sheng, 2010)

2.3 Interfacial Tension

Interfacial tension is a force per unit length along an interface of two immiscible fluids. When referred to an interface of a liquid and gas it is called surface tension. In literature the symbol is often given as γ or σ and its unit in mN/m .

Molecular interdependency is the fundamental reason for those forces to occur. Whereas cohesive forces are mainly interacting within the bulk of the fluid we do have additional adhesive forces at the interface which determine interfacial tension. IFT is mainly influenced by temperature, composition of the oil and water phases and only minorly by the pressure.

Widely used methods for measuring are the pendant drop and du Noüy ring method, the later was introduced by the French physicist (du Noüy, 1925). Even though both are simple and fast to execute their downside are their measurable range. Both methods do only hold for values down to 10^{-1} mN/m.

Since the goal is the formation of (micro-)emulsions and consequently reaching ultra-low IFTs, which according to literature are 10^{-2} mN/m and lower (Thomas, 2008), a different way of measuring needs to be considered. The most well-known technique for measuring those is the spinning drop tensiometer, which has been applied throughout this thesis. However, also other techniques are proposed, like a modified sessile drop (Chatterjee, et al., 1998), the micropipette (Afshar & Yeung, 2011) or laser light scattering method (Zhang, et al., 2001).

2.3.1 IFT measurement via pendant drop method

The pendant drop method is a very common known method for measuring the IFT of two immiscible fluids. It is easy to execute and with the help of modern computers and cameras the drop shape can easily be obtained and analyzed. The method relies on the balance between hydrostatic pressure, gravitational and surface forces. From those the IFT can be calculated by the use of Laplace-Youngs equation.

$$\left(\frac{1}{R_1} + \frac{1}{R_2}\right) = -\frac{\Delta\rho g y}{\gamma} + f(R_0)$$

Where $(1/R_1 + 1/R_2)$ is the mean curvature of the droplet, $\Delta\rho$ the density difference, g the gravitational acceleration, γ the IFT and R_0 the radius at $y = 0$. With the help of differential geometry, the mean curvature can be expressed as a function of the y position see Figure 2-3 (Zeppieri, et al., 2001).

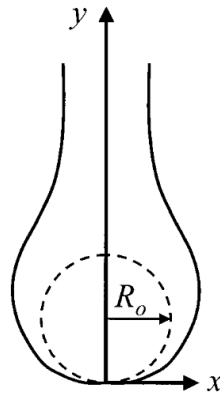


Figure 2-3 Pendant drop showing the geometrical variable (Zeppieri, et al., 2001)

As mentioned before is the method limited when trying to measure low IFT values, because then the droplet only slightly deviates from a spherical form and detaches from the needle before forming a proper measurable size.

2.3.2 IFT measurement via spinning drop tensiometer

In 1942 a new method of measuring the interfacial tension between two immiscible fluids by rotating a vessel at a known speed was suggested (Vonnegut, 1942). Due to the spinning centrifugal forces arise. Consequently, the suspended fluid migrates towards the center of rotation and forms a droplet around this axis. If no interfacial forces are present the droplet elongates until it either reaches the sides of the container or is infinitesimal narrow, considering the container is indefinitely long. However, since interfacial forces are present, the suspended fluid rather will take up a spherical shape, especially for low rotational speeds and high IFT. This is to minimize interfacial energy until a force balance is reached. With increasing speed, the forces acting upon the fluid lead to an elongation of the droplet see Figure 2-4.

When the forces are at equilibrium the droplet takes a stable shape. Since the mathematical description of this shape is quite complex Vonnegut proposed that this shape can be neglected if the radius is quite small compared to its length (Vonnegut, 1942).

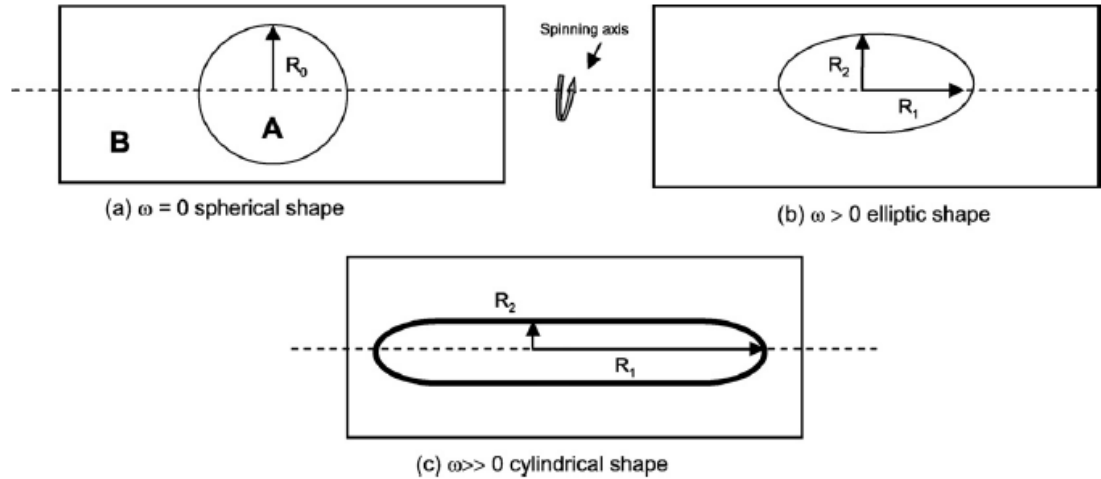


Figure 2-4 Drop shapes depending on the rotational speed when gravitational forces are neglected (Viades-Trejo & Gracia-Fadrique, 2007)

These assumptions then lead to the following function for the interfacial tension

$$\gamma = \frac{\Delta\rho\omega^2}{4}R^3$$

with $\Delta\rho$ being the density difference, ω the rotational speed and R the radius of the droplet in z -direction. However, this only holds if the radius is much smaller than the length ($R \ll L$). The theory was later proven by Rosenthal as well as Princen, Zia and Mason who did a full-shape analysis of the droplets so IFT could also be measured for lower speeds (Rosenthal, 1962) (Princen, et al., 1967). Furthermore, they showed that Vonneguts approach only holds if the ratio between diameter and length is below 4.

Due to their achievement it is now possible to calculate the IFT with the help of the Laplace-Young equation. The expression is

$$\Delta P = \gamma \left(\frac{1}{R_1} + \frac{1}{R_2} \right)$$

for non-spherical droplets, with ΔP being the pressure difference and R_1 and R_2 being the principal curvature radii whereas both need to be orthogonal to each other. By linking the pressure difference to the forces applied and using Princens and others system of differential equations to fit the profile of the droplet we get the following expression for the interfacial tension.

$$\gamma = \frac{\Delta\rho\omega^2}{2\alpha}a^3$$

With a being the radius at the cap and α being the shape factor. The formula already shows that the cap radii of the droplet are needed to measure the IFT via the Laplace-Young method.

Caius, Schechter and Wade went one step further and showed that with knowing the length and width an even more accurate way of determining the IFT is possible, especially for low values (Caius, et al., 1975). Therefore, when measuring with the CSW-Method one makes use of the same formula as before mentioned, however with the major difference that instead of a fitting procedure as compared to the LY-Method but rather an iterative calculation procedure to obtain the shape parameter is used.

In Figure 2-5 the shape parameter is plotted as function of the width to height ratio. Its values range from 0 to $\frac{16}{27}$, however when getting close to zero theoretically the interfacial tension rises to infinity. The shape parameter has a high increment for width/height ratios close to one. It supports the statement that those measurement methods withhold only for non-spherical droplets. Especially since the shape parameter is in the denominator, a decrease of the value towards zero does have a crucial influence. Whereas for ratios above one the shape parameter is clearly defined and above a value of 4 the changes are negligible small, so the shape parameter can be assumed as $\frac{16}{27}$.

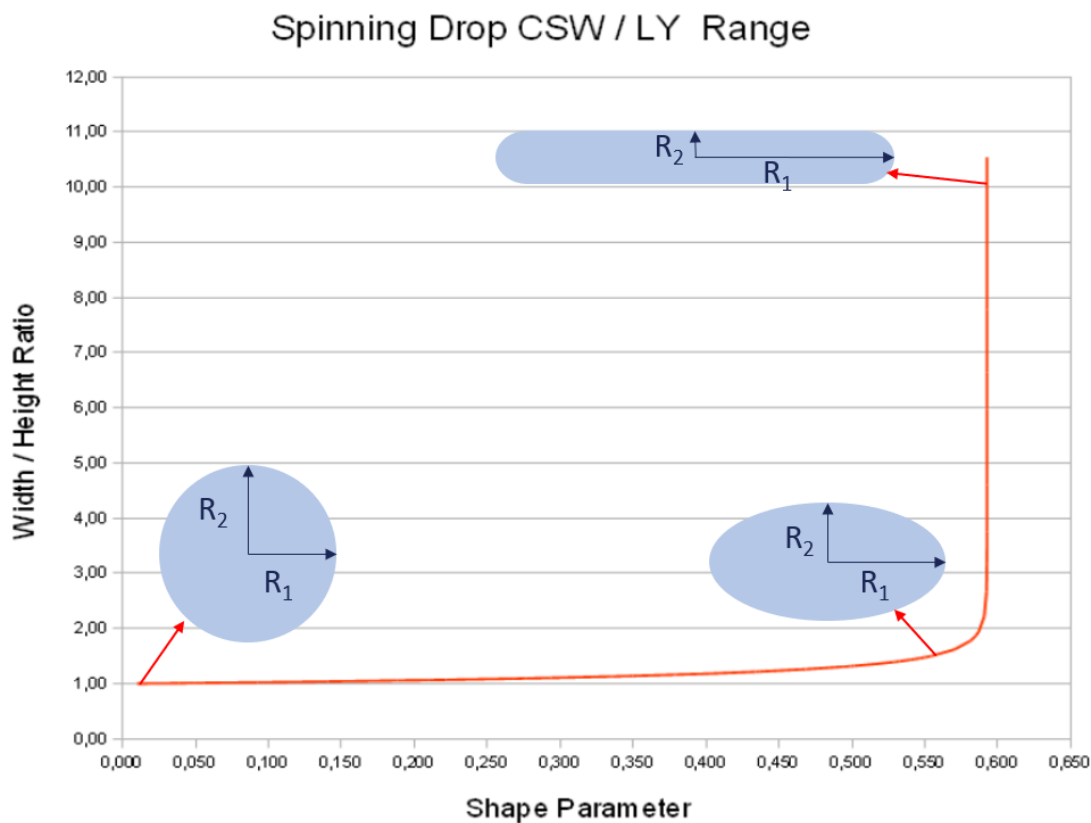


Figure 2-5 Shape parameter for usage of CSW- and LY-Method calculations (Dataphysics, 2013)

2.3.3 Temperature dependency of IFT

As discussed earlier, the interfacial tension of oil/water systems is mainly influenced by the temperature and composition of the oil and water. Even though the composition is the most influencing factor, the temperature dependency is of interest as well. Especially since in-situ surfactants are formed by chemical reactions which are in general influenced by temperature.

The effect of temperature on the IFT was studied by a series of people, however most of them used synthetic oils. It was found that with increasing temperature the IFT decreases (Hassan, et al., 1953) (Bowman, 1967). Hjelmeland, Larrondo and Flock, Le and Gibeau on the other hand found mixed results when conducting the experiments with different crude oils. (Hjelmeland & Larrondo, 1986) (Flock, et al., 1986)

When including alkaline and therefore generating in-situ surfactants the entire system becomes more sensitive to temperature. Furthermore, it was found that IFT is time dependent and therefore will have its minimum depending on time and temperature (Babu, et al., 1984). They showed that both of their oil samples had minima with respect to time. On the one hand for increased temperatures, the obtained minima were lower whereas on the other hand the time interval until the IFT started to increase was significant shortened. In addition, Ye and others showed that for oils with gemini surfactants the minimum reached is also lower with increasing temperature (Ye, et al., 2008). On the other hand, the system becomes more unstable with respect to the temperature, which also coincides with Babus and others observations.

2.3.4 Capillary Number

To describe the influence of IFT on the oil remaining in the reservoir the capillary number, N_c , is used. It is a dimensionless number which is defined as the ratio of viscous over capillary forces. Its simplest definition on the microscopic scale is,

$$N_c = \frac{v\mu}{\gamma}$$

where v is the velocity of the displacing fluid, μ the viscosity and γ the interfacial tension. In some literature the denominator also includes the contact angle $\cos \theta$. From the equation it can be seen that with decreasing IFT the capillary number increases, which results in a change of residual oil saturation, which is one of the targets in EOR. In Figure 2-6 a schematic depiction of this can be seen. Depending on the fluid type the residual saturation is constant until the critical capillary number is attained, after which the desaturation part of the curve is reached, where the residual saturation declines. The capillary number is plotted on a logarithmic scale, which implies that order of magnitude changes of the formula values are needed to reach the

desaturation zone. The capability of changing the velocity and viscosity is rather limited, therefore a change in IFT is pursued.

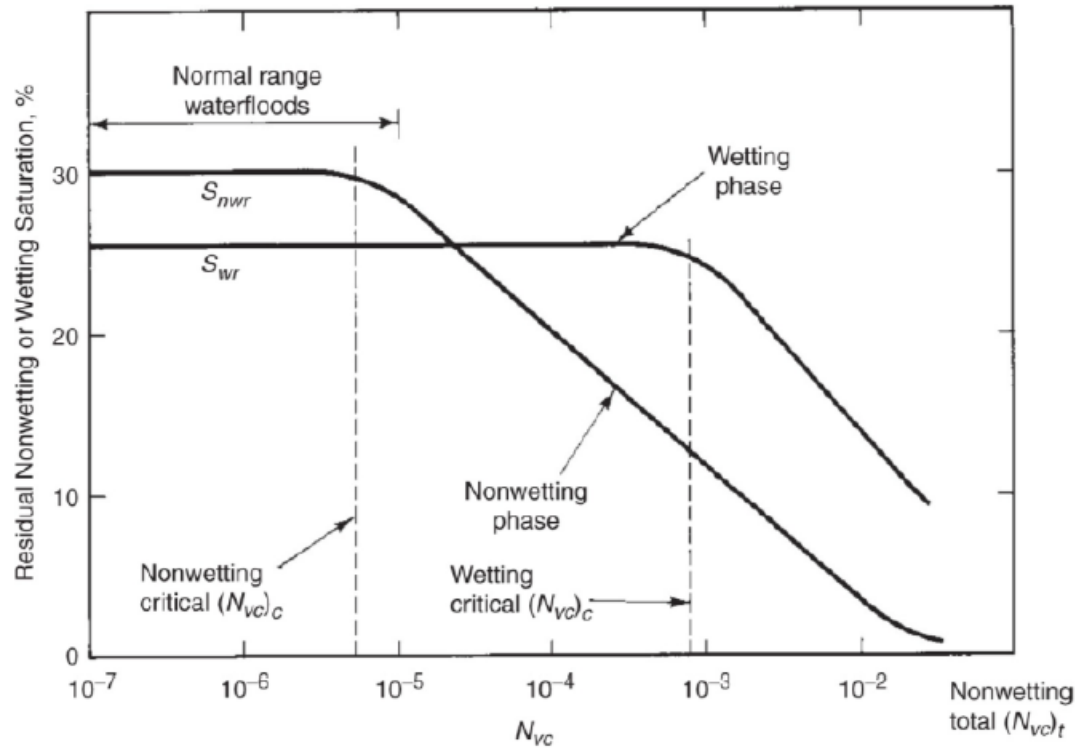


Figure 2-6 Schematic capillary desaturation curve (Lake, et al., 2014)

Chapter 3

Experimental preparation and set up

In this section I will describe the workflow including experimental set up, the cleaning procedures and the preparation of solutions. In all experiments the same steps were carried out to ensure consistency and reproducibility of experiments.

3.1 Materials

- **Distilled water**

The water used for preparation of solutions and basic measurements is manufactured by the company C+V Pharma-Depot GmbH and is in accordance with VDE 0510 and DIN 43530.

- **Synthetic water**

To obtain more realistic values for the IFT a synthetic solution was fabricated. By mixing distilled water with 22.09 g/l NaCl and 1.5 g/l NaHCO₃ it represents a brine with a total salinity of around 23500 ppm.

- **Oils**

Two different oils were used with different properties but a similar TAN. They are both from different reservoirs within the same field.

Table 3-1 Oil samples properties

Oil	Crude 8	Crude 16
TAN [mg KOH/g oil]	1.96	1.56
Density @15°C [g/cm³]	0.9339	0.9104
Density @20°C [g/cm³]	0.9306	0.9070
API°	19.88	23.78

- **Alkali Agent**

Sodium Carbonate, Na₂CO₃ was used as alkali agent within a range from 3 g/l to 12 g/l, which corresponds to concentrations of 3,000 ppm up to 12,000 ppm.

- **Spinning Drop Tensiometer**

The main device used to measure the IFT is the SVT 20N from Dataphysics in combination with their SVT20 software. It consists of a measuring cell where the capillary is located which can be heated or cooled down allowing a temperature range from -30 to 180°C. The capillary can be spun up to a rotational speed of 10,000 rpm in steps of 100 rpm. Furthermore, it has a camera with an optical zoom lens which allows magnifications between 0.7 to 4.0x enabling measurements of different drop sizes. The cell has an adjustable LED-lighting system giving a broad illumination range. In Figure 3-1 the SVT 20N is shown.

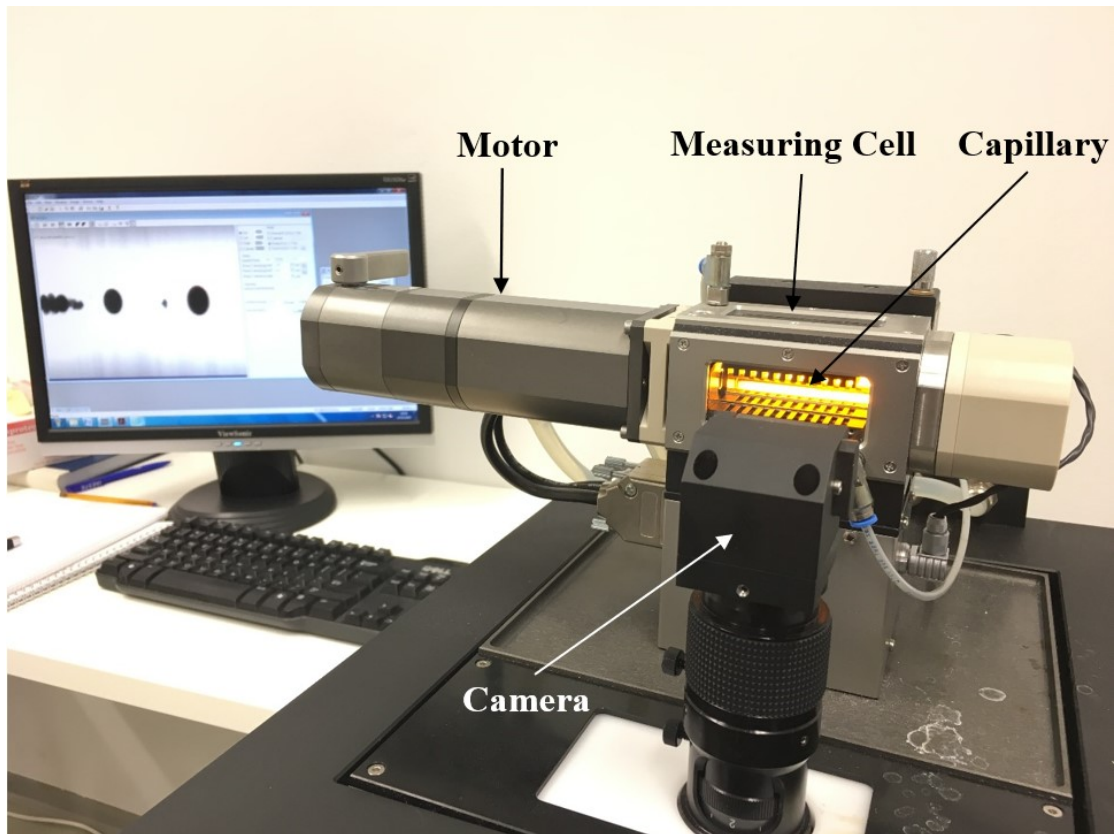


Figure 3-1 Spinning Drop Tensiometer SVT 20N set up

- **OCA 100**

Another device for measuring the IFT is the OCA 100 from Dataphysics. It consists of different dispensing units and a camera with optical zoom ranging from 1.0 x to 7.0 x of magnification. A bended needle is lowered into a cuvette filled with water or brine and droplets of oil are released, this pendant drop method is then evaluated by the included software SCA20_U.

- **Capillary tube**

During measurements the two immiscible fluids are contained within a fast exchange capillary from the type FEC 622/400-HT (see Figure 3-2), which is put inside the measuring cell. The capillary tube is able to withstand the same temperature range as the measuring device. It has an inner diameter of 4.0 mm and a visible glass window length of 50 mm.

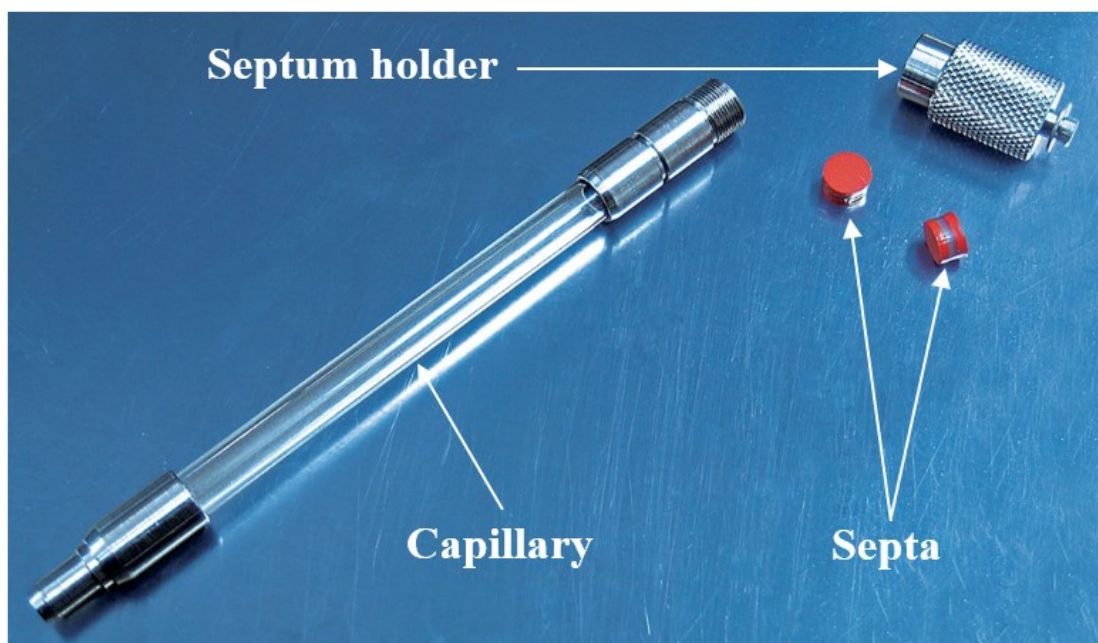


Figure 3-2 FEC 622/400-HT capillary

- **Syringe and needle**

BRAUN 1 ml single-use syringes attached with 0.80 x 120 mm needles, were used for disposing the liquids into the capillary. The needles have a sharp tip, so the septum of the capillary tube can be penetrated.

For the pendant drop measurements gas-tight Hamilton syringes (500 μ L) were used in combination with SNC 052/026 bended stainless-steel needles.

- **Glass cuvette**

The cuvette made of optical glass with dimensions of 40x40x40 mm was used for pendant drop measurements.

- **Test tubes**

For observing the phase behavior between the oils and different alkali solutions test tubes with standardized ground joints were used. Each has a scaling of 10 ml with a 0.1 ml grading.

- **Precision balance**

All weight related measurements were conducted with KERNs EW 620-3NM which has a readout of 0.001g and is of accuracy class I.

- **Chemicals**

Chemicals used for preparation of solutions and cleaning are from the company Sigma-Aldrich:

- NaCl
- NaHCO₃
- Na₂CO₃
- Acetone
- Decane ($\geq 95\%$)

3.2 Measurement Set up

3.2.1 Preparation of solutions

All solutions were prepared by weighing with the precision balance. Due to the volumetric limit of the solution containers, badges of 250 ml each were prepared.

For getting as accurate as possible volumes the density at the measured room temperature was taken to calculate the weight of 250 ml distilled water. Water density values were obtained from (Weast, 1972).

The balance was then tared, and the salts were added according to the amounts needed. Next, the solution was stirred with the help of a magnetic stirrer to make sure they are dissolved within the water.

3.2.2 Phase behavior

The test tubes have a graduation for 10 ml and were therefore filled with 5 ml solution and 5 ml oil, giving a ratio of 5:5. Since the solutions are denser than the oils, those were filled in first. To ensure a comparability the bottom of the meniscus was used as reference. After adding the oil, all test tubes were closed by their ground joints and shaken by hand before being placed into the test tube holder and left for at least 48h at room temperature.

3.2.3 Syringes

After filling the syringe with the desired liquid, it is important to make sure that no air bubbles are within the system. If any air is visible the needle is held vertical and some liquid together with the air is exerted into a paper towel. For spinning drop measurements additionally, the air needs to be squeezed out of the cannula before injecting into the system.

3.2.4 Pendant drop

3.2.4.1 Setting up the system

The set up for a pendant drop is quite plain. At first the densities of the two immiscible fluids at the present temperature need to be known. Furthermore, the outer diameter of the needle needs to be known since it is needed as reference size when measuring dimensions of the droplet. After the data is inserted into the program, the red lines need to be adjusted to the tip of the needle and below as in Figure 3-3.

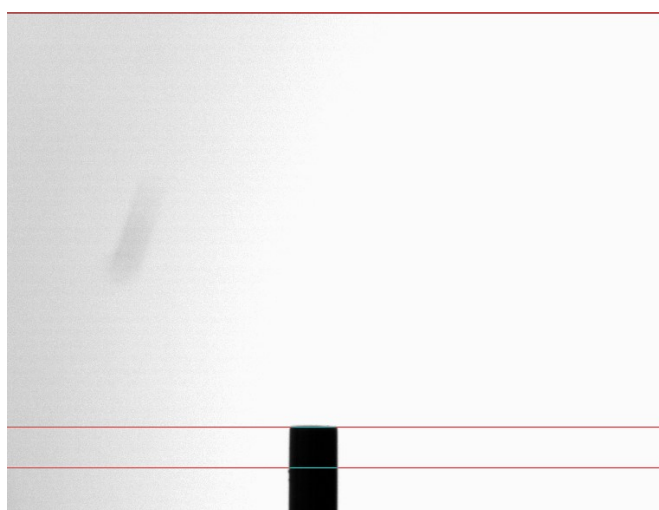


Figure 3-3 Set up for pendant drop measurement

3.2.4.2 Measurement

If the program is set up correctly the oil is dispensed and forms a droplet whose form is captured by a camera.

It is important that the cuvette is parallel to the camera to avoid any optical effects like bright refractions. To make sure to have a constant sharp image with no reflections on the droplet natural light needs to be eliminated and preferably the room light is kept on as an artificial source.

Before measuring a droplet dispense at least 2-3 droplets so any air within the needle gets pushed out. For accurate measurements the dispensed droplet should have a sufficient size, so it deviates as much as possible from a spherical shape. However, it should be noted that for small IFT values the droplet easily detaches from the needle and therefore the dispensable volume is limited.

3.2.5 Spinning Drop

3.2.5.1 Setting up the system

Differing from the pendant drop, the spinning drop has two ways of referencing the system. Option one is an inbuilt function from Dataphysics. For this a stable and clearly defined droplet is needed. The program detects the droplet and then moves the camera to the left and right, so the droplet leaves the screen. By knowing the position of the camera and where the droplet was located it can then calculate how much pixels are there per mm. Systems with emulsions in them can lead to a wobbling of the oil, therefore it is not an option for those.

Option two is the referencing via a needle. The capillary is filled with liquid and inserted into the measuring cell. A needle, whose outside diameter was measured beforehand by a caliber, is punctured into the capillary and held still. Via the camera a part of the needle, which is not sharpened is selected and the calibration window accordingly adjusted. Furthermore, the measured outside diameter need to be entered as reference size. It is important to make sure that a clear image is visible otherwise the focus needs to be adjusted. To ensure an accurate calibration the needle should be horizontal and not bended down. The downside of this option is that with the needle sizes available in the lab only calibrations for magnification between 0.7x to 2.0x are possible. Others need to be calculated by multiplying the pixel/mm of another magnification with the factor the magnifications differ from each other.

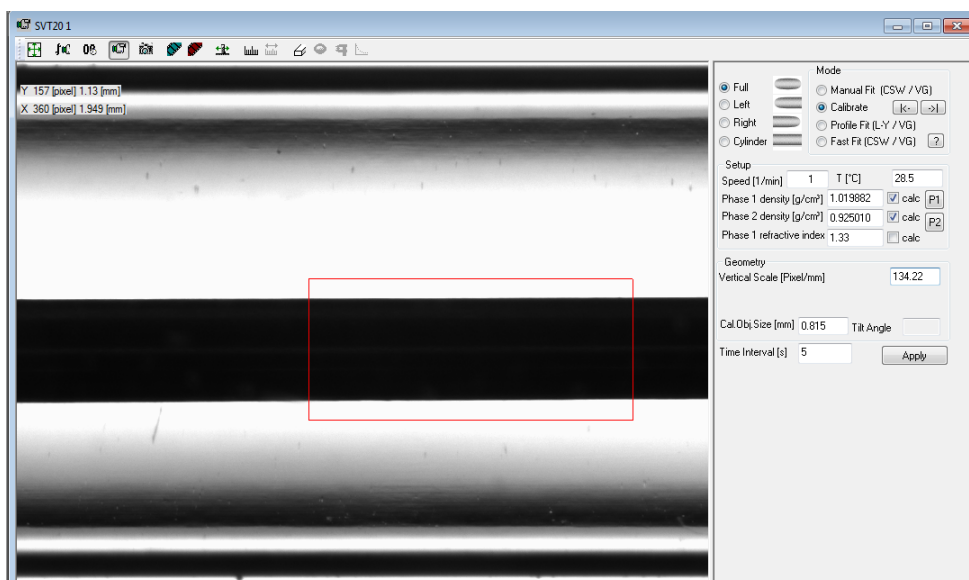


Figure 3-4 Calibration via needle for a magnification of 1.0x

Table 3-2 Calibration values for the spinning drop

Magnification	Calibration [pixel/mm]
0.7x	83.08
1.0x	134.32
2.0x	267.77
3.0x	401.66

Additionally, to calibrating the system a density input is needed. In general, the density of both fluids needs to be entered at the temperature the system is measured in. When doing temperature dependent measurements, the thermophysical properties of the liquids need to be entered into a substance window. In this substance window there is then the possibility to use different approximations to fit the data, so only a few data points are needed. Water and brine densities were taken from tables which are attached in the appendix, whereas the oil densities were calculated after Russia's GOST R 8.610-2004 standard (Gossudarstwenny Standart (GOST), 2004).

Before preparing flush the capillary at least twice with the fluid which is going to be used. This ensures the removal of any residuals of acetone from before performed procedure.

The proposed way of preparing the sample is to fill the capillary with the higher density liquid first. When filling it up a convex meniscus of the liquid needs to be on top. The septa holder is screwed on top and the excessive liquid is pushed out of a small hole, which ensures that there is no air in the system. After inserting the capillary into the measuring cell, the drop is injected via a sharpened needle which is punctured through the septum. By rotating the system with a speed of 500 rpm while injecting a contact between droplet and capillary wall is avoided. However, this way of preparation holds some downsides, especially for low to ultra-low IFT systems. One of the frequently occurring problems is the co-injecting of air which mainly comes from within the cannula. Furthermore, it is hard to exert a controlled volume, especially for high viscous oil, which is a major problem when measuring low IFTs where minimal amounts are needed.

Therefore, another way of preparing is filling two-thirds of the capillary with the denser fluid. Then a small droplet of the other fluid is set to the wall of the capillary. While holding it horizontal the rest is filled with the denser fluid until a convex meniscus can be seen. After screwing the septa holder on top the capillary is inserted into the measuring cell. Before the

start of the measurement the system needs to be rotated with very high rpms, so the liquid detaches from the capillary wall. The downside of this method is the defilement of the glass. It makes measurements in the right part more difficult as well as the detection of microemulsions, since they are hard to differ from defilements.

3.2.5.2 Measurement

When the system is set up a proper mode needs to be selected for measuring the IFT. If a single droplet is available a rectangular box is set around it and the measurement can be started. The modes Profile Fit and Fast Fit work completely automatically as long as the droplet is within the box. Manual fit is the least accurate one, since a predefined form is fitted around the droplet which is done by eye. In general, the Profile Fit mode is preferable even though it is a bit more complex than the Fast Fit mode. However, it delivers values for all three measuring methods (L-Y, CSW and VG), explained in Chapter 2.3.2, and is the most accurate one. The profile is actually fitted around the droplets outline instead of taking predefined forms. This is especially important if the shape is not axisymmetric.

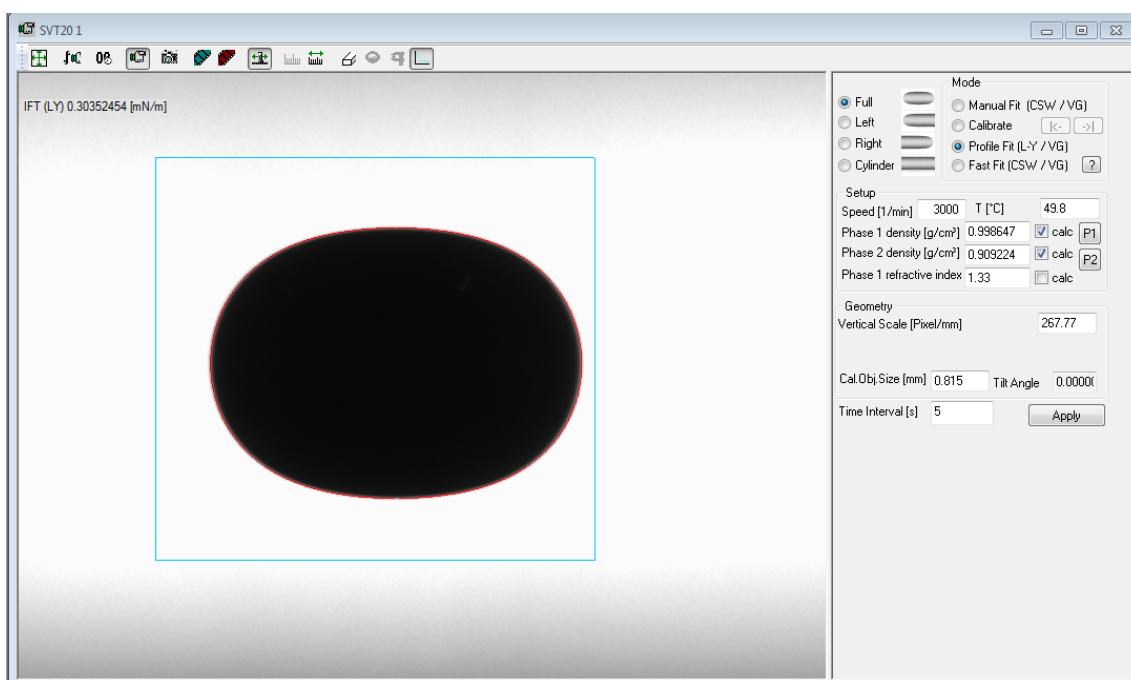
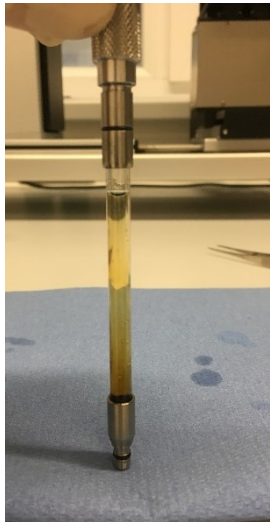


Figure 3-5 Example of a droplet within the measuring box

3.3 Cleaning Procedure

To ensure a reproducibility all capillaries were cleaned by the same procedure. First an alkene is used to dissolve the oils, which is then replaced by a ketone.

1. Fill the capillary with n-Decane (95%) at least two-third, close with septum holder then shake and flush out. Repeat.
2. Fill the capillary up to the top with n-Decane (95%) and put it into a beaker filled with water. Insert the beaker into the ultrasonic bath for 10 minutes. Flush the n-Decane (95%) out.
3. Fill the capillary with acetone at least two-third, close with septum holder then shake and flush out. Repeat.
4. Fill the capillary up to the top with acetone and put it into a beaker filled with water. Insert the beaker into the ultrasonic bath for 10 minutes. Flush the acetone out.



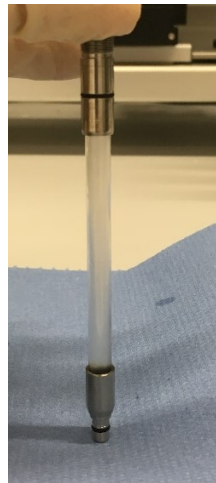
First flush with n-Decane



Second Flush with n-Decane



Beaker with capillary before ultrasonic bath



After usage of ultrasonic bath filled with n-Decane



After being flushed twice and being put into the ultrasonic bath

Figure 3-6 Cleaning steps of the capillary

Chapter 4

Experimental observations

This section of the thesis presents the observations, findings and results of the previously described IFT measurements. The start was made by phase behavior experiments to see whether a three-phase system is present or not and if a clear microemulsion phase is forming. Next, pendant drop and spinning drop experiments were executed. Former was used for referencing results from the spinning drop since it cannot handle IFTs below 1 mN/m very well.

4.1 Phase Behavior

4.1.1 Phase behavior distilled water solutions

The phase behavior for the oils with alkali distilled water solutions were prepared in a 5:5 ratio as described in chapter 3.2.2. After filling the test tubes with alkali distilled water solutions of 1,500 ppm steps starting at 3,000 ppm up to 12,000 ppm Na_2CO_3 the oil was added, and the tube shaken. In Figure 4-1 the results can be seen. Pictures were taken 48h after the test tubes were shaken and put down for settling.

The crude 8 oil has a high TAN number, therefore a strong reduction of IFT with alkali is expected, leading to pronounced emulsion formation. With increasing concentration of alkaline a distinction between phases gets less possible. Before the samples were shaken the relative volume of both phases was 50/50 in all cases. For a concentration of 3,000 ppm an oil phase and a cloudy water phase are visible. The ratio seemed to shift to a ratio of 65/35. In addition to a dulling of the water phase a change in the relative volumes can be observed, respectively to 70/30, 74/26 and 79/21 for the next three consecutive concentrations. Furthermore, a small white ring is visible between phases. Beyond a concentration of 7,500 ppm a phase distinction is not possible anymore. They look like mixtures with a grading of brown to black from bottom to the top.

The crude 16 oil has a lower TAN (1.56 mg KOH/g oil) than the crude 8 oil (1.96 mg KOH/g oil), yet it is still comparatively high. A similar trend was therefore expected. In difference to the phase behavior of the crude 8 oil two phases can be identified throughout the entire concentration range. At the first glance it can be observed that the water phase beclouds from left to right. Furthermore, it is visible that the oil phase is swollen in the range of the 4.0 ml to 4.5 ml mark. Starting at a concentration of 6,000 ppm the oil phase looks marmorated at the test tube wall with something of light brown color. Those patterns increase with the concentration. An even brighter, almost white ring can be visible at all phase borders. However, at a concentration of 7,500 ppm it is biggest and best visible.

A swelling of the oil means that there is water within the oil phase whereas in parallel the cloudy water hints that oil is within the water phase. The results seem to be a mixture of the Winsor Type I and II, which were explained in chapter 2.2. It appears that with increasing Na_2CO_3 concentration the system turns from an immiscible two-phase system into one miscible solution.

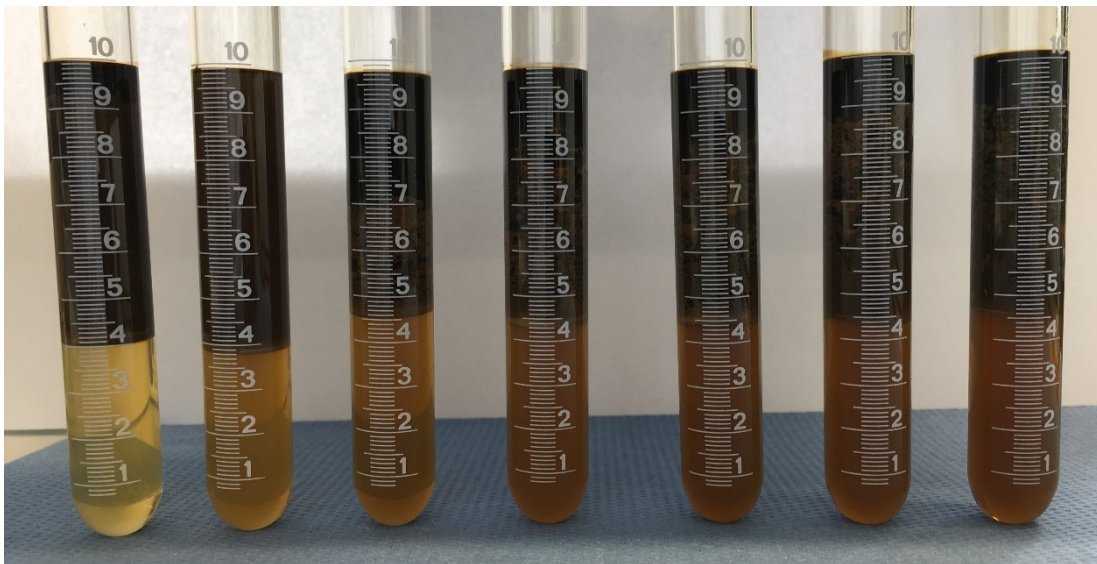
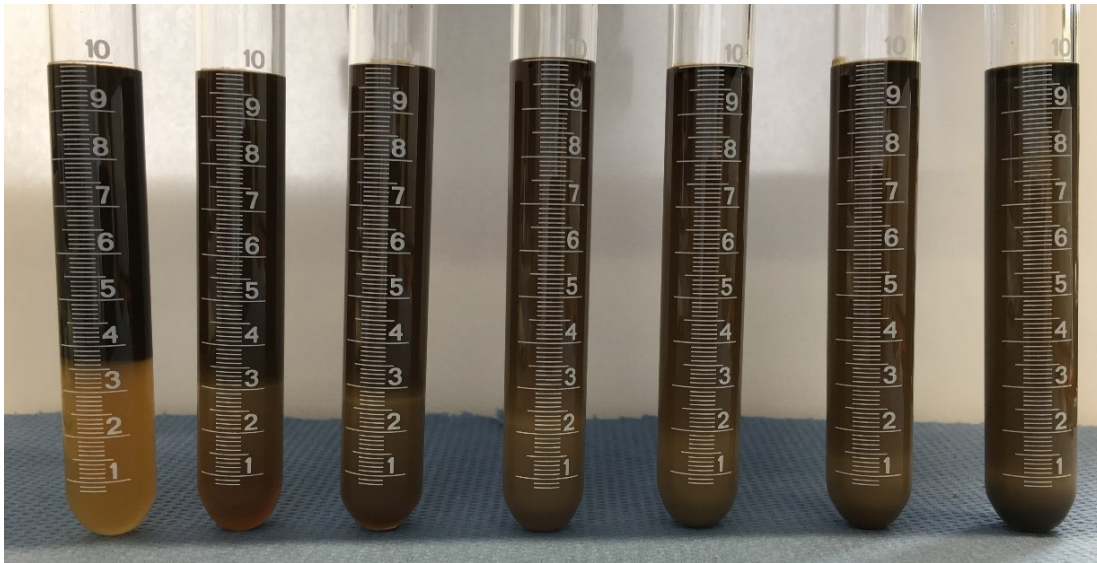


Figure 4-1 Phase behavior of crude 8 (top) and crude 16 (bottom) oil with alkali solutions prepared with distilled water (left to right: 3,000, 4,500, 6,000, 7,500, 9,000, 10,500, 12,000 ppm)

4.1.2 Phase behavior synthetic water solutions

In earlier sections it was mentioned that the phase behavior between oil and brine systems depend on the salinity therefore different results are expected. Since no optimum could be observed yet, the phase behavior was restricted to pure synthetic water, with 3000 ppm, 7500 ppm and 12000 ppm alkali solutions.

The results can be seen in Figure 4-2. In a first glance two clearly distinguishable phases are observed. In case of the crude 8 oil a slight oil swelling with increasing sodium carbonate concentration is visible. At the 3,000 ppm solution a white ring of about 1 mm formed between both phases indicating that we are closer to an optimum thus to a formation of a third phase, then for any of the other cases. In addition, emulsions can be seen in the oil phase for higher concentrations. However, those are visible by eye but do not show on the pictures. From those observations I would conclude to have Winsor II types which correlate to the literature where those are mentioned for high salinity brines.

In case of the crude 16 oil the oil swelling is even more apparent. A white ring as with the crude 8 oil did not form for any of the concentrations. The biggest oil swelling did appear for the 7,500 ppm concentration, however no clear trend is visible. All of them seem to be Winsor type II like in the crude 8 oil case. All concentrations show the formation of emulsion within the oil phase, which is not clearly visible in the picture. It is especially obvious by eye for the 3,000 and 7,500 ppm solutions. In conclusion, if there is an optimum it is probably between those concentrations. Yet it is also possible that due to the high degree of salinity no optimum is reached at all.

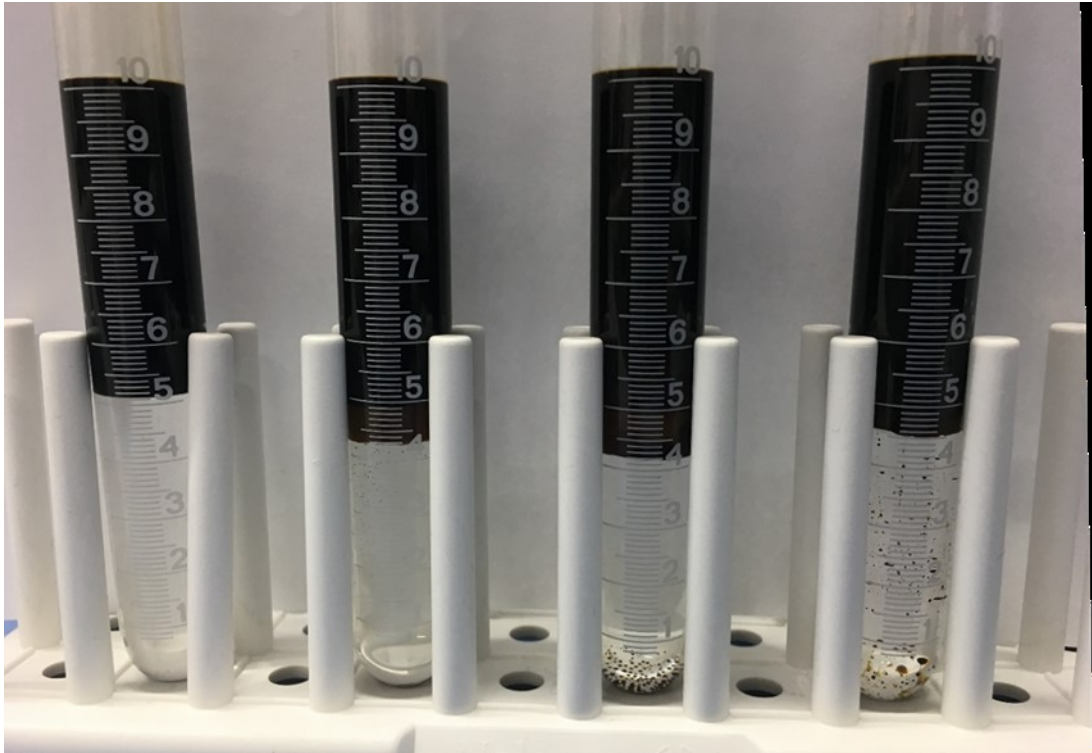
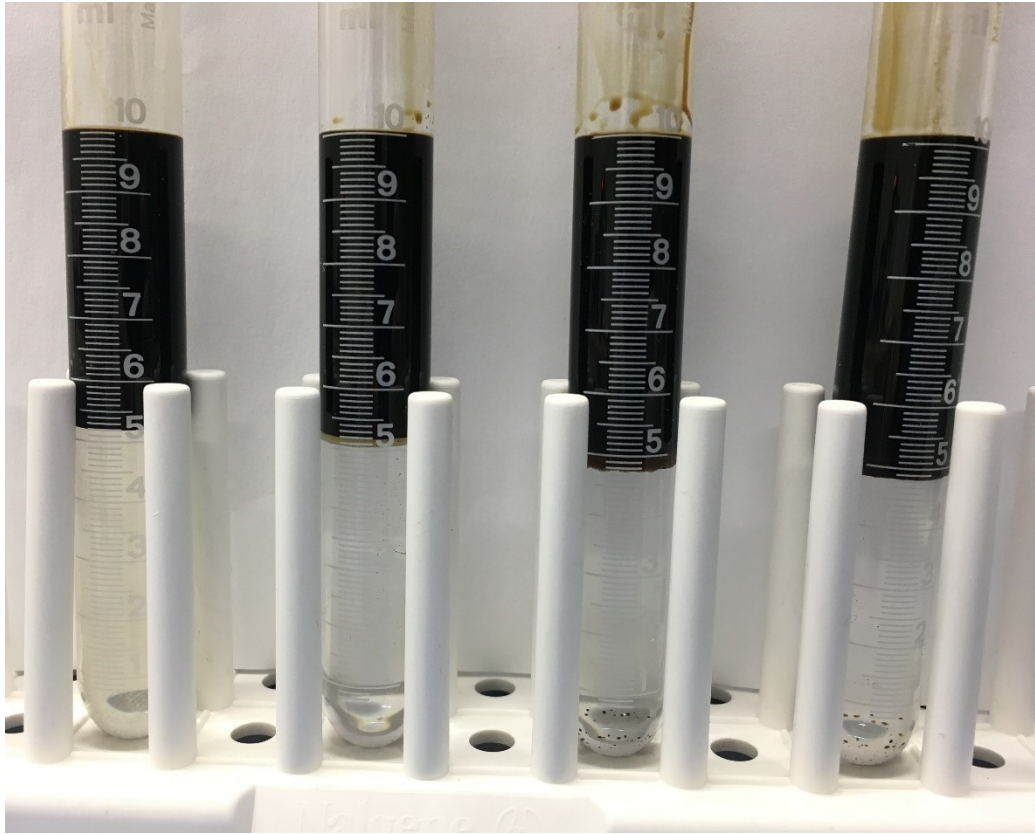


Figure 4-2 Phase behavior of crude 8 (top) and crude 16 (bottom) oil with alkali solutions prepared with synthetic water (left to right: pure synthetic water, 3,000 ppm, 7,500 ppm and 12,000 ppm)

4.2 IFT measurements

4.2.1 Pendant Drop

The bulk of experiments in this thesis were performed using the spinning drop technique. Additionally, some pendant drop experiments were performed for the purpose of having independent datasets for benchmarking. Knowing that for IFT values below 1 mN/m the possibility of obtaining measurable droplets greatly decreases measurements were performed with distilled and synthetic water without alkali. All measurements were performed at room temperature ($25^{\circ}\text{C} \pm 1^{\circ}\text{C}$).

4.2.1.1 Distilled Water

To get a general idea of the behavior of the oils within the solutions they were measured first in distilled water. In general, the idea is to dispense the maximum volume of oil so the shape deviates from a spherical one. The crude 8 oil has a much lower IFT compared to the crude 16 therefore dispensed volumes were much lower since the crude 8 kept detaching from the needle tip. Meaning crude 8 oil drop volumes are around 1.5 μL as for crude 16 oil they are around 17 μL .

As soon as the desired volume was dispensed the measurement started. IFT values were measured every 5 seconds for at least 1.5 hours. The time was mainly limited by the detaching of the crude 8 oil from the needle. In Figure 4-3 the results can be seen. Both oils show a similar trend of exponential IFT decay right after being dispensed. After an initial strong decline, the curves start to flatten out.

The obtained values after 100 minutes are around 1 mN/m and 16 mN/m for both oils respectively as seen in Figure 4-3. IFT values for the crude 16 oil still slightly decreased and had not leveled yet. Therefore, the measurement was continued for another 5h until the IFT did not change any further, resulting in an IFT value of 15.2 mN/m.

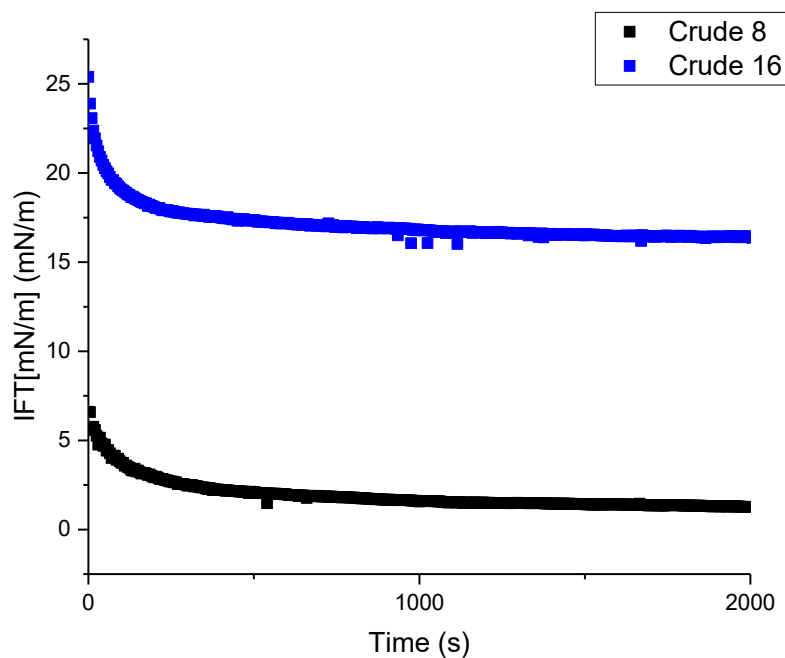


Figure 4-3 IFT vs. time of crude 8 and crude 16 oil in distilled water via pendant drop

4.2.1.2 Synthetic water

The same measurements were repeated in synthetic water. Measuring values in synthetic water was only possible for the crude 16 oil since the crude 8 would detach from the needle within a minute. IFT values decreased greatly within seconds and even when dispensing volumes below 1 μL it was not possible that a droplet formed which stayed attached to the tip of the needle, therefore no reliable IFT reading could be obtained for the crude 8 oil. Compared to that did the IFT of the crude 16 drop by almost one order of magnitude. It was possible to have readings for around an hour until the droplet also detached from the needle tip. The results can be seen in Figure 4-4.

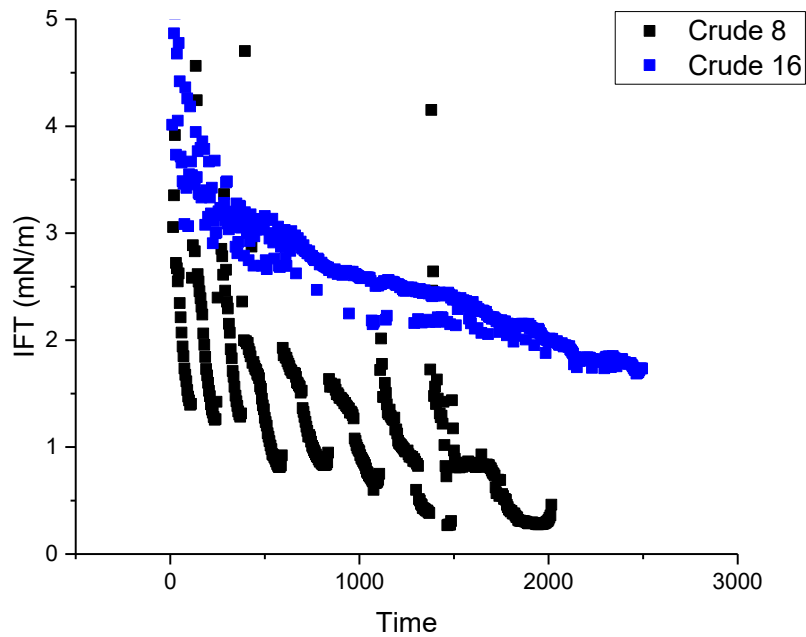


Figure 4-4 IFT vs. time of crude 8 and crude 16 oil in synthetic water via pendant drop

Not only did the readings drop, but also the volume dispensable went down to 1.5 μl and lower. This can be seen in the results which scatter a lot more. Furthermore, the change over time is much higher, even though the initial decline is not as high as for the synthetic water. The IFT values were still decreasing when the droplet detached, therefore it can be assumed that the actual IFT readings are much lower.

4.2.1.3 Alkali solutions

As mentioned before are IFT readings below 1 mN/m not measurable. When adding the alkali agent to the waters it is expected that the IFT values decrease significantly. Therefore, no droplets are forming making it impossible to make any further measurements with the pendant drop. Those presumption were verified when trying to measure the IFT within a distilled water 3,000 ppm solution. The result of this attempt can be seen in Figure 4-5.

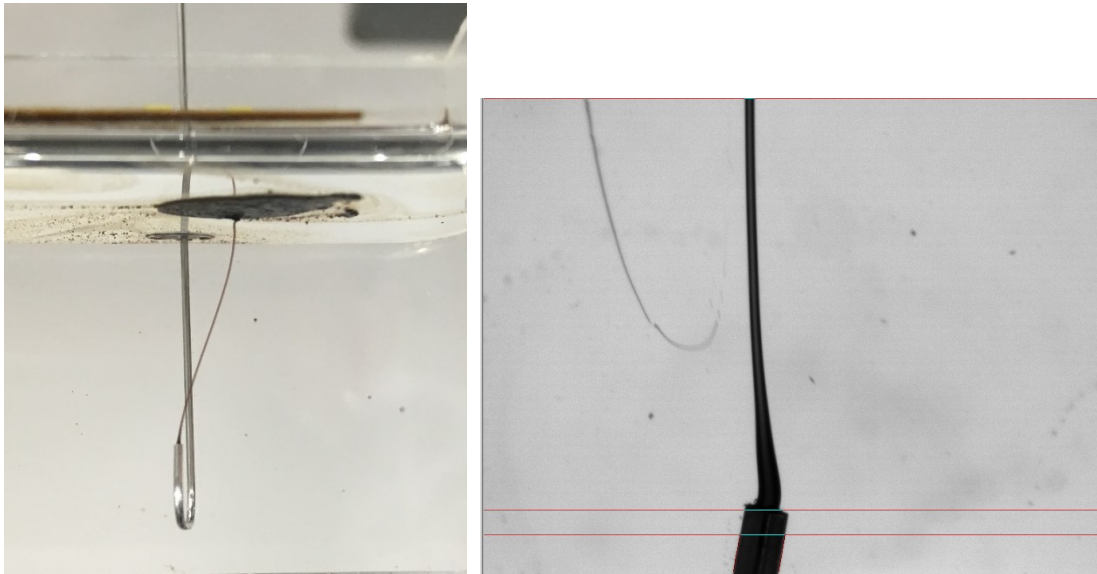


Figure 4-5 No droplet formation of crude 8 oil in distilled water with 3,000 ppm Na_2CO_3 (left: picture of needle inside cuvette; right: picture within the software)

4.2.2 Spinning Drop

Spinning drop measurements are a bit more complex compared to pendant drop measurements. This is due to the fact that there are a lot more parameters which need to be considered when measuring. First of all, there are different drop types and calculations methods, an overview can be seen in Figure 4-6. In addition, can the rotation speed be adjusted in steps of 100 rpm up to a speed of 10,000 rpm. Furthermore, the temperature can be controlled with accuracies of $\pm 0.1^\circ\text{C}$ enabling measurements up to 50°C . Every experiment was started at 20°C since the oils densities are explicitly known for this temperature. Furthermore, the effect of alkali concentrations on the IFT was measured at that temperature. Later thermal dependency was investigated as well.





Table of available calculation methods				
		Vonnegut (VG)	Cayias Schechter Wade (CSW)	Laplace Young (LY)
Drop Type	Profile Mode			
	Manual + Fast Mode			
		YES	YES	YES
		YES	YES	YES
	YES	YES	YES	
	YES	NO	NO	

Figure 4-6 Overview of drop types and calculation methods

4.2.2.1 Drop type comparison

As shown in Figure 4-6 there are four drop types which can be measured. Neglecting the cylinder type, where only calculations after Vonnegut are possible a comparison between the other three was necessary. To identify which one is the most accurate one, each side and the entire droplet was measured over 10 minutes each. Obtained values were statistically analyzed by calculating the median and standard deviation for each drop type. The results are plotted in Figure 4-7.

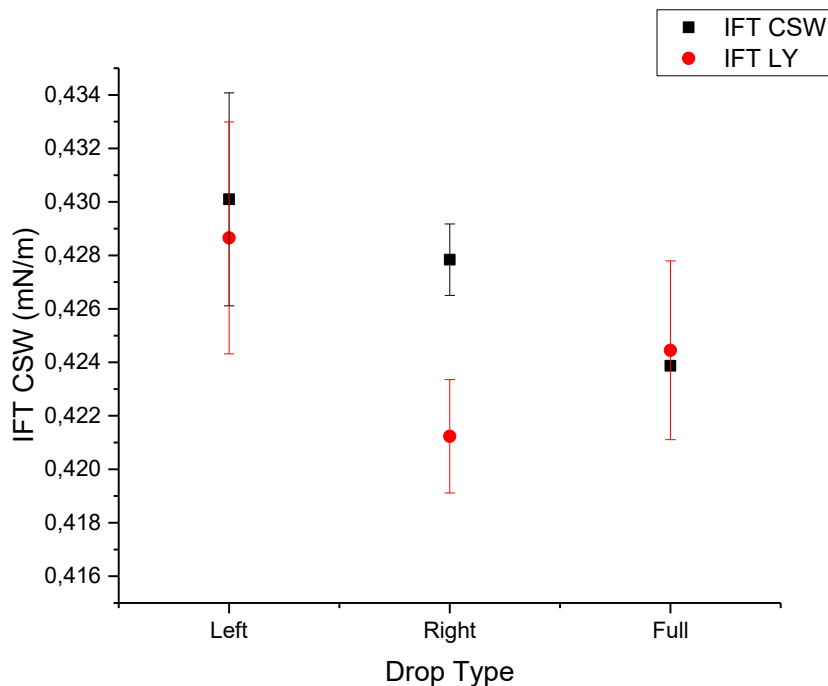


Figure 4-7 Drop Type comparison with standard deviation

Since the object of this thesis is the measurement of ultra-low IFTs a stable droplet with relatively low IFT was taken, to get a sense which drop type measurement should be taken for further experiments. Crude 16 oil in synthetic water seemed with an IFT reading below 0.5 mN/m suitable for that.

Looking at the calculation method CSW it can be seen that left and right type have a much higher standard deviation. The error bar for the full droplet is not even shown since it is so small, meaning that readings obtained by the full type method are the most constant ones. However, in general it can be said that all three types are very constant considering the error being below 1%. Furthermore, it can be seen that the CSW calculation method is more accurate

and delivers less deviation. Therefore, when possible, all further measurements were performed using the entire drop and the calculation method CSW.

4.2.2.2 Calculation method

In chapter 2.3.2 the theory behind the different calculation methods was thoroughly discussed. The drop type IFT value comparison, seen in Figure 4-8, supports the claim that the CSW method is the most accurate one. Therefore, are the other calculating methods referenced to it. Furthermore, the VG methods inaccuracy regarding the horizontal to vertical ratio was investigated.

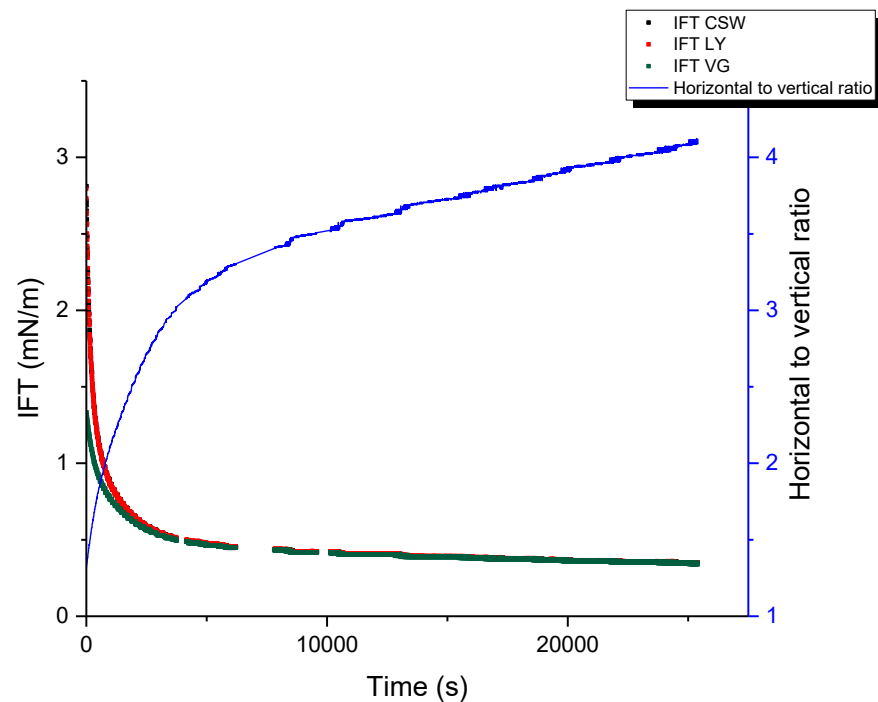


Figure 4-8 IFT of all three calculation methods vs. time with horizontal to vertical ratio

The IFT readings difference between the calculation methods decreases with an increasing horizontal to vertical ratio. It is also proven that Vonneguts method works very accurately when the ratio is above 3.5 which can be seen in Figure 4-9. As expected do both LY and CSW method give good readings. This was expected since the droplets shape deviates from a spherical one which is shown by the ratio which is above one.

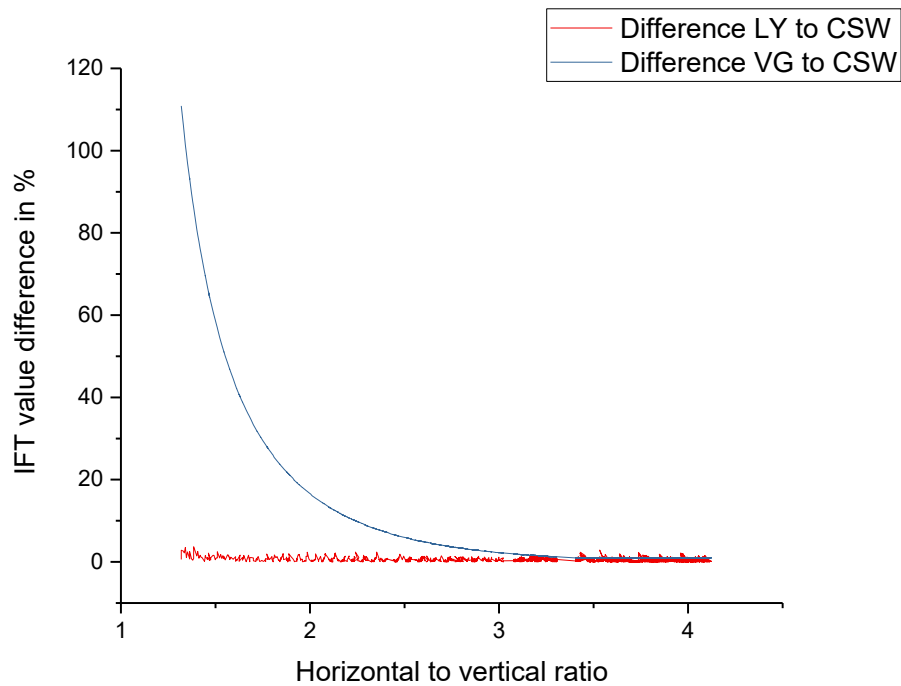


Figure 4-9 Measured IFT difference to the ratio of the drop

However, when the droplets horizontal to vertical ratio is one the LY calculation method does not work anymore because it cannot fit the outline of the drop. Therefore, obtained values are extremely scattered without any clear trend. The CSW method on the other hand delivers some evident values, which can be seen in Figure 4-10. It seems like the reading can be between 0.16 and 0.36 mN/m, which depends on the horizontal to vertical ratio. Since each run is a measurement every 5 seconds the ratio solely depends on what the program defines as the outline of the drop, since the values obtained are within a constant range.

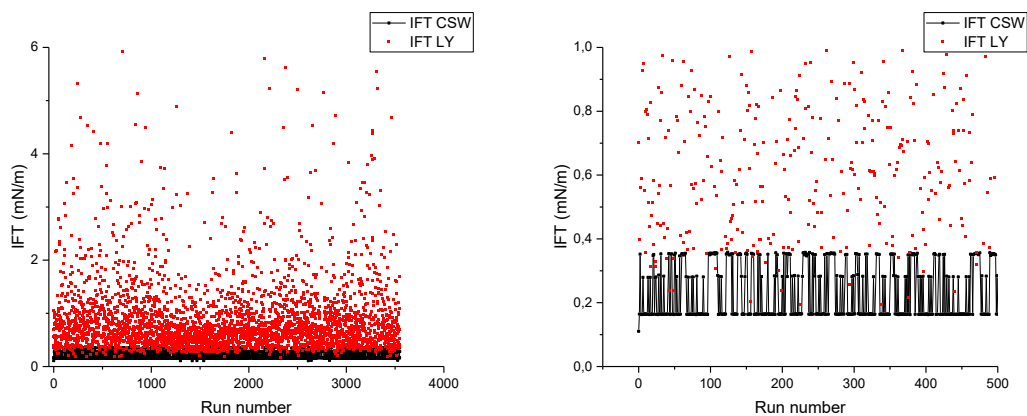


Figure 4-10 Measured IFT values with LY and CSW method for a droplet with a ratio of 1.01

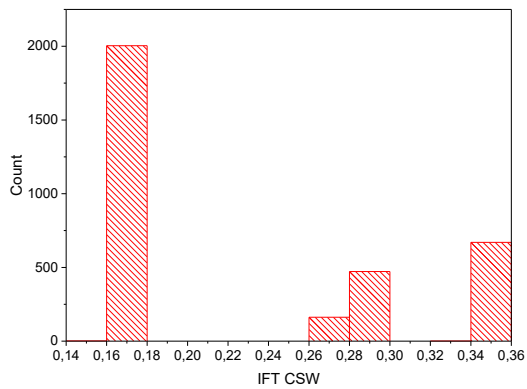


Figure 4-11 Histogram of IFT values for almost spherical drop

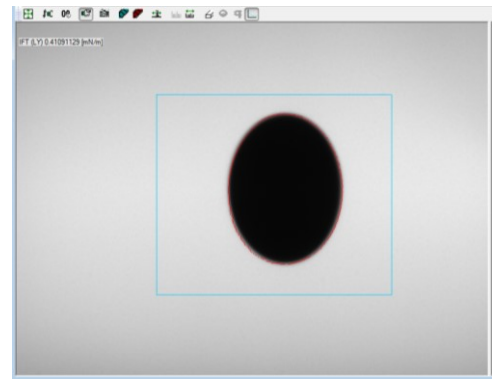


Figure 4-12 Almost spherical drop view via software

The histogram (Figure 4-11) shows that the most frequent obtained values are between 0.16 and 0.18 mN/m. As a result, when having constant oscillating readings, a distribution fit should be done.

In general, it was shown that the CSW calculation method is the only one which can be taken for spherical as well as an ellipsoidal shape. Therefore, all further experiments were conducted using it.

4.2.2.3 Rotational speed

One of the parameter influencing the measurement is the rotational speed. In general, increasing rpms stabilize the droplet since the gravitational forces acting on it increase as well. This statement holds for big droplets as well as for systems with IFT values above the order of 10^{-1} mN/m. However, it is not valid anymore when microemulsions are present and the IFT reduces to very low values. One thing is that due to high rotational speeds, the droplet elongates to a point where it is touching both sides of the capillary, making the measurement unreliable. Since the volume dosage of the oil is rather tricky it is a reoccurring problem. The dependency on rotational speeds was measured after the system equilibrated, therefore it was started after 12,500 seconds.

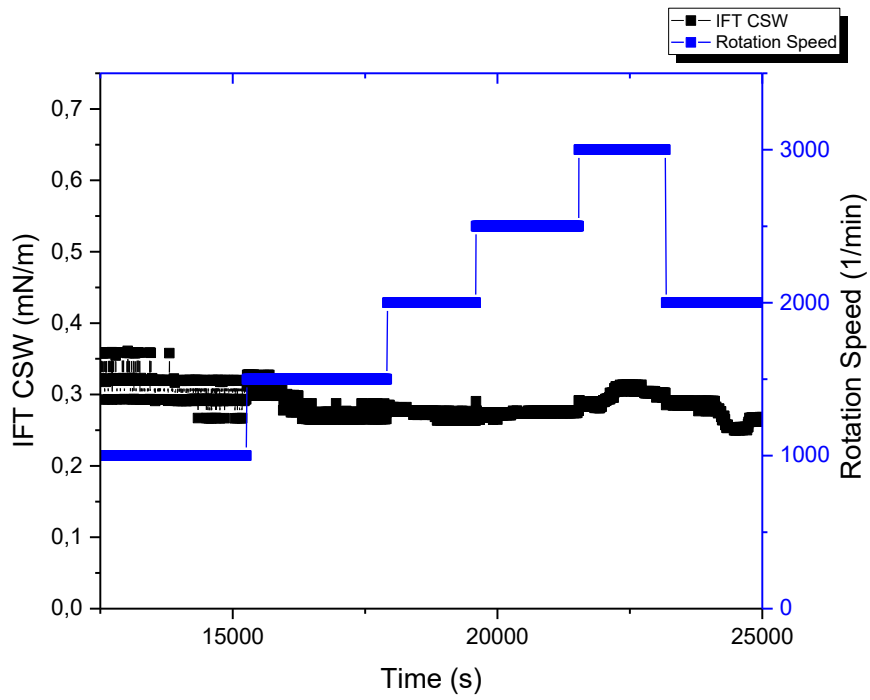


Figure 4-13 IFT dependency on rotational speed

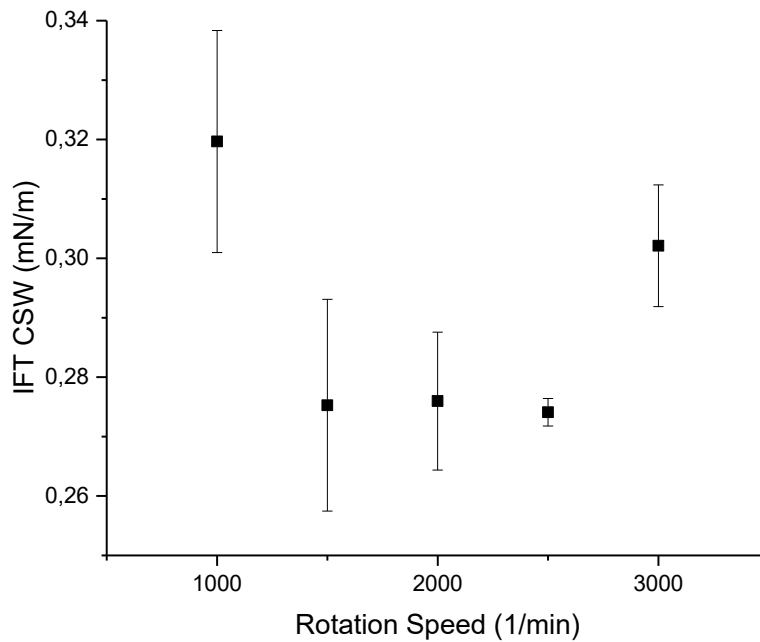


Figure 4-14 IFT median with standard deviation depending on rotational speed

From the Figure 4-13 and Figure 4-14 it can be seen that with higher rpms the obtained IFT values have less deviation. However, the differences are not very high. Therefore, it is also interesting to take the minimum and maximum values into account. Those show that for higher rpms the difference between the extremes is much less compared to those at lower speeds.

Table 4-1 Statistics for rotational speed dependency

Rotational Speed [1/min]	Minimum [mN/m]	Median [mN/m]	Maximum [mN/m]	Standard Deviation [mN/m]
1000	0,26653	0,31966	0,36118	0,01868
1500	0,26528	0,27528	0,32755	0,01782
2000	0,24965	0,27598	0,29092	0,01161
2500	0,26472	0,27411	0,29057	0,00232
3000	0,28107	0,30212	0,31352	0,01024

Therefore, if possible measurements were executed with rotational speeds of 3,000 rpm. For measurements of ultralow IFTs a rotational speed of at least 1,000 rpm is sought.

4.2.3 Distilled water

In chapter 4.2.1 we obtained already first IFT values for the two oils. It also showed that a certain amount of time will be necessary until the system equilibrates. Therefore, an IFT change over time is expected. Furthermore, the expected readings are different since the ambient temperature at which the experiments were conducted are different.

The IFT readings, seen in Figure 4-15, show a similar trend like they did for the pendant drop. However, it drops even further down than it did for the pendant drop. Furthermore, much longer measurements are possible since the drop cannot disappear like it does when detaching from the tip of the needle. The gap at around 8,000 seconds is because the drop moved out of the measuring box and the automatic drop tracking from the software did not readjust accordingly. Thus, manual adjustments needed to be done which sometimes can take a while. Yet there still is a clear trend reducing the influence of that measurement gap. Since the crude 8 oil drop is very stable within distilled water rotational speed was set to 3,000 rpm. The obtained IFT after around 7h was 0.35 mN/m.

Pictures of the droplets, which are shown in Figure 4-16, were taken at the end of the measurements, this also holds for the next chapters unless otherwise stated.

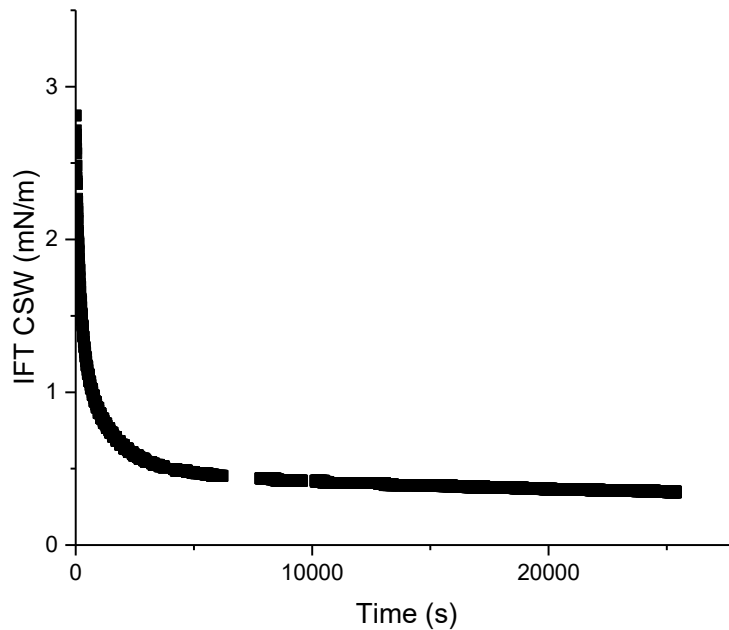


Figure 4-15 IFT vs. time of crude 8 oil in distilled water via spinning drop

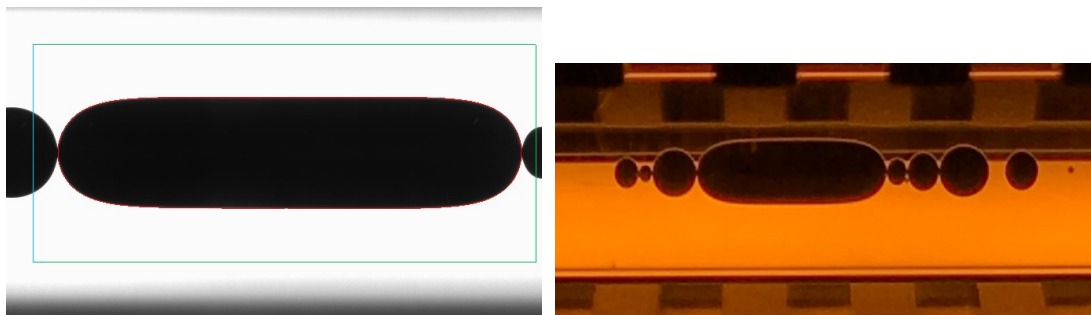


Figure 4-16 Crude 8 oil in distilled water

When measuring the crude 16 oil with distilled water via pendant drop we obtained good measurements in the sense of a droplet which stayed attached to the needle. Therefore, a reference value with 15.2 mN/m is given. This value was obtained after 5h of measuring meaning it had a long equilibration time. In case of the spinning drop it did equilibrate much faster as seen in Figure 4-17. IFT readings of 12.5 mN/m were reached after a little bit more than 1h. Even though the volume of the droplet is with $\sim 23 \mu\text{L}$ higher than for the pendant drop it actually took less time to equilibrate. Comparing with the crude 8 it was also much faster. When observing the drop shape, which is shown in Figure 4-18, the higher IFT displays with the drop having a lower horizontal to vertical ratio.

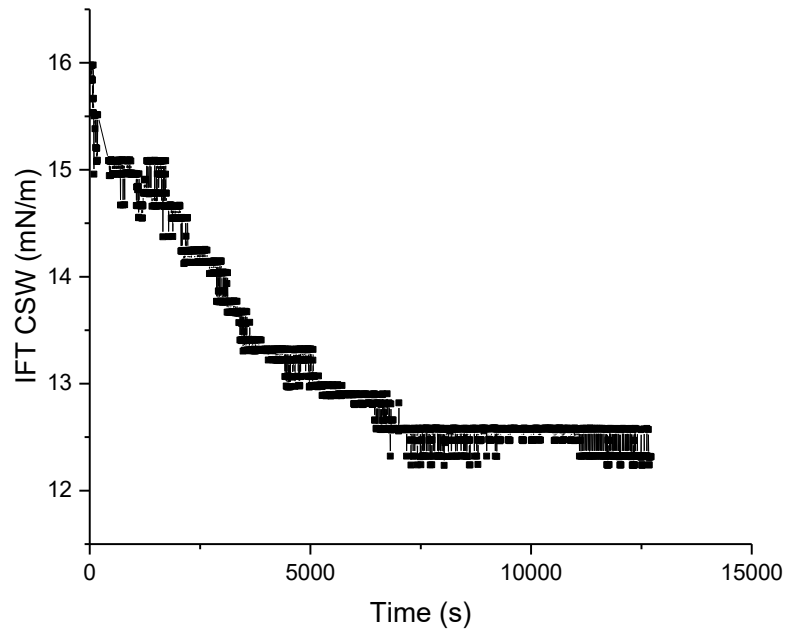


Figure 4-17 IFT vs. time of crude 16 oil in distilled water via spinning drop

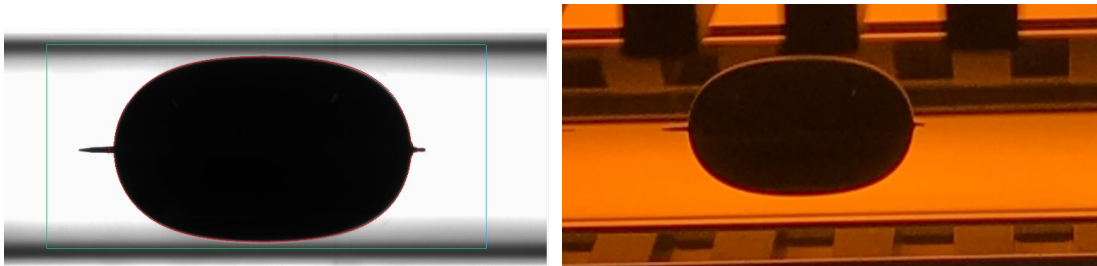


Figure 4-18 Crude 16 oil in distilled water

4.2.4 Synthetic water

Since it was not possible to obtain values from the pendant drop method it was already expected that either very long ellipsoidal droplets form or many small ones. Droplets which have a high horizontal extend can only be measured at the sides or somewhere in between by applying the VG's calculation method on cylindrical shapes.

After starting the experiment with the crude 8, the made presumptions confirmed, one big elongated drop and two smaller droplets formed. Since the smaller droplets could be measured in their entirety they were used for obtaining IFT values. A slow increase in IFT can be observed until the values stabilized around 0.0325. Yet it could be observed that the distance between the droplets reduced over time. After around 2,000s after the start of the experiment the first smaller droplet conjoined with the bigger one and after another 700s the droplet used for

obtaining IFT values got observed as well. In Figure 4-19 this event can be seen by the switch of the measuring method from full drop to left side measurement. After the system stabilized it can be seen that the obtained values are the same as before the conjoining of the drops.

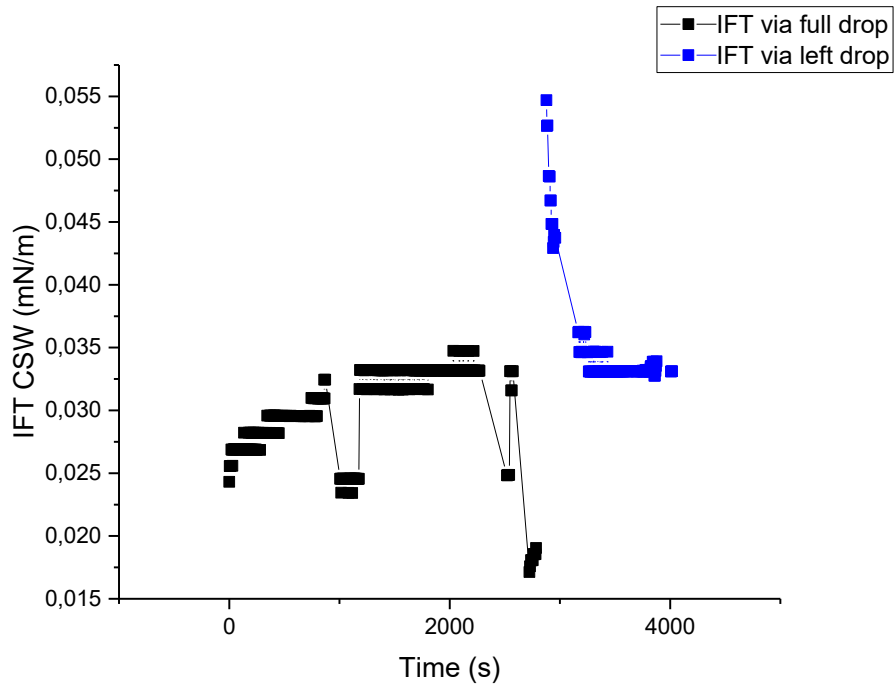


Figure 4-19 IFT vs. time of crude 8 oil in synthetic water

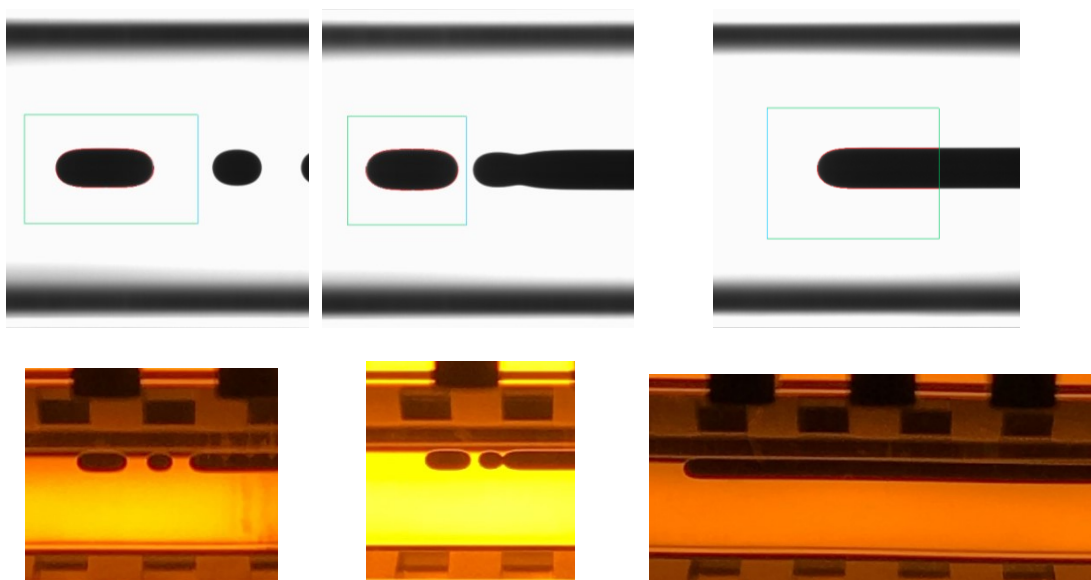


Figure 4-20 Crude 8 oil in synthetic water over time

For the crude 16 oil a droplet formation similar to that of crude 8 oil in distilled water was expected. From the pendant drop results it is known that the IFT value is around 1 mN/m which means stable drops should form.

After the measurement started those assumptions proved to be right because multiple bigger droplets formed. The biggest one was then taken for obtaining readings, which are plotted versus time in Figure 4-21. Even though the drop was very stable the measured values oscillate quite a lot. Anyhow this is due to the low horizontal to vertical ratio of around 1.1, which influence on the measurement accuracy was discussed earlier. The droplets form, which is close to being spherical can be seen in Figure 4-22. When looking at the distribution in between the time range of 13,200s to 26,400s, it shows that the obtained IFT value is 1.49 mN/m.

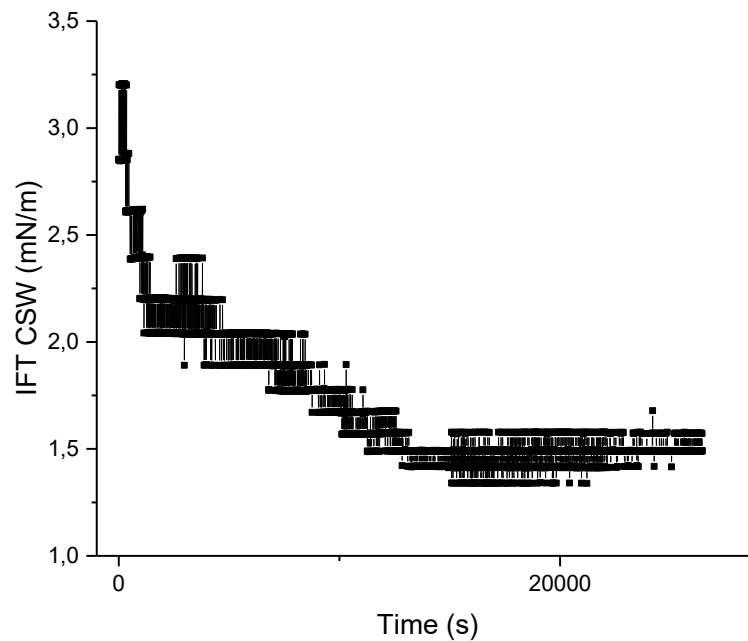


Figure 4-21 IFT vs. time of crude 16 oil in synthetic water

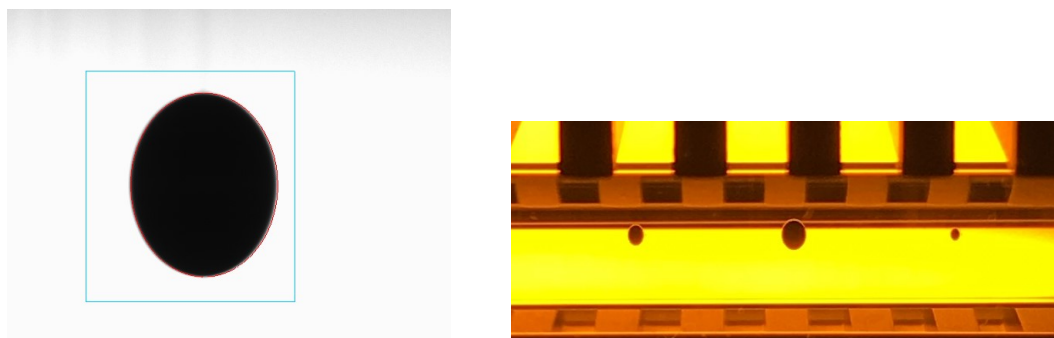


Figure 4-22 Crude 16 oil in synthetic water

4.2.5 Alkali solutions

Measurements of the oils in different alkali concentration solutions are much more complex compared to in distilled water. One of the main reasons is the formation of emulsions furthermore are the expected IFT readings much lower than those obtained yet. Earlier experiments showed that smaller droplets are harder to measure, especially focusing them. All experiments were firstly conducted under the same ambient conditions.

Early experiments showed that if too much oil is present a single elongated oil phase is forming which touched both sides of the capillary making the experiment unreliable. Especially since the sides of the capillary are not visible making it impossible to judge whether oil accumulates at those ends or not. Furthermore, only a measurement via VG is possible whose values highly depend where the oil is measured since the vertical extend is different along the capillary. The amount of oil injected in Figure 4-23 is the same as when measuring a single droplet in distilled water. However, due to oil swelling and the reduction of IFT to very low values it extends.



Figure 4-23 Example of oil touching both sides of the capillary

Alkali concentration measurements were conducted for three different concentrations to see if there is an obvious trend. By taking 3,000, 7,500 and 12,000 ppm concentrations the extremes as well as the mean of them is covered. The ambient temperature for those experiments was 20°C.

4.2.5.1 Crude 8 oil in alkali solutions with distilled water

The start was done with 3,000 ppm Na_2CO_3 prepared with distilled water. From the phase behavior we know that two phases are still visible and that we are not within an optimum, therefore a thermodynamic stable microemulsion is not expected. However, since we have a Winsor Type III microemulsions within the oil phase are expected which reduce the IFT.

The experiment was started at very low rotational speeds since the entire system was not very stable. A steady increase from ultralow IFT values of $2.5 \cdot 10^{-4}$ mN/m to 0.015 mN/m could be observed (see Figure 4-24). Especially the drop shape changed from an elongated to spherical drop, as seen in Figure 4-25, leading to a fluctuation of the obtained values. In addition to that did the droplet become more unstable. As a result, the rpms were increased. It can be seen that it leads to even more fluctuation of obtained readings. Since the drops shape kept changing it

was decided to the system for a longer time at 1,500 rpm to make sure the system equilibrated. After that the speed was increased slowly to the desired 3,000 rpm leading to more stable readings. In addition, does it lead to drop shape change towards a spherical drop. The obtained values at 3,000 rpm are around 0.065 mN/m.

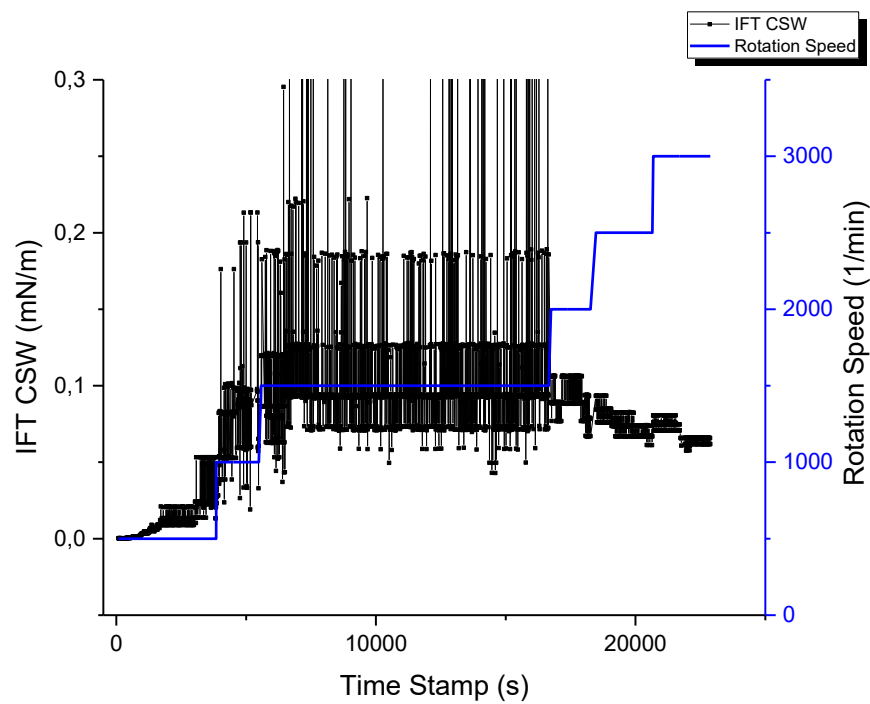


Figure 4-24 IFT vs. time of crude 8 oil in 3,000 ppm distilled water solution

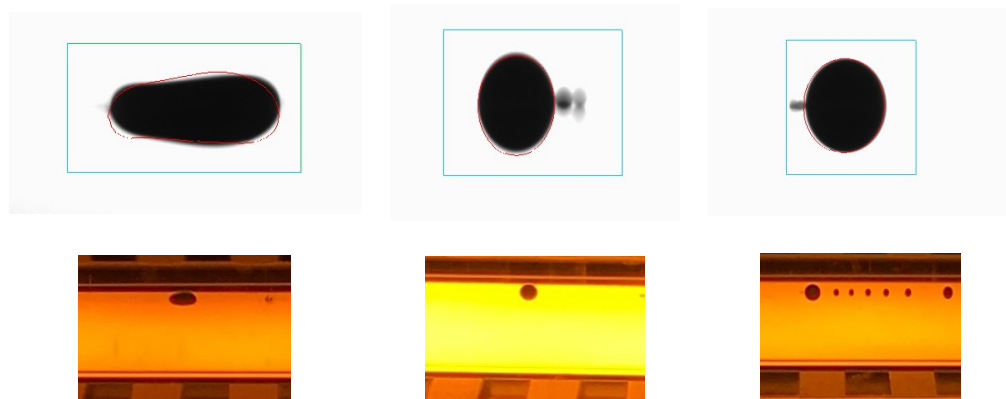


Figure 4-25 Crude 8 oil in 3,000 ppm distilled water solution over time (left to right: 274 s, 6450 s, 20600 s)

Next was the 7,500 ppm concentration. From the phase behavior it is expected that even more emulsions are forming. The measurements were performed in the same way as for the 3,000 ppm. However, from the start emulsions could be seen which were attached to the oil droplets. They were detectable within the software as well as by the eye. In general, the droplets which

formed were much more stable from the start than those measured before. On the other hand, it could also be observed that a group of many small droplets attached next to each other forming an accumulation. In Figure 4-27, this can be observed at the first two photos taken by camera. The accumulations are between the two bigger droplets. Those were wobbling a lot, especially since they seem to be attached to the end of the milky stuff, which for now is assumed as an emulsion. The emulsion accumulated between both bigger droplets and was in constant change. Within the emulsion droplets formed after a while, some of them combined with the bigger droplets. A similar IFT value trend as for the 3,000 ppm measurement can be seen. At the beginning the obtained values are very low starting at 0.0059 mN/m which raised within minutes to values of 0.065 mN/m. After around 1,500 second the speed was increased to 1,000 rpm which lead to a very interesting behavior of the oil drop.

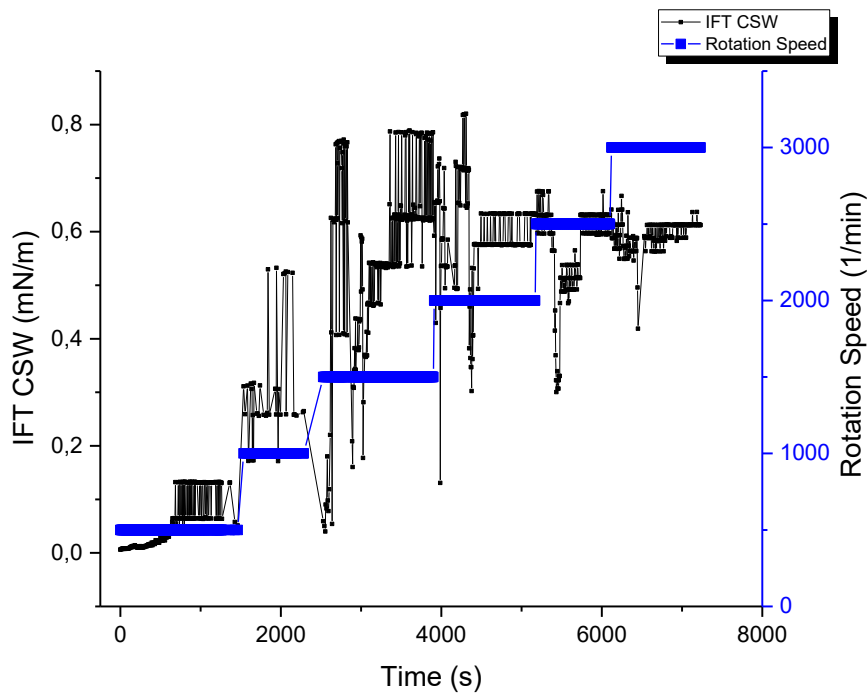


Figure 4-26 IFT vs. time of crude 8 oil in 7,500 ppm distilled water solution

The drop detached from the emulsion and immediately moved to the left. In addition, no emulsion close to the drop was visible anymore. This lead to a strong increase in IFT. At the end values which represent the IFT between crude 8 oil and distilled water ($\gamma_{o-dw} \sim 0.35$ mN/m) were reached. It seems that too high rpms lead to a separation of oil and emulsion. In Figure 4-27 it can be seen more clearly. Furthermore, the other oil drops did conjoin into one big droplet. Even before increasing the speed the drop was moving towards the right end of the

capillary consequently it was necessary to tilt the measuring cell. However, it is interesting that with increasing speed and the separation also the attraction of the drop towards the capillary sides reversed which means a tilt into the other direction was needed. This can be seen in the last two photos of Figure 4-27.

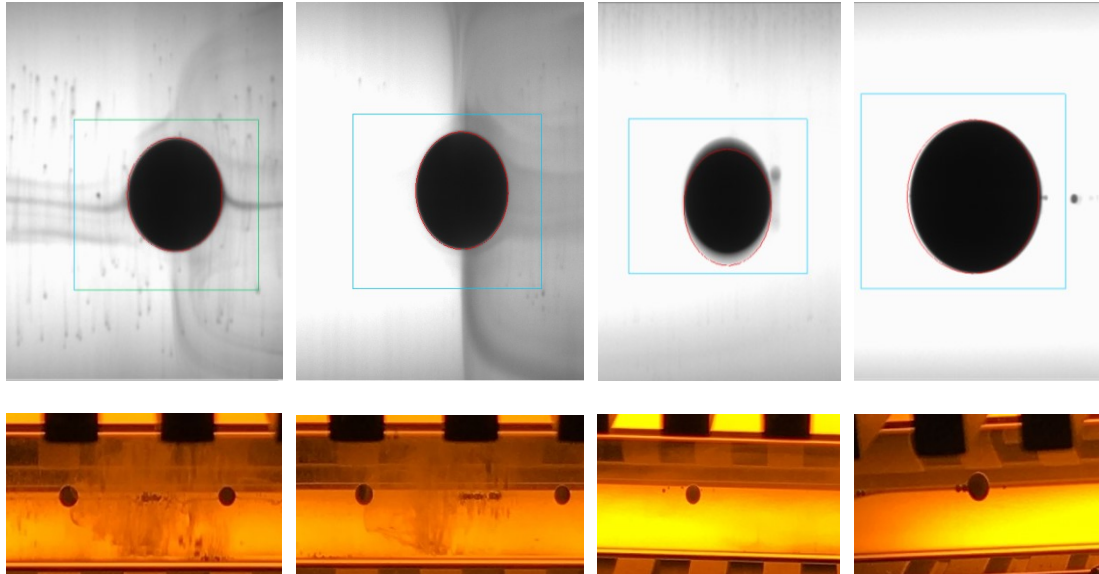


Figure 4-27 Crude 8 oil in 7,500 ppm distilled water solution over time (left to right: 10 s, 380 s, 1730 s, 6300 s)

Since the obtained values were close to those within pure distilled water, the rotational speed was decreased to 500 rpm at 700 seconds to see whether the emulsion would attach to the droplet again. The IFT values dropped immediately after the rpm reduction, but it took quite a while time until stable low values were reached again. Yet this shows that somehow the system equilibrium changed. In Figure 4-29 the reattachment of the emulsion can be seen. Values obtained are around 0.1 mN/m.

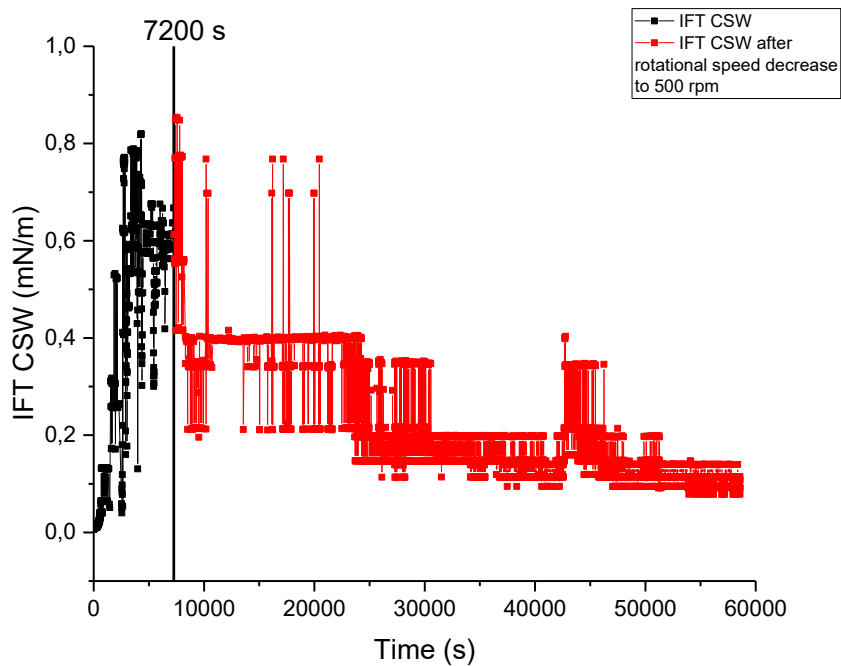


Figure 4-28 IFT vs. time of crude 8 oil in 7,500 ppm distilled water solution with rpm decrease

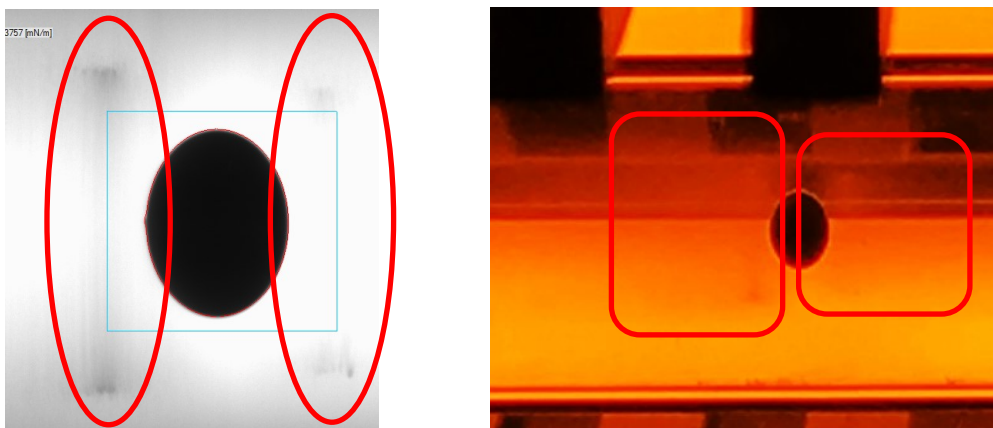


Figure 4-29 Crude 8 oil in 7,500 ppm distilled water solution after emulsion reattached

From the phase behavior experiments we know that emulsions will form. Therefore, similar results like in the previous cases are expected. At the beginning many droplets of different sizes formed. In between the bigger drops many small ones accumulated next to each other appearing as one small line. As predicted emulsions formed between the droplets. After a while they were only barely visible and instead small satellites formed next to the drops. This is also visible in the IFT vs. time readings which are at the beginning not very stable and in the order of 10^{-2} mN/m. However, after the seemingly visible emulsions vanished and the smaller satellites

appeared the IFT instantaneously jumped up by one order of magnitude and more steady readings were obtained.

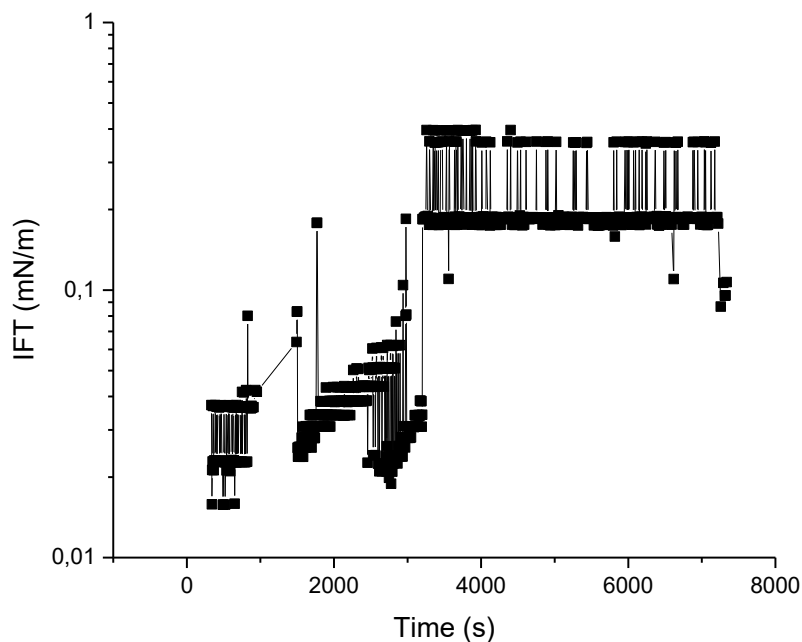


Figure 4-30 IFT vs. time of crude 8 oil in 12,000 ppm alkali distilled water solution

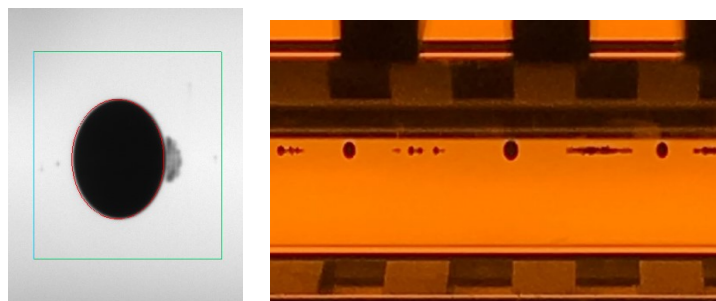


Figure 4-31 Crude 8 oil in 12000 ppm distilled water solution

With changing alkali concentration no clear trend was yet monitored. In case of the 7,500 ppm solution the most emulsions were visible, however did it not lead to a significant difference in the obtained IFT values.

4.2.5.2 Crude 16 oil in alkali solutions with distilled water

From previous experiments as well as the phase behavior experiments it was expected that emulsions will form. Especially the phase behaviors of both oils look similar for the low concentration. The experiments were conducted the same way as those for the crude 8 oil.

Unlike in the crude 8 case right from the start stable droplets formed for the 3,000 ppm distilled water solution. In addition, to that emulsions are clearly visible. At the beginning the biggest droplet was measured. After stable values were obtained over a longer period of time, a smaller one was measured, which was engulfed in emulsions. The obtained readings differ by one order of magnitude, which can be seen in Figure 4-32 as opaque squares. The experiment was then repeated, and measured data was added in the graph as small transparent triangles. Though the droplets volume was slightly higher in the second experiment, are the obtained values closer to those of the smaller drop in the first experiment. In Figure 4-33 and Figure 4-34 the droplets of both experiments can be seen. For the second experiment only, the bigger droplet could be measured.

However, in both cases it can be seen that the shape ratio is below one, which gives rise to the question whether the values are reliable.

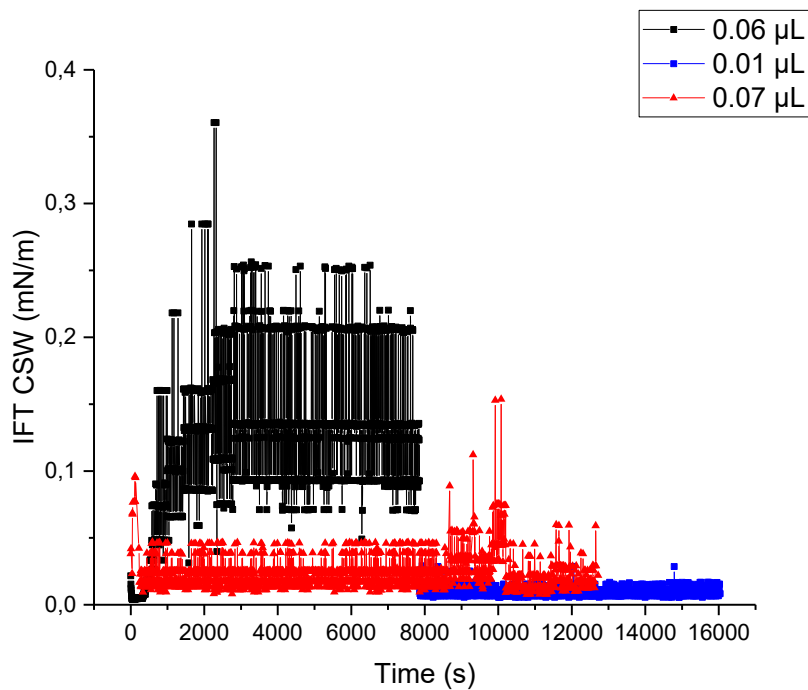


Figure 4-32 IFT vs. time of crude 16 oil in 3,000 ppm alkali distilled water solution

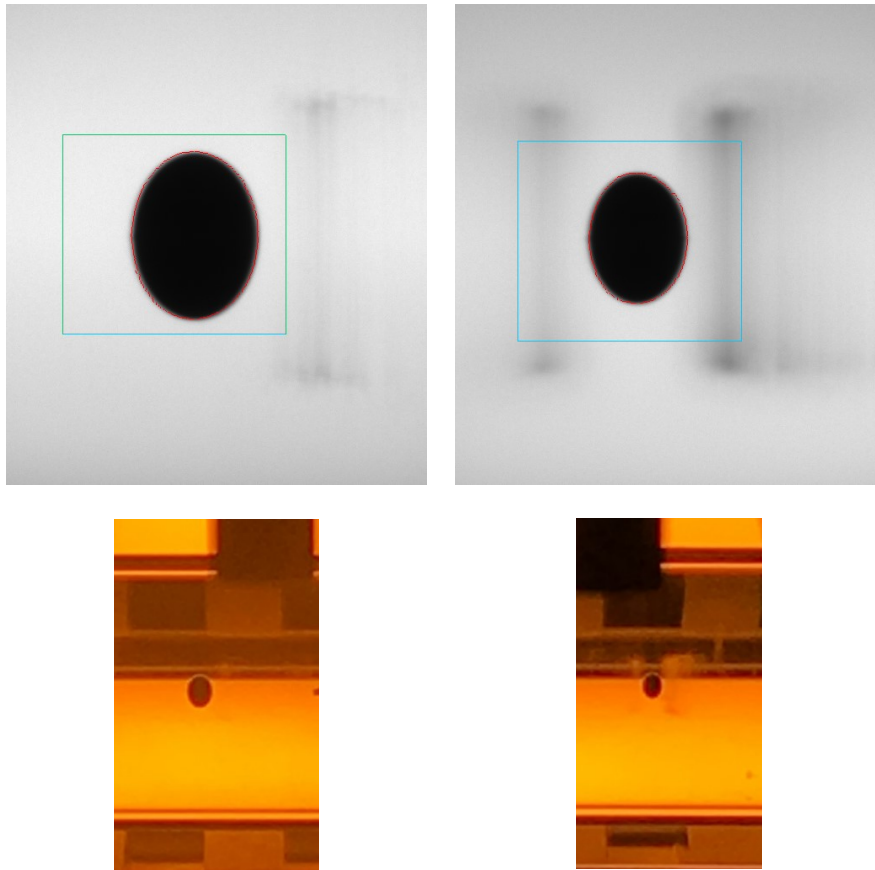


Figure 4-33 Crude 16 oil in 3,000 ppm distilled water solution (first experiment)

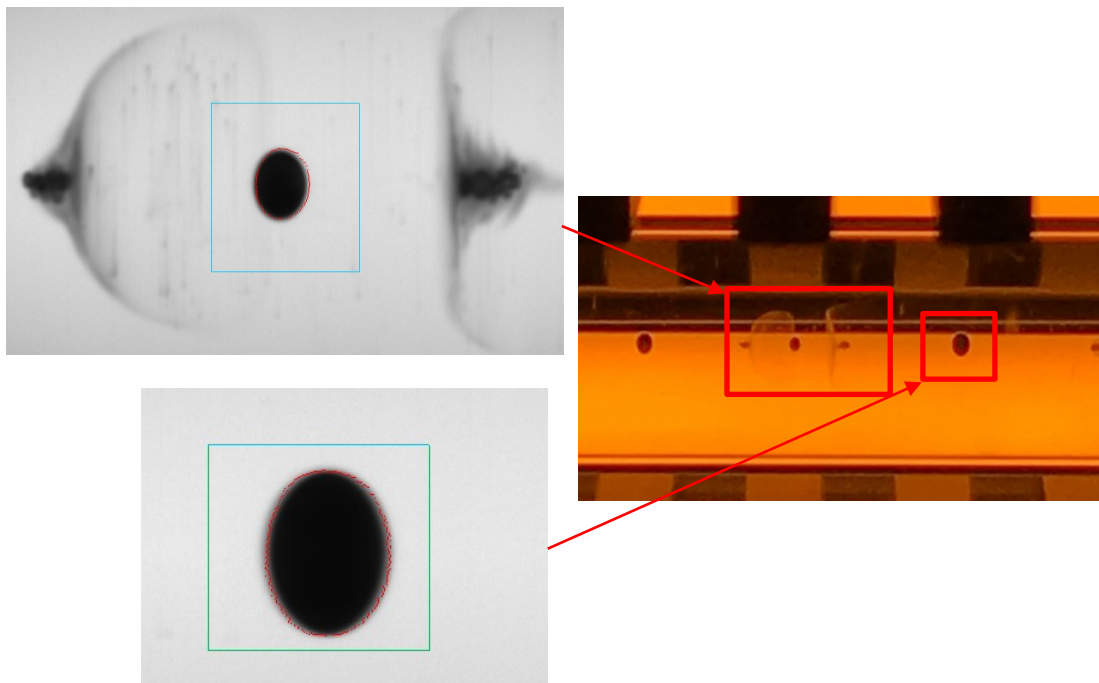


Figure 4-34 Crude 16 oil in 3,000 ppm distilled water solution (second experiment)

Measurements of the crude 16 oil in the 7,500 ppm solution turned out to be quite more complex than those before because it took around 40 minutes until the first real droplets were forming which enabled a measurement of the IFT. At the beginning the oil consisted of multiple elongated drops. Emulsions started to form around those leading to a destabilizing of the elongated drops. After a while parts of the oil moved out of the diluted portion where it started to form a more stable drop. As soon as one big stable drop was present the measurement started. Therefore, IFT readings are obtained starting at 2,600 seconds.

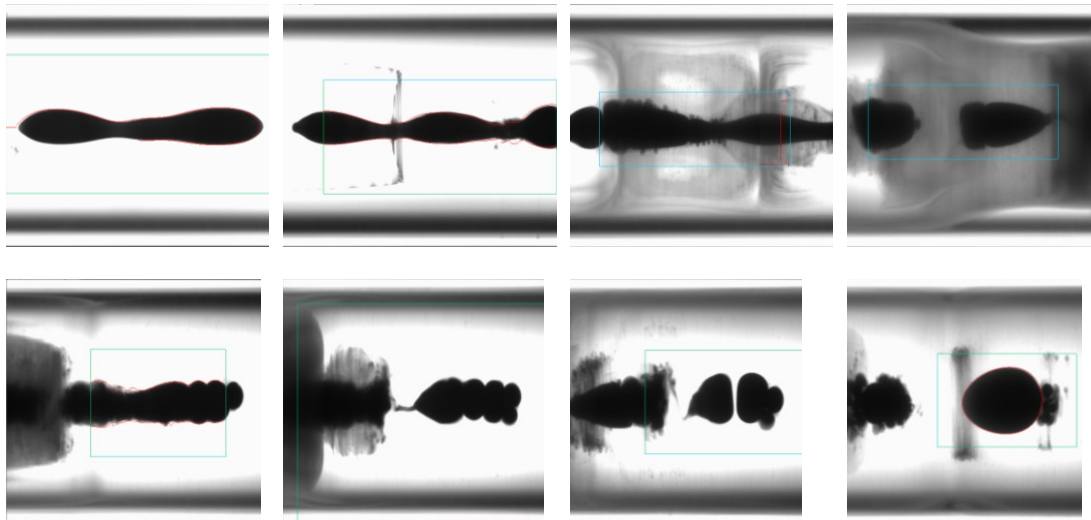


Figure 4-35 Evolution of crude 16 oil drop formation in 7,500 ppm distilled water solution software (left to right: 33s, 140s, 470s, 714s, 1031s, 1110s, 1400s and 2640s)

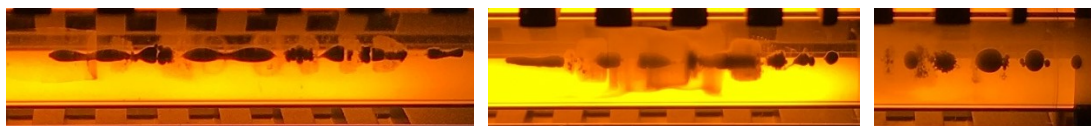


Figure 4-36 Evolution of crude 16 oil drop formation in 7,500 ppm distilled water solution photos (left to right: 145s, 720s, 2700s)

The drop continued to change its shape for another 50 minutes until it got more spherical and stabilized. IFT values obtained at the end are around 0.02 mN/m for a drop volume of around 0.9 μL which is quite a large volume compared to previous experiments. Before continuing the measurement with the next higher concentration, the measurement was immediately repeated to check whether the long equilibration time is due to the amount of oil expelled in the solution. Additionally, it was checked whether the drop volume influences the obtained IFT.

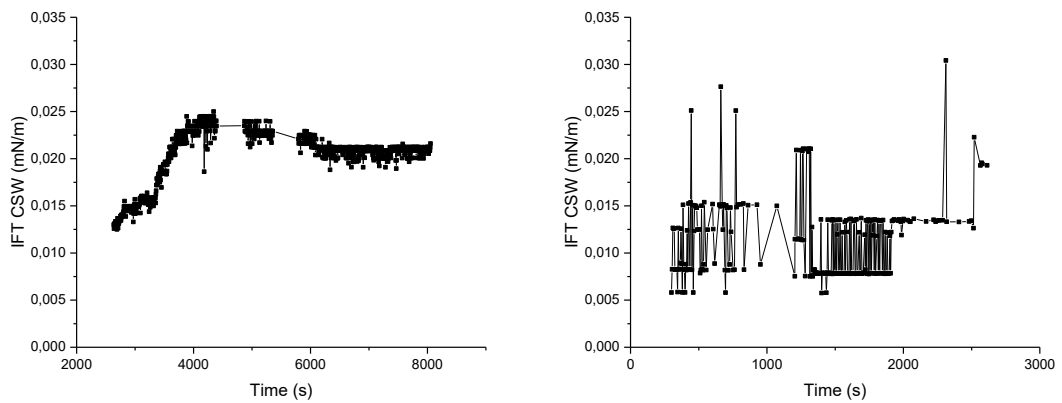


Figure 4-37 IFT vs. time crude 16 oil in 7,500 ppm distilled water solution of two different experiments with different drop volumes (left: 0.9 μ L; right: 0.03 μ L)

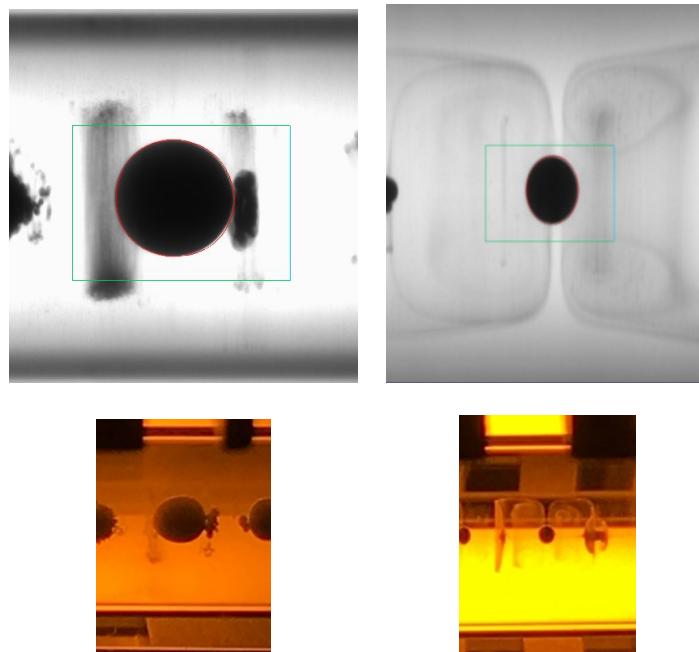


Figure 4-38 Crude 16 oil in 7,500ppm distilled water solution of two different experiments with different drop volumes (left: 0.9 μ L; right: 0.03 μ L)

Even though the volume of both droplets differs by a factor of 30, the obtained IFT values are alike. Furthermore, it can be observed that the time until the start of measurement changed from 40 minutes to 5 minute, which is the time until a stable droplet formed. Though it can be observed that the obtained values are oscillating much more for the smaller volumes. This is also due to the shape of the droplet. In the left picture it can be seen that the horizontal to vertical ratio is above one. The obtained values are therefore more reliable than in the case of the smaller drop where the ratio is clearly below one. However, the values do not deviate too much from each other, leading to the assumption that a ratio below one leads to an underestimation of IFT.

The last experiment conducted with the distilled water alkali solutions were with the 12,000 ppm concentration. A stable droplet formed from the start enabling measurements. The obtained IFT values are very stable and do not change over time. Next to the droplet an elongated accumulation of much smaller droplets gathered yet they did not bother the bigger droplet at all.

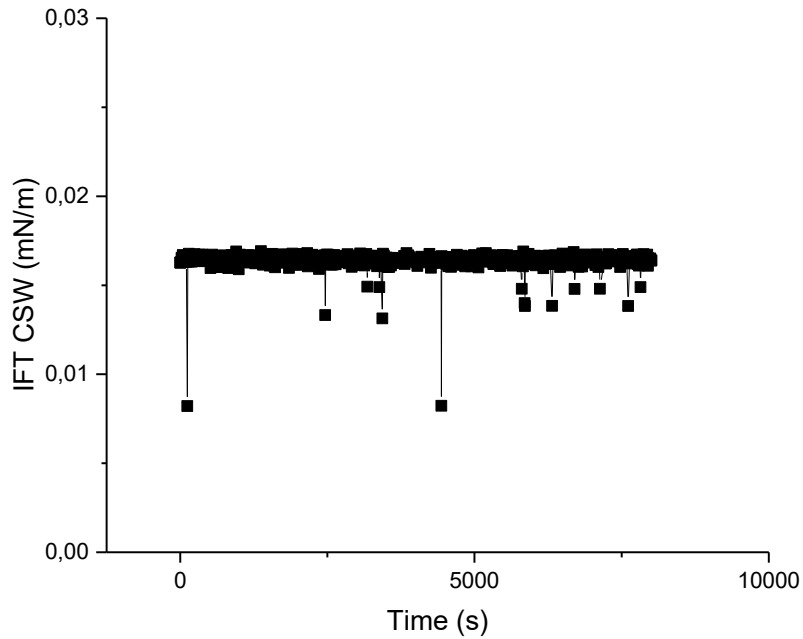


Figure 4-39 IFT vs. time of crude 16 oil in 12,000 ppm distilled water solution

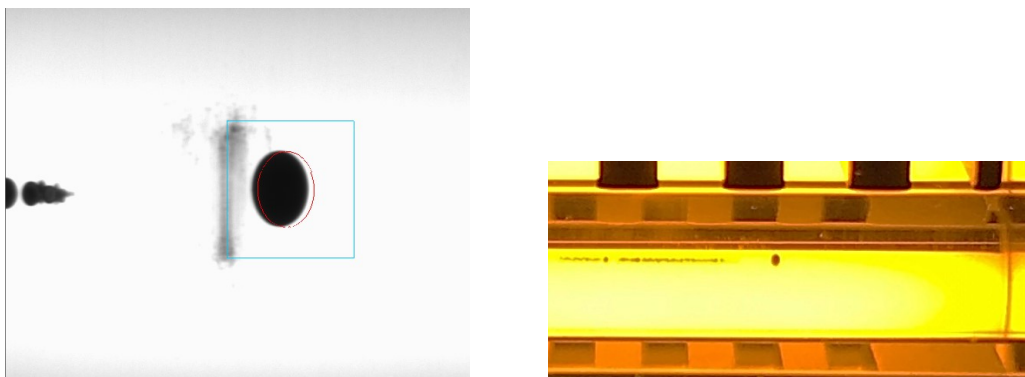


Figure 4-40 Crude 16 oil in 12,000 ppm distilled water solution

4.2.5.3 Crude 8 oil in alkaline synthetic water solutions

From the phase behavior experiments it is not expected that visible emulsions are forming. Earlier experiments have shown that IFTs obtained from crude 8 oil within synthetic water are very low ($\gamma_{o-sw} \sim 0.035$). Therefore, similar results are expected but in contrast to those measurements with synthetic water solutions no visible emulsion formations are expected.

After starting to rotate many small droplets formed. Those aligned with almost equal spacing to each other. The IFT readings started at very low values and steadily increased until reaching some sort of equilibrium (see Figure 4-41). Since they seemed stable the speed was increased which lead to less oscillation of the values, which is also due to the fact that the elongation in horizontal direction increased. After $\sim 4,000$ s and with a rotational speed of 2,000 1/min the IFT reading is around 0.15 mN/m which is a magnitude of order higher than the ones obtained within pure synthetic water. Furthermore, no emulsions were visible only some small satellite next to the droplet. The droplets shape is almost spherical, with a slightly higher

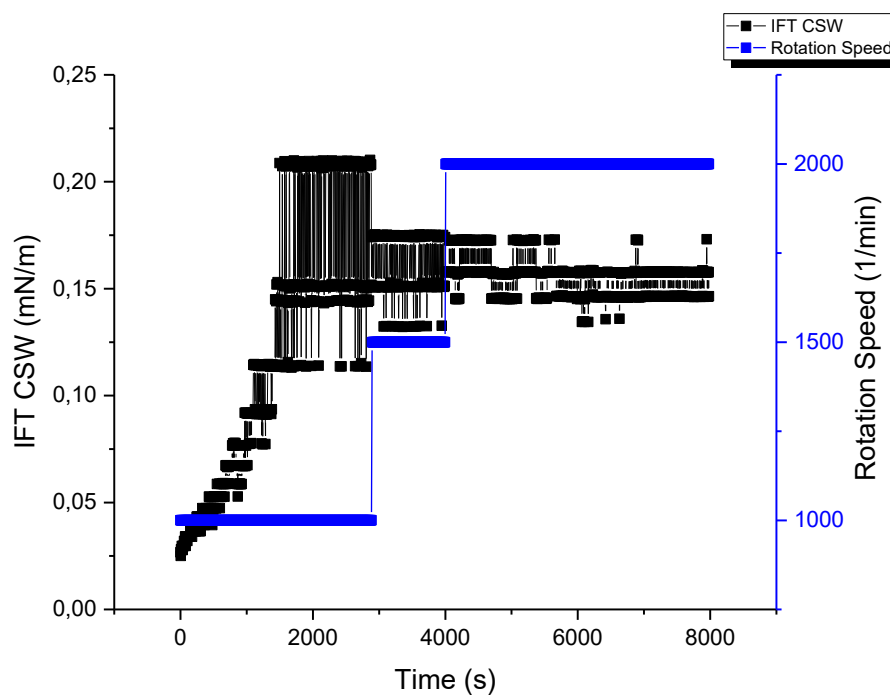


Figure 4-41 IFT vs. time of crude 8 oil in 3,000 ppm synthetic water solution

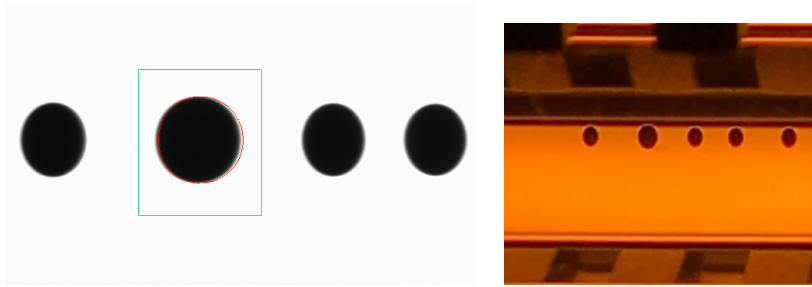


Figure 4-42 Crude 8 oil in 3,000 ppm synthetic water solution

In case of the 7,500 ppm alkali synthetic water solution no drastic change was expected. After the start several separate drops arranged close to each other. With time those approached each other until they started conjoining the biggest one with advancing time. Right after conjoining the IFT increased to a maximum. Subsequently the IFT decreased again to a stable value of around 0.3 mN/m. In Figure 4-43, both the increase to a maximum as well as the afterward decline can be seen. Since the obtained values were still oscillating and the observed ratio seemed to be below one the rotational speed was increased. It shows that with increased speed the IFT does not majorly change, however the form of the drop deviates further from a spherical one, which makes the obtained data more reliable. Furthermore, even after very long times of exposure it can be seen that the system is not in perfect equilibrium since the IFT is still minorly changing. In addition to the stabilization did satellites form next to both sides of the drop, after the increase in rotational speed.

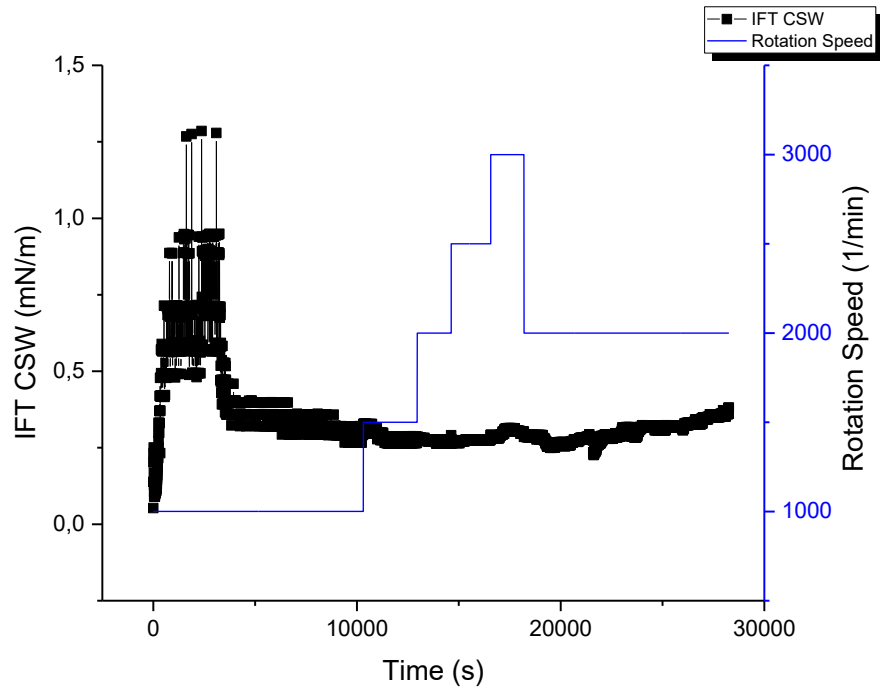


Figure 4-43 IFT vs. time and rotational speed of crude 8 oil in 7,500 ppm synthetic water solution

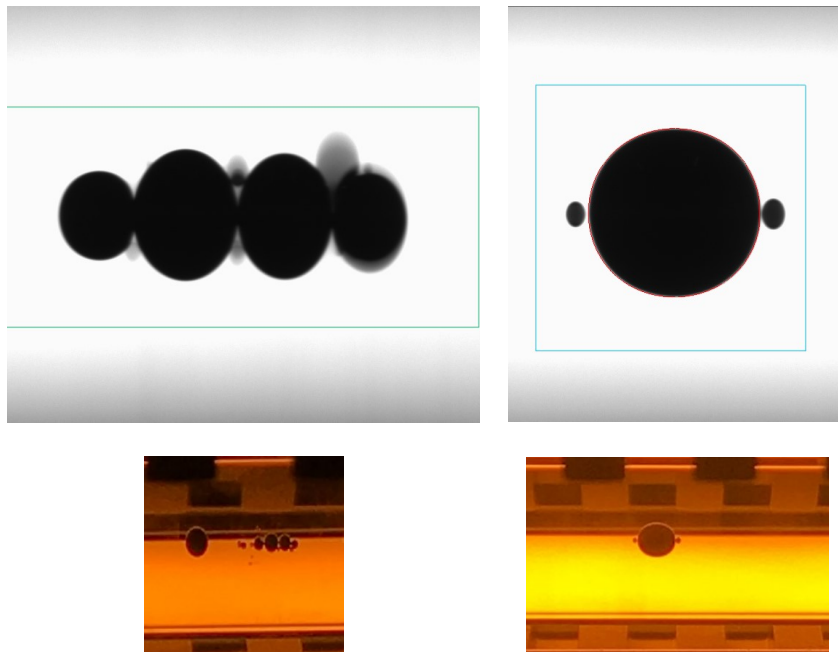


Figure 4-44 Crude 8 oil in 7,500 ppm synthetic water solution

The crude 8 oil showed the same characteristics as within the other two measured alkali synthetic water solutions. After an IFT increase with time stable drops formed which also approached each other over time. The only difference was that the droplets did not conjoin the big one during the experiment.

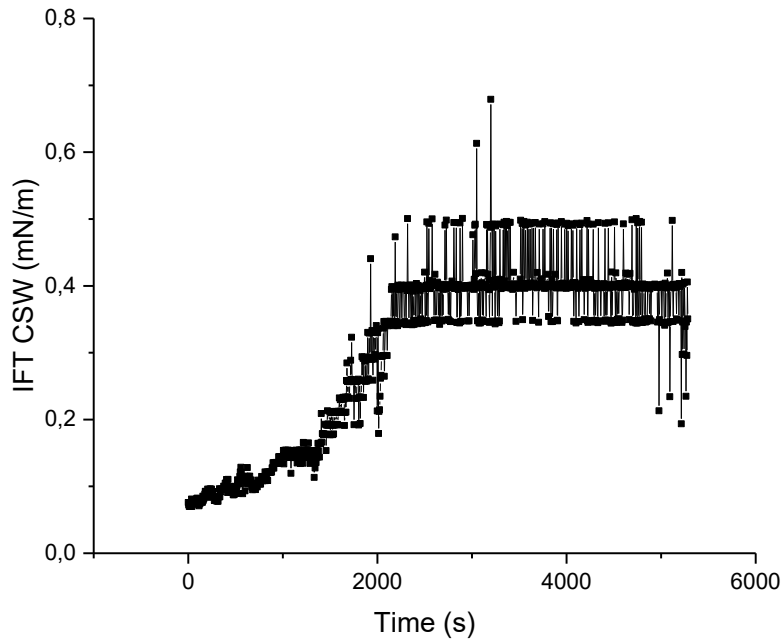


Figure 4-45 IFT vs time of crude 8 oil in 12,000 ppm synthetic water solution

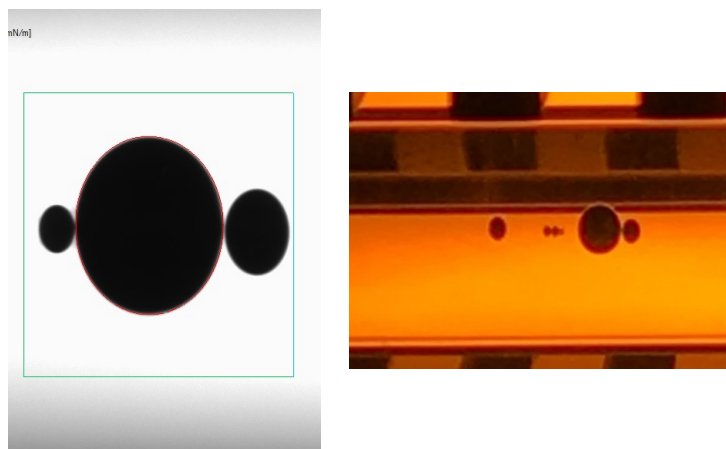


Figure 4-46 Crude 8 oil in 12,000 ppm synthetic water solution

4.2.5.4 Crude 16 oil in alkaline synthetic water solutions

The phase behavior of the crude 16 oil was quite similar to that of the crude 8 oil, with the only difference that a white ring was not visible, only oil swelling. Therefore, alike results were expected when conducting these.

Just as expected droplets of similar size formed, which later conjoined to a bigger stable one. The drops shape is rather elliptical with a bigger vertical than horizontal extend (Figure 4-49)

inducing a high oscillation of obtained IFT readings (Figure 4-47). In the histogram it gets more evident, that the measured values are around 2.5 mN/m. No visible emulsions formed.

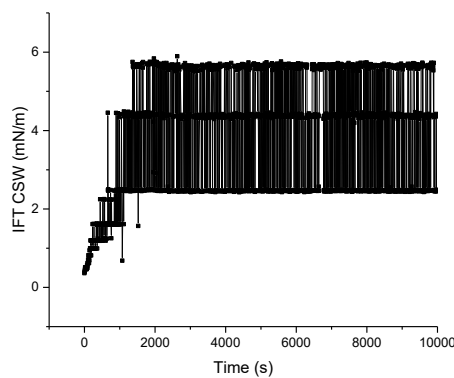


Figure 4-47 IFT vs. time of crude 16 oil in 3,000 ppm synthetic water solution

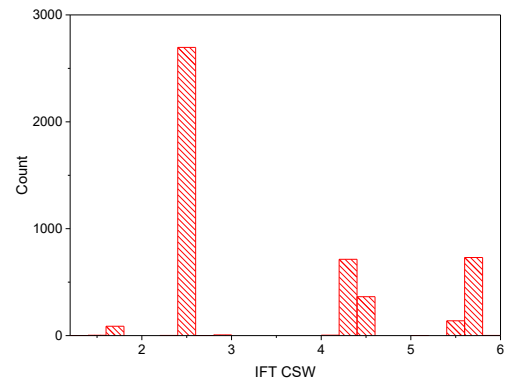


Figure 4-48 Histogram of stable crude 16 oil drop in synthetic water solution

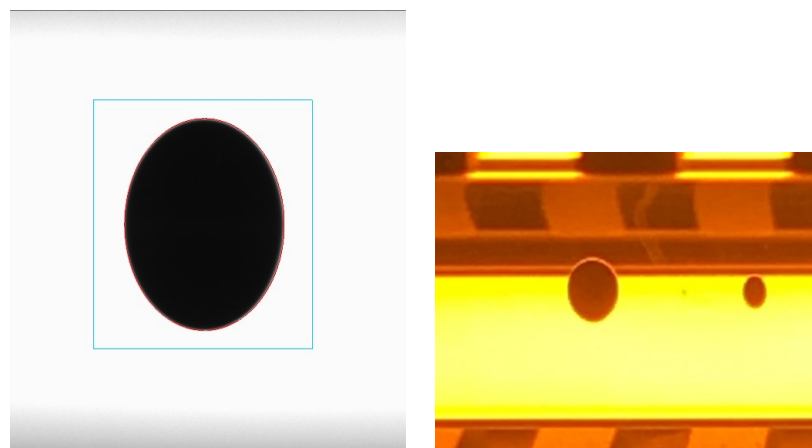


Figure 4-49 Crude 16 oil in 3,000 ppm synthetic water

In case of an alkali concentration of 7,500 ppm a similar behavior was observed. At the beginning many smaller droplets formed, which relatively fast started conjoining shaping one big stable droplet. Obtained readings do not oscillate as much as in the case of the 3,000 ppm since the drops form is less elliptical than in the previous case. After a while a small satellite formed, however it did not interrupt the system.

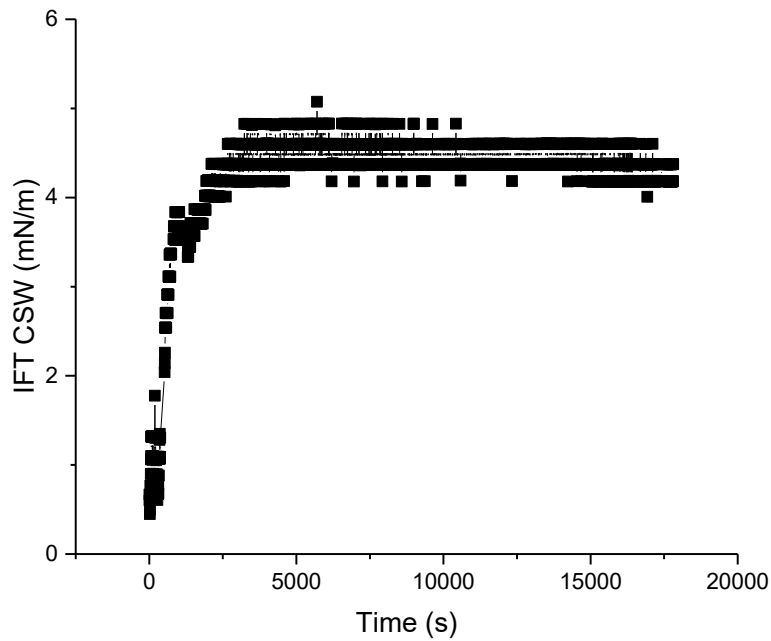


Figure 4-50 IFT vs. time of crude 16 oil in 7,500 ppm synthetic water solution

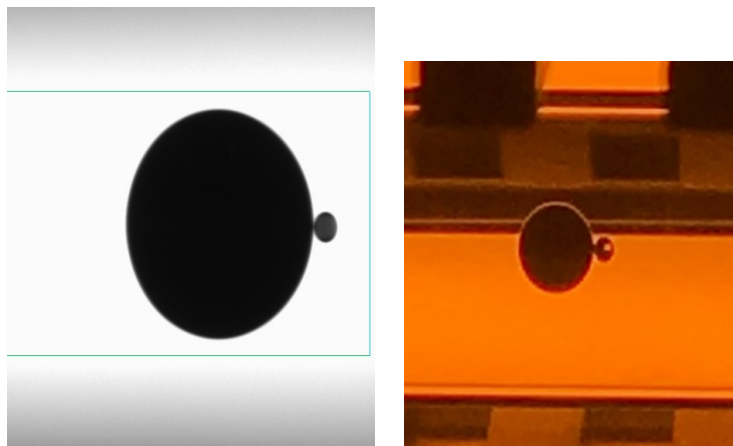


Figure 4-51 Crude 16 oil in 7,500 ppm synthetic water solution

In general, did the crude 16 oil in 12,000 ppm synthetic water solution show a similar trend to the preceding experiments. However, higher rotational speeds needed to be used that a stable measurable drop formed. Even though many drops were present, they did in opposition to the other experiments not conjoin and not approach each other. Due to the drops form the obtained IFT values are less clearly distributed than in other measurements. This can be seen in the histogram. Other than that, was the drop still stable and neither emulsions nor satellites formed close to the measured drop.

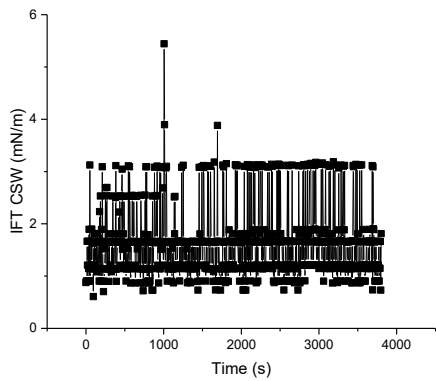


Figure 4-52 IFT vs. time of crude 16 oil in 12,000 ppm synthetic water solution

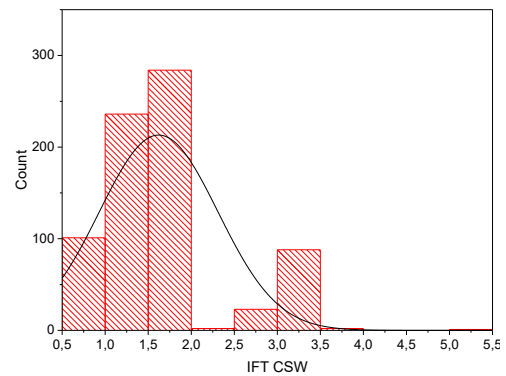


Figure 4-53 Histogram of crude 16 oil in 12,000 ppm synthetic water solution

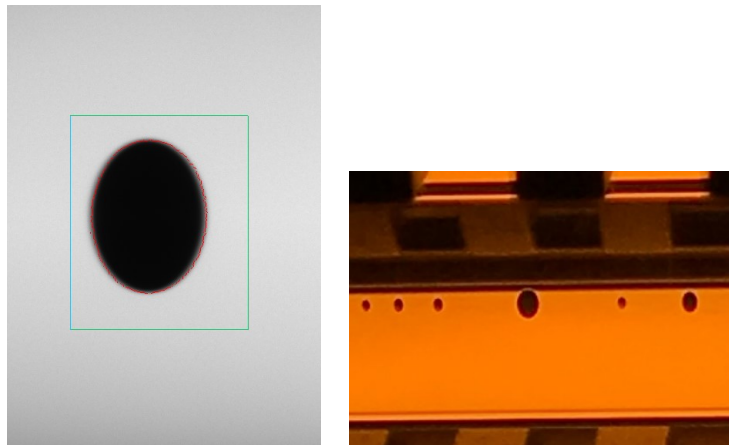


Figure 4-54 Crude 16 oil in 12,000 ppm synthetic water solution

4.2.6 Temperature

Temperature dependency measurements were always started at 20°C. Each of them was conducted the same way by increasing in 5°C steps. A drop was considered stable at a temperature if its IFT and volume did not change over the course of 20 min. The obtained readings at this time span were taken as the IFT value. Since some of them showed oscillating behavior, they were statistically analyzed and the mean which was also the most common count of value was taken as value for plotting. Only one alkali concentration was measurement each, since the goal was to see what influence the alkali addition has to the system.

From literature it was known that with crude oils the observed IFT change with increasing temperature can go both ways. Furthermore, it was known that surfactants destabilize the system, especially at higher temperatures. In general, the 16 oil showed almost no sensibility

to the temperature. After increasing the temperature, the systems stabilized rather fast enabling the measurement of the IFT. In case of the crude 16 in synthetic water the temperature was also measured from high to low, which is plotted in Figure 5-3 as hollow triangles. The results did not change much emphasizing the low sensibility to temperature changes. Only in case of the crude 16 in 3,000 ppm synthetic water a slight trend of decreasing IFT over time was observed.

The crude 8 oil on the other side was rather tricky to measure. Only for the distilled water measurements clear values could be obtained throughout the temperature increase. In general, especially for higher temperatures it was harder to obtain IFT values. In two cases a minimum showed at 25°C. The measurement was repeated from high to low temperature in the case of the crude 8 in synthetic water, which lead to a change of the minimum to 30°C, which can be seen in Figure 5-3. Furthermore, the readings did increase with increasing temperature even if just slightly. The crude 8 oil with 3,000 ppm distilled water solution marks a rather special case since it is initially increasing and then strongly decreasing with the higher temperatures.

In general, it was observed that if more than one droplet were present that with increasing temperature the droplets started to distant away from each other, as seen in Figure 4-56. Furthermore, in case of the crude 8 in 3,000 ppm distilled water the droplet elongated with increasing temperature, which led to a significant reduction of the IFT. However more importantly due to the elongation the droplet started to distinguish further from a spherical shape, not only reducing obtained IFT values, but also the oscillation of those (see Figure 4-55). When the temperature was increased from 45°C to 50°C the IFT steeply decreased only to stabilize again at even lower values.

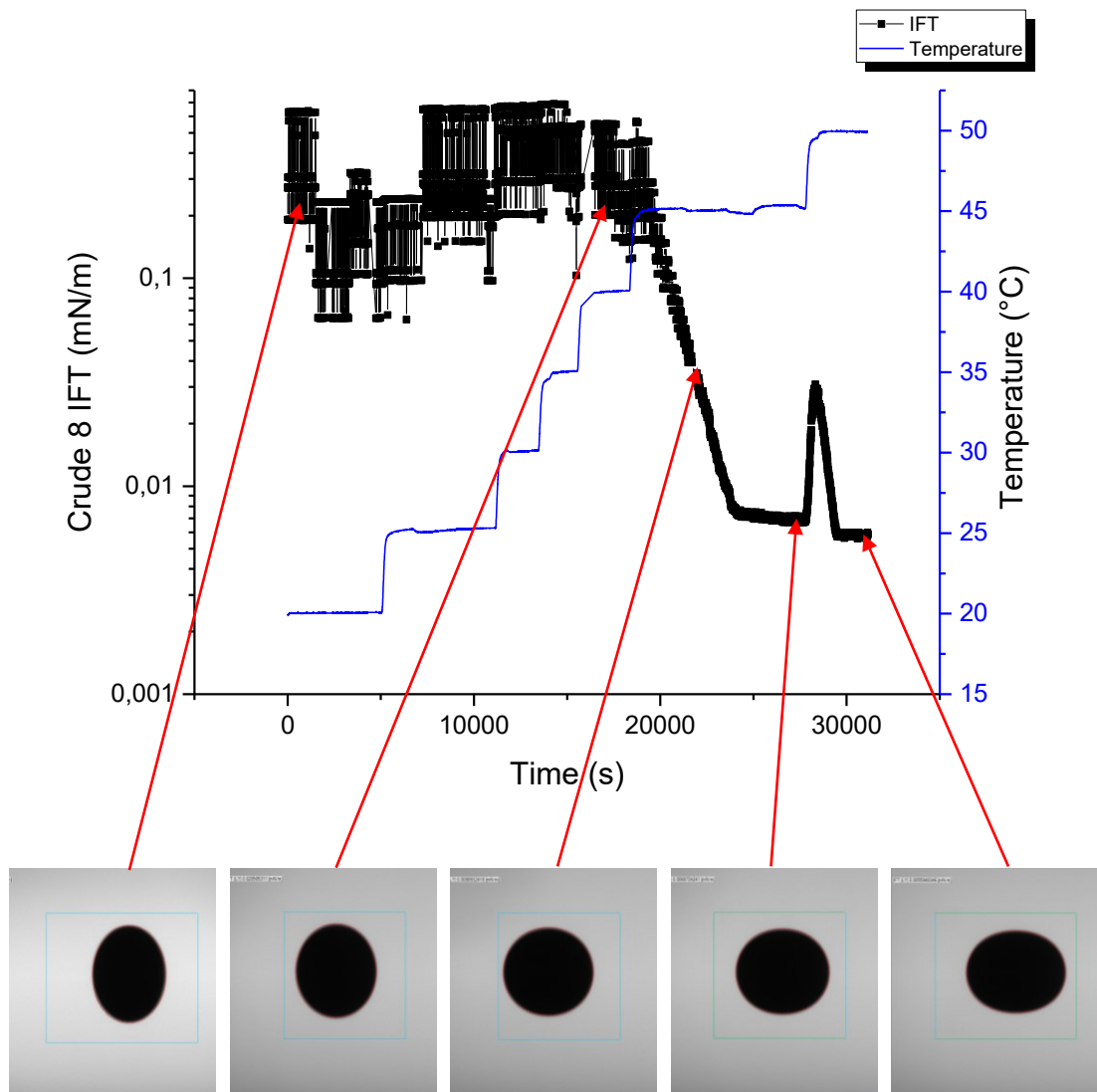


Figure 4-55 IFT vs. time and temperature of crude 8 oil in 3,000 ppm distilled water solution

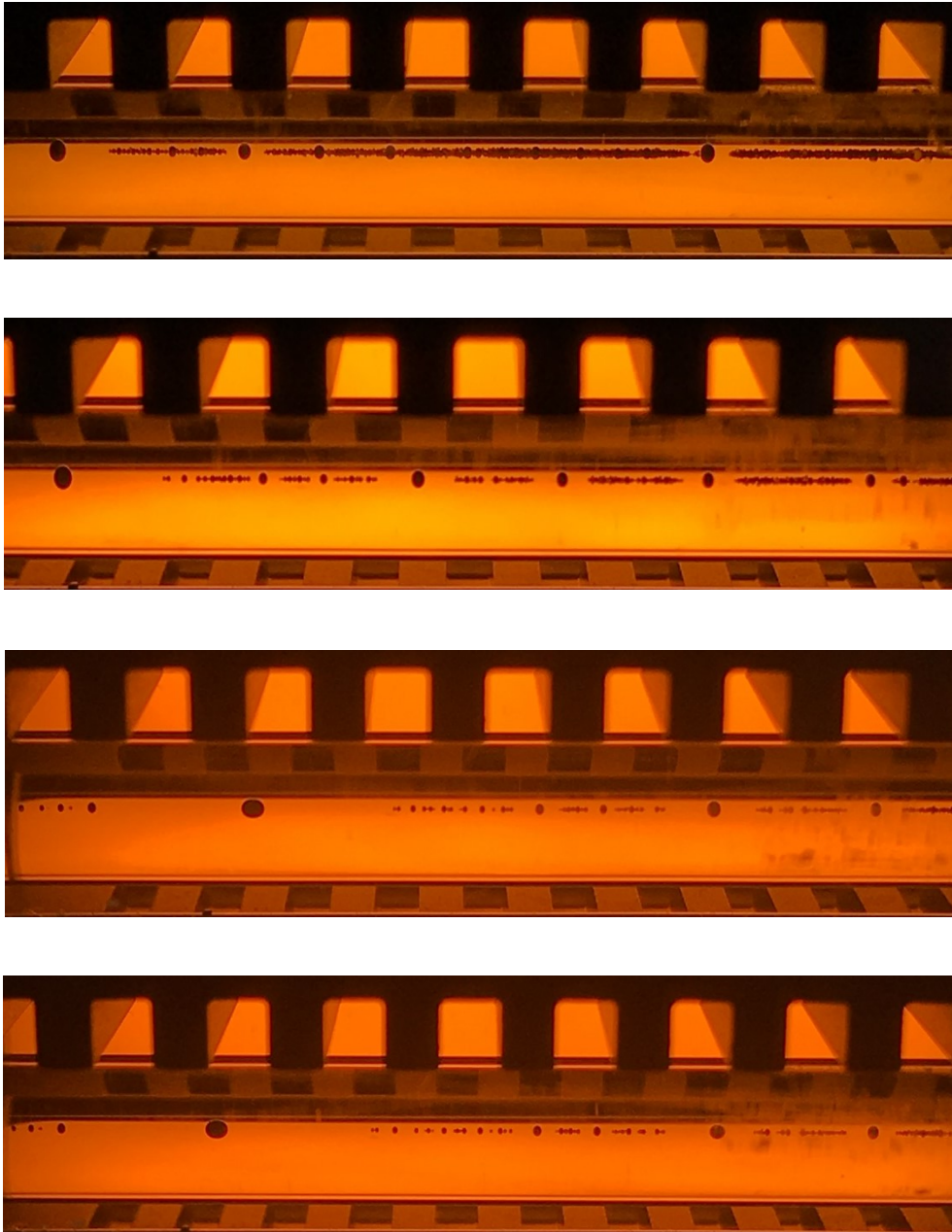


Figure 4-56 Distancing and conjoining of droplets exemplary in the case of crude 8 and 3000 ppm distilled water solution (top to bottom: 20, 30, 40 and 50°C)

Chapter 5

Results and conclusions

In this chapter results of the previous observations and findings are discussed.

5.1 Alkali concentration dependency

At the beginning it was shown that the pendant drop method cannot deliver IFT values below 1 mN/m. Since either no drop forms at the tip of the needle or it detaches. Therefore, it can only be used as reference system for higher IFT systems.

In this study, no values below an order of magnitude of 10^{-2} mN/m were measured. The small to very small droplets which formed cannot be measured by the system. Due to the resulting picture quality and focus with increasing magnification it is rather hard to capture them. Especially in cases where the smaller droplets were within an emulsion cloud it would have been interesting to measure and compare those values with the bigger drops. Furthermore, the readings would be quite inaccurate since most of the droplets shape are spherical or even elliptical an elongation in vertical direction, especially smaller ones. In later cases the actual IFT values are different but the shape cannot be processed by the program due to the horizontal to vertical ratio, which is below one. Since the shape factor (see chapter 2.3.2) does not exist below a ratio of one and in case of a sphere it equals zero, the IFT would be infinite. Therefore, the program assumes a ratio close to one, so the IFT can be calculated. Thus, obtained values are wrong, especially since the program takes the vertical radius as cap radius and assumes an almost spherical shape. This leads to an overestimation of the surface area as well as the volume. On basis of this the IFT would be overestimated since the radius is taken to the power of three within the IFT formula. Furthermore, the shape factor is not defined for those ratios thus the value taken is that of an almost spherical droplet, which results in very low values. The shape factor α is in the denominator therefore the smaller α the greater the IFT, which could also lead to an overestimation of the IFT. Therefore, obtained values for horizontal to vertical ratios below one are considered as unreliable, since the formula used for calculating them does not hold.

On a first glance this behavior does not seem to be physical, since a drop will take the shape of sphere to minimize the energy needed to maintain that form. Therefore, when centrifugal forces are applied, the drop should elongate in horizontal direction. Yet the experiments showed that in most cases, especially when many small droplets formed, and emulsions are present, the drop elongates in vertical direction. An explanation could be that the emulsion, even though not always visible, accumulates for density reasons around the axis of rotation (at the sides of the droplet). Since the IFT between oil and emulsion can be assumed to be smaller than between oil and the aqueous phase, the drop minimizes the interfacial energy considering the variation of interfacial tension between oil and water. In this situation the minimum of interfacial energy does not correspond to a minimum in interfacial area. The droplet takes on an elliptical shape symmetric to the rotational axis elongated in vertical direction, corresponding to the variation of interfacial tension (see Figure 5-1). The denotation O is the oleic phase, E the emulsion phase and W the aqueous phase.

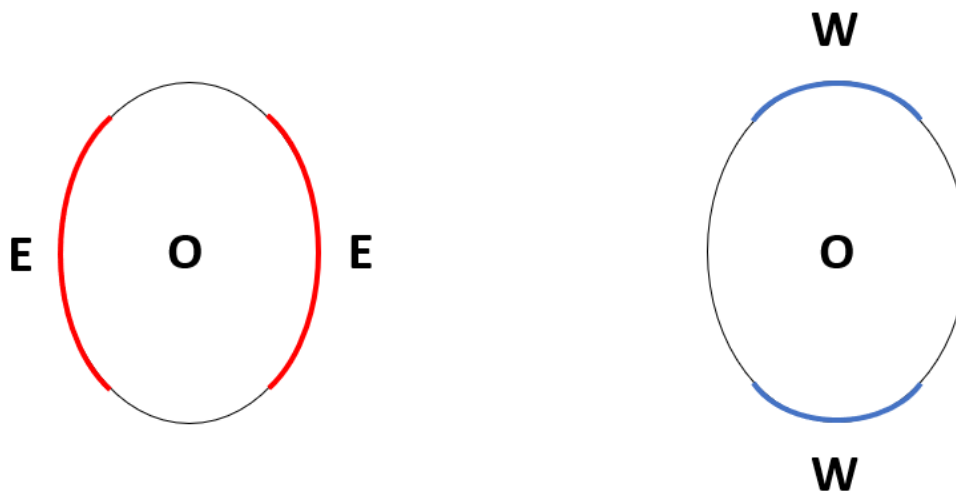


Figure 5-1 Schematic of an elliptical droplet with different phase contacts

The observed oscillating behavior of IFT values can be explained by measurements taken every 5s. For each measurement, the program has taken the most suitable detection of the droplets shape by fitting 100 points around it. Therefore, the cap radius of the drop is alternating as well as the horizontal to vertical ratio. As explained in chapter 2.3.2, for ratios close to one the shape parameter α can take up a wide range of values explaining the IFT behavior. Especially, since the program is assuming a spherical shape for the drops, as explained before. Even though the obtained values seem to be oscillating between three explicit values, there is still a variation of

those values, which show that the obtained IFT really relies on the shape and points of the contour captured at that specific moment. When looking at the distribution of those values it can be seen that one is always more common than the others.

When injecting greater amounts of oil small droplets accumulated next to each other throughout the entire capillary. If a certain amount of oil was present the droplets conjoined into one, which extended to both sides of the capillary. Therefore, it was not possible to enlarge the volume of the smaller droplets thus changing their shape.

In almost all experiments a time dependency of the obtained readings could be seen. Yet due to the preparation of the capillaries, where the oil initially is attached to the wall, it is not possible to make distinct statements about those. Additionally, for some droplets measurements were not possible until they stabilized.

It can be said that when using distilled water, the alkali agent did cause the expected IFT reduction. However, no clear trend between each concentration step is visible. Surprisingly lower IFT values were achieved when using the crude 16 oil, which has a lower TAN. For both oils the most emulsions formed when using the 7,500 ppm solution. It was shown that if emulsions form the IFT is much more dependent on the rotational speed than in cases of no obvious emulsion formation. At the beginning they form between bigger drops in a cloud like structure. In addition to that it seems that with advancing time that those form satellites next to bigger drops, especially for higher rotational speeds. Though it was also observed that they can disappear, whereas they either conjoined a big droplet or moved to the non-visible sides of the capillary. Yet once a bigger drop stabilized it does not seem disturbed by those.

The experiments with synthetic water showed quite different results than those with the distilled water. First of all, from the phase behavior two clear phases are visible, which was not the case for the distilled water-based experiments. In addition to that, only minor oil swelling has been observed indicating that emulsions have not formed as in the previous case. Another surprising result was that already in case of the synthetic water, the obtained IFT values were already in the lower range. Especially in case of the crude 8 oil a rather unique behavior displayed, immediately a large portion of the oil conjoined to form a long-elongated drop. With advancing time, the other drops approached it to form one single one. The crude 16 oil on the other hand formed a couple of stable drops which did not conjoin even after long exposure times. Comparing the behavior of the crude 8 in synthetic water with other cases where the IFT was in the same range, the behavior is unique. Normally smaller and bigger droplets form which stay stable in a certain distance to each other, especially since the emulsions seem to stabilize those distances. However, in this case the oil conjoined immediately, no emulsion was visible. Still, even though a single big drop formed, ultra-low IFT was measured.

The results show an increase of IFT with the addition of alkali to the mixtures, which is reported in literature when being outside of the optimum concentration range. There is a maximum at a 12,000 ppm with crude 8 oil and 7,500 ppm with crude 16 oil. This corresponds to the maximum oil swelling from the phase behavior experiments, which could mean that these points deviate most from an optimum.

The mean obtained values with an error margin at each concentration were plotted in Figure 5-2. Errors were estimated on basis of the minimum and maximum obtained readings for stable drops. In general, the smaller the IFT values, which often comes along with having small droplets, the higher the absolute error. The data points, where the ratio was below one, are plotted as empty symbols. As discussed earlier they are considered as unreliable.

In none of the experiments a third phase formed or was visible, therefore it can be said that no optimum was found for any of the cases.

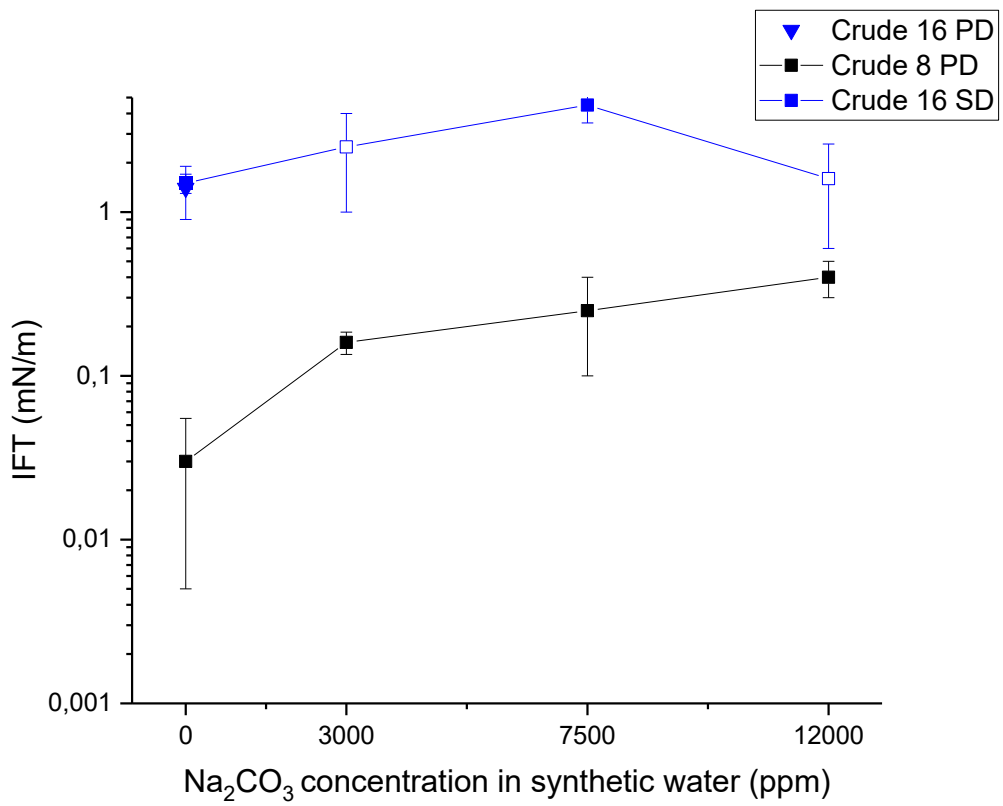
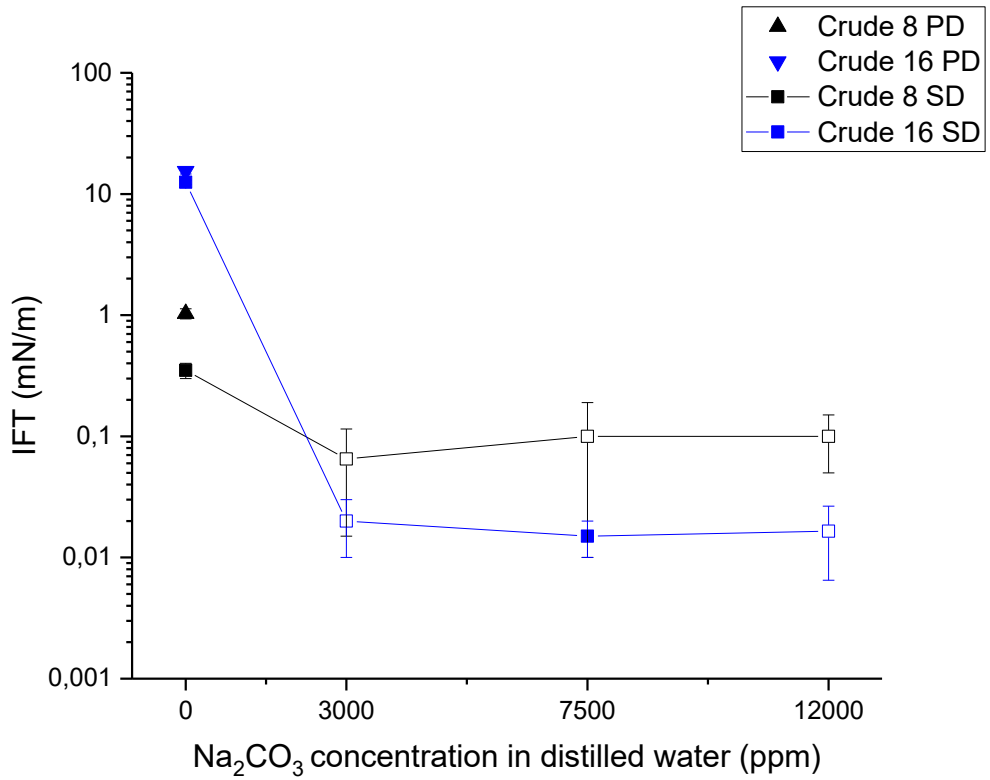


Figure 5-2 IFT vs. Na_2CO_3 solutions prepared with distilled (top) and synthetic (bottom) water

5.2 Temperature dependency

The results, plotted in Figure 5-3, show that IFT readings are temperature dependent. Data points with full symbols are obtained from droplets with a horizontal to vertical ratio of one or greater. In case of the crude 8 oil no general statement is possible. With pure distilled and synthetic water, a minimum at 25°C can be observed. Furthermore, the increase in IFT is rather high even on a logarithmic scale. Comparing with those where sodium carbonate is present, it seems that those systems are less sensitive to temperature changes. Rather interesting is the behavior of the crude 8 in 3,000 ppm distilled water which shows for higher temperatures a rapid decrease of IFT readings. In addition to that did the drop elongate and other droplets present removed themselves from each other, which fits low IFT behavior. Since IFT measurements are conducted over rather long periods of time, aging could be a reason for this behavior.

The crude 16 oil showed less sensitivity towards temperature changes. In contrast to the other measurements are there no extrema within the results. In general, is there a minor increase of IFT with temperature, only in case of the 3,000 ppm synthetic water mixture a decreasing trend is observed?

In most cases it was observed that smaller droplets are attracted to bigger ones and therefore approached those and eventually conjoined them. However, when increasing the temperature droplets showed opposite behavior by distancing from each other. Even though the IFT was not changing it seems that the systems equilibrium is disturbed and somehow changing.

In general, it was observed that systems with alkaline present took less time until stable IFT values could be read. When observing the emulsions, they were not influenced by the temperature and could be a reason for a stabilization of the system.

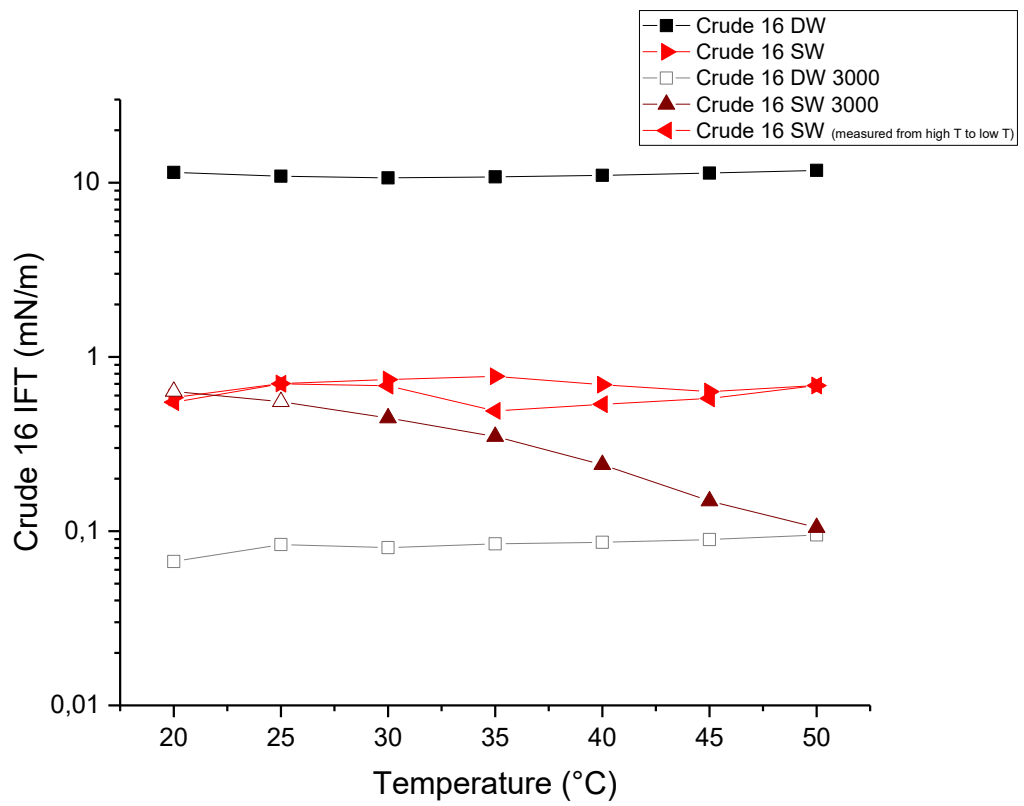
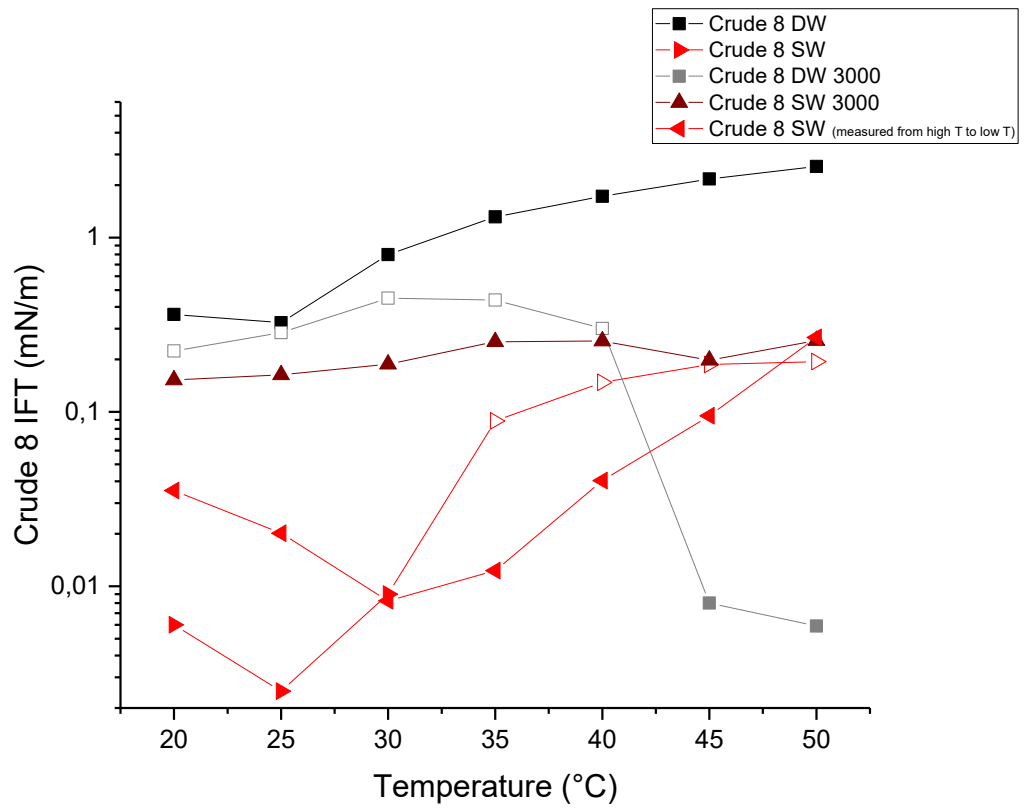


Figure 5-3 IFT vs. temperature of crude 8 (top) and crude 16 (bottom) oil

5.3 Summary

In this thesis the influence on the IFT of two different crude oils and various alkaline mixtures has been studied. The effect of different parameters such as,

- Total acid number of the oils
- Alkaline concentration
- Salinity
- Temperature

has been studied. In none of the tried cases an optimum emerged. Both oils have similar TAN but showed different behavior. Hence, it can be assumed that not the total number of acids but rather the composition and type of acid present influences the system.

For alkali mixtures prepared with distilled water an IFT reduction have been observed in all cases accompanied by extensive emulsion formation. Yet, no trend between each concentration step was visible within the obtained data. When using synthetic water, which has an increased salinity, the addition of an alkaline agent led to a slight IFT increase in the case of the crude 8 oil whereas in contrast for the crude 16 oil IFT values decreased. Therefore, it can be assumed that we are outside the optimum concentration window for this salinity.

In almost all cases of very low interfacial tension small droplets formed, whose shape was spherical or elliptical elongated in vertical direction. Since the calculation method used by the program does not hold for those, it can be assumed that those IFTs are deviating what was obtained.

Furthermore, was shown that the temperature influences the system. However, the extent of influence as well as trend seems to greatly rely on the type of oil. Generally, it was observed that increased temperatures lead to less interaction between oil droplets. For mixtures with alkaline it took much less time until the drop stabilized after a temperature increase, leading to the assumption that the alkaline has a stabilizing effect on the system.

5.4 Future Work

The conducted experiments showed that oil-alkaline systems are rather complex and sensitive to many parameters. There are a couple of things which need to be investigated in future work.

1. Possibility to reliably measure IFT values below the order of 10^{-2} mN/m.
2. Establishing and reliable measuring actual three-phase systems by spinning drop technique and to measure the IFT between microemulsion-oil and microemulsion-water/brine.
3. Phase behavior at higher temperatures to see whether some of the IFT measurements can be better understood.
4. CT-scan of the phase behavior tubes to grasp the actual composition.
5. Reevaluation of the capillary preparation method and injection of second phase. In this thesis the oil was attached to the wall and then filled with the rest of the water mixtures ensuring no disturbance by air bubbles but preventing time dependent measurements of the IFT. Furthermore, it would be interesting whether an injection/placement of constant volume droplets is possible by any means.
6. Performing reliable time dependent measurements.
7. More extensive screening of the parameter space in the present thesis, especially the salinity dependence to find best salinity to be able to design the injection water.
8. Investigation of the resulting droplet size and droplet merging behavior.
9. It can be expected that a lot of EOR-relevant systems are affected by phase separation as observed and discussed in previous chapters. Investigation of the influence of emulsion separation – the “three phase” system – on the measurements. How can droplets with inverse aspect ratio be interpreted and respectively analyzed? Can such multiphase systems be reliably measured at all?

Chapter 6

References

Afshar, S. & Yeung, A., 2011. Considerations when determining low interfacial tensions. *Journal of Colloid and Interface Science*, Issue 364, pp. 276-278.

Anon., 2018. *Machinery Lubrication*. [Online] Available at: <http://www.machinerylubrication.com/Read/1052/acid-number-test> [Zugriff am 23 April 2018].

Babu, D. R., Hornof, V. & Neale, G., 1984. Effects of Temperature and Time on Interfacial Tension Behavior Between Heavy Oils and Alkaline Solutions. *The Canadian Journal of Chemical Engineering*, Issue 62, pp. 156-159.

Bowman, C. W., 1967. *Molecular and interfacial properties of Athabasca tar sands*. Mexico City, Mexico, World Petroleum Congress.

Cayias, J. L., Schechter, R. S. & Wade, W. H., 1975. Measurement of Low Interfacial Tension via the Spinning Drop Technique. *ACS Symposium Series*, pp. 234-247.

Chatterjee, J., Nikolov, A. & Wasan, D. T., 1998. Measurement of Ultralow Interfacial Tension with Application to Surfactant-Enhanced Alkaline Systems. *Industrial & Engineering Chemistry Research*, Issue 37, pp. 2301-2306.

D664, A., 2018. *Test Method for Acid Number of Petroleum Products by Potentiometric Titration*, s.l.: s.n.

Dataphysics, 2013. *SVT_Help*. Filderstadt, Germany: Author: s.n.

Deutsche Bank, 2013. *Oil and Gas for Beginners*, United Kingdom: Deutsche Bank Markets Research.

deZabala, E. F., Vislocky, J. M., Rubin, E. & Radke, C. J., 1982. A Chemical Theory for Linear Alkaline Flooding. *Society of Petroleum Engineers Journal*, Issue 22, pp. 245-258.

- du Noüy, P. L., 1925. An interfacial tensiometer for universal use. *The Journal of General Physiology*, pp. 625 - 632.
- Eremin, N. & Nazarova, L. N., 2003. *Enhanced Oil Recovery Methods*. Moscow, Russia: Russian State Gubkin University of Oil and Gas.
- Flock, D. L., Le, T. H. & Gibeau, J. P., 1986. The effect of temperature on the interfacial tension of heavy crude oils using the pendant drop apparatus. *The Journal of Canadian Petroleum Technology*, pp. 72-77.
- Gong, H. et al., 2016. Effect of wettability alteration on enhanced heavy oil recovery by alkaline flooding. *Colloids and Surfaces A: Physicochemical and Engineering Aspects*, Issue 488, pp. 28-35.
- Gossudarstwenny Standart (GOST), 2004. *R 8.610-2004, State system for ensuring the uniformity of measurements. Density of oil. The tables for recalculation*, s.l.: s.n.
- Hamilton, W., Wagner, L. & Wessely, G., 1999. Oil and Gas in Austria. *Mitt. Österr. Geol. Ges.*, Issue 92, pp. 235-262.
- Hassan, M. E., Nielsen, R. F. & Calhoun, J. C., 1953. Effect of pressure and temperature on oil-water interfacial tensions for a series of hydrocarbons. *Petroleum Transactions, AIME*, Issue 198, pp. 299-306.
- Hjelmeland, O. S. & Larrondo, L. E., 1986. Experimental Investigation of the Effects of Temperature, Pressure and Crude Oil Composition on Interfacial Properties. *SPE Reservoir Engineering*, pp. 321-328.
- Johnson, C. E., 1976. Status of Caustic and Emulsion Methods. *Journal of Petroleum Technology*, pp. 85-92.
- Lake, L., Johns, R. T., Rossen, W. R. & Pope, G. A., 2014. *Fundamentals of Enhanced Oil Recovery*. s.l.:s.n.
- Morrow, N. R., 1990. Wettability and its effect on oil recovery. *Journal of Petroleum Technology*, pp. 1476-1484.
- Muggeridge, A. et al., 2013. Recovery rates, enhanced oil recovery and technological limits. *Philosophical Transactions of the Royal Society A: Mathematical, Physical and Engineering Sciences*, 372(2006), p. 20120320.
- Owens, W. W. & Archer, D. L., 1971. The Effect of Rock Wettability on Oil-Water Relative Permeability Relationship. *Journal of Petroleum Technology*, Issue 251, pp. 873-878.

- Princen, H. M., Zia, I. Y. Z. & Mason, S. G., 1967. Measurement of Interfacial Tension from the Shape of a Rotating Drop. *Journal of Colloid and Interface Science*, pp. 99-107.
- Rosenthal, D. K., 1962. The shape and stability of a bubble at the axis of rotation. *Journal of Fluid Mechanics*, pp. 358-366.
- Sheng, J. J., 2010. *Modern Chemical Enhanced Oil Recovery: Theory and Practice*. s.l.:Elsevier.
- Sheng, J. J., 2014. A comprehensive review of alkaline-surfactant-polymer (ASP) flooding. *Asia-Pacific Journal of Chemical Engineering*, Issue 9, pp. 471-489.
- Thomas, S., 2008. Enhanced Oil Recovery - An Overview. *Oil & Gas Science and Technology*, Issue Vol 63, pp. 9-19.
- Viades-Trejo, J. & Gracia-Fadrique, J., 2007. Spinning drop method: From Young-Laplace to Vonnegut. *Colloids and Surfaces A: Physicochemical and Engineering Aspects*, pp. 549-552.
- Vonnegut, B., 1942. Rotating Bubble Method for Determination of Surface and Interfacial Tensions. *Review of Scientific Instruments*, Issue 13, pp. 6-9.
- Weast, R. C., 1972. *CRC Handbook of Chemistry and Physics*. 53 Hrsg. s.l.:s.n.
- Winsor, P. A., 1948. Hydrotrophy, solubilisation and related emulsification processes. *Transactions of the Faraday Society*, Issue 44, pp. 376-398.
- Winsor, P. A., 1956. Solvent Properties of Amphiphilic Compounds. *Fette, Seifen, Anstrichmittel*, Issue 12, pp. 1103-1104.
- Ye, Z. et al., 2008. The effect of temperature on the interfacial tension between crude oil and gemini surfactant solution. *Colloids and Surfaces A: Physicochemical and Engineering Aspects*, Issue 322, pp. 138-141.
- Zeppieri, S., Rodríguez, J. & López de Ramos, A. L., 2001. Interfacial Tension of Alkane + Water Systems. *Journal of Chemical Engineering Data*, Issue 46.
- Zhang, H. R., Bjørkvik, B. J. A. & Moffatt, B. J., 2001. Determination of Low Interfacial Tension with a Laser Light Scattering Technique and a Comparative Analysis with Drop Shape Methods. *Journal of Colloid and Interface Science*, Issue 237, pp. 11-20.

Appendix A

Appendix Title

A.1 Densities

Water density

Table 6-1 Water density depending on temperature [g/ml] (Weast, 1972)

	0	0.1	0.2	0.3	0.4	0.5	0.6	0.7	0.8	0.9
15	0.999099	0.999084	0.999069	0.999054	0.999038	0.999023	0.999007	0.998991	0.998975	0.998959
16	0.998943	0.998926	0.99891	0.998893	0.998877	0.99886	0.998843	0.998826	0.998809	0.998792
17	0.998774	0.998757	0.998739	0.998722	0.998704	0.998686	0.998668	0.99865	0.998632	0.998613
18	0.998595	0.998576	0.998558	0.998539	0.99852	0.998501	0.998482	0.998463	0.998444	0.998424
19	0.998405	0.998385	0.998365	0.998345	0.998325	0.998305	0.998285	0.998265	0.998244	0.998224
20	0.998203	0.998183	0.998162	0.998141	0.99812	0.998099	0.998078	0.998056	0.998035	0.998013
21	0.997992	0.99797	0.997948	0.997926	0.997904	0.997882	0.99786	0.997837	0.997815	0.997792
22	0.99777	0.997747	0.997724	0.997701	0.997678	0.997655	0.997632	0.997608	0.997585	0.997561
23	0.997538	0.997514	0.99749	0.997466	0.997442	0.997418	0.997394	0.997369	0.997345	0.99732
24	0.997296	0.997271	0.997246	0.997221	0.997196	0.997171	0.997146	0.99712	0.997095	0.997069
25	0.997044	0.997018	0.996992	0.996967	0.996941	0.996914	0.996888	0.996862	0.996836	0.996809
26	0.996783	0.996756	0.996729	0.996703	0.996676	0.996649	0.996621	0.996594	0.996567	0.99654
27	0.996512	0.996485	0.996457	0.996429	0.996401	0.996373	0.996345	0.996317	0.996289	0.996261
28	0.996232	0.996204	0.996175	0.996147	0.996118	0.996089	0.99606	0.996031	0.996002	0.995973
29	0.995944	0.995914	0.995885	0.995855	0.995826	0.995796	0.995766	0.995736	0.995706	0.995676
30	0.995646	0.995616	0.995586	0.995555	0.995525	0.995494	0.995464	0.995433	0.995402	0.995371

Oil density calculation

For calculating the oil densities at different temperatures, the following standard was used.

GOST R 8.610-2004 “State system for ensuring the uniformity of measurements. Density of oil. The tables for recalculation.”

$$\rho_T = \rho_{15} e^{-\alpha_{15}(T-15)(1+0.8\alpha_{15}(T-15))}$$

With T being the temperature in °C and ρ the density in kg/m³.

$$\alpha_{15} = \frac{K_0 + K_1 \rho_{15}}{\rho_{15}^2}$$

$$K_0 = 613,97226, \quad K_1 = 0$$